



Cite this: *Chem. Soc. Rev.*, 2023, 52, 663

# Recent advances in fluorescent and colorimetric chemosensors for the detection of chemical warfare agents: a legacy of the 21st century

Vinod Kumar, <sup>a</sup> Heejeong Kim, <sup>b</sup> Bipin Pandey, <sup>d</sup> Tony D. James, <sup>\*c</sup> Juyoung Yoon <sup>\*b</sup> and Eric V. Anslyn <sup>\*d</sup>

Chemical warfare agents (CWAs) are among the most prominent threats to the human population, our peace, and social stability. Therefore, their detection and quantification are of utmost importance to ensure the security and protection of mankind. In recent years, significant developments have been made in supramolecular chemistry, analytical chemistry, and molecular sensors, which have improved our capability to detect CWAs. Fluorescent and colorimetric chemosensors are attractive tools that allow the selective, sensitive, cheap, portable, and real-time analysis of the potential presence of CWAs, where suitable combinations of selective recognition and transduction can be integrated. In this review, we provide a detailed discussion on recently reported molecular sensors with a specific focus on the sensing of each class of CWAs such as nerve agents, blister agents, blood agents, and other toxicants. We will also discuss the current technology used by military forces, and these discussions will include the type of instrumentation and established protocols. Finally, we will conclude this review with our outlook on the limitations and challenges in the area and summarize the potential of promising avenues for this field.

Received 30th July 2022

DOI: 10.1039/d2cs00651k

rs.c.li/chem-soc-rev

<sup>a</sup> Process and Technology Development Division, Defence Research & Development Establishment, Jhansi Road, Gwalior 474002, India. E-mail: vkpal77@yahoo.co.in

<sup>b</sup> Department of Chemistry and Nanoscience, Ewha Womans University, Seoul 03760, Korea. E-mail: jyoona@ewha.ac.kr

<sup>c</sup> Department of Chemistry, University of Bath, Bath, BA2 7AY, UK. E-mail: t.d.james@bath.ac.uk

<sup>d</sup> Department of Chemistry, The University of Texas at Austin, Austin, Texas 78712-1224, USA. E-mail: anslyn@austin.utexas.edu

## 1. Introduction

The area of supramolecular chemistry emerged through inspiration from nature. Biological systems utilize a range of non-covalent interactions, such as hydrogen bonding, electrostatics, and  $\pi$ - $\pi$  stacking, to facilitate essential processes, such as the functioning of proteins and nucleic acids. Over the last 50 years, supramolecular chemists have devoted their attention



Vinod Kumar

Vinod Kumar is a Senior Scientist in the Defence Research and Development Establishment, Gwalior (India). He is working on the synthesis of bioactive molecules and the development of chemical sensor/detection system for chemical warfare agents and other toxicants.



Heejeong Kim

Heejeong Kim obtained her BSc from Ewha Womans University in 2020. Currently, she is pursuing her PhD degree under the supervision of Prof. Juyoung Yoon at Ewha Womans University. Her research interest is focused on supramolecular nano-agents and AIE theranostic agents.



to mimicking these interactions and designing new chemical systems for a variety of different applications, such as catalysis<sup>1</sup> and chemosensing,<sup>2</sup> as well as the fabrication of molecular switches,<sup>3</sup> smart materials,<sup>4</sup> molecular machines,<sup>5</sup> medicine,<sup>6</sup> and nanomedicine.<sup>7</sup> Notably, the design of new chemical sensors for analyte detection is crucial for chemical, biomedical, and defense applications. The detection of environmental pollutants, explosives, and chemical warfare agents (CWAs) is of particular interest to the scientific as well as the medical community. Next-generation molecular sensors and detection systems must focus more on prudent designs to control supramolecular interactions and enhance current properties. This review primarily focuses on the introduction of each type of lethal and non-lethal chemical weapon (conventional and novel CW agents) identified by the Chemical Weapon Convention (CWC). Examples of currently used detection methods/techniques/devices will also be discussed. We will discuss examples of currently reported chemical sensors with a particular focus on chromogenic and fluorogenic probes for CW detection. We hope that this review reveals how much this field has grown over just two decades to become a recognized and established branch of chemistry.

A nuclear, chemical or biological weapon can cause widespread destruction and kill large numbers of people at

one time. Chemical weapons are classified as weapons of mass destruction (WMD), like nuclear and biological weapons.<sup>8</sup> Formerly, the term 'NBC' (*i.e.*, nuclear, biological, and chemical) was coined to designate a WMD. At present, an accepted abbreviation is 'CBRNE' which describes chemical, biological, radiological, nuclear, and explosive weapons.<sup>9</sup> Chemical, biological, and non-nuclear explosives have been demonstrated to cause extensive damage to the nervous system and/or have neurobehavioral effects in victims. Technically, chemical weapons are both the CW agents, and the used delivery systems such as bombs, rockets, artillery shells, and aerosols.<sup>9</sup> CW agents are generally assumed to be gaseous (as depicted by movies), but they can also be in the liquid or solid-state. Therefore, to achieve the desired effect, CWAs are mostly delivered and disseminated in the form of aerosols. The release of aerosolized samples allows the particles to remain airborne for an indefinite period. The method of exposure of the CWAs depends on their physical and/or chemical properties. For example, if they have low vapor pressure, the likely route of exposure is *via* skin contact, and highly volatile CWAs are most likely exposed *via* respiratory, oronasal, and conjunctiva mucosal tissues. These exposures irritate the eyes, nose, and skin immediately.



**Bipin Pandey**

*Bipin Pandey obtained his BS in Biochemistry for The University of Evansville in 2020. Currently, he is pursuing his PhD degree under the supervision of Prof. Eric V. Anslyn at The University of Texas at Austin. His PhD work focuses on sequence-defined oligourethanes and their applications.*



**Tony D. James**

*Tony D. James is Professor at the University of Bath and Fellow of the Royal Society of Chemistry. He was a Royal Society University Research Fellow (1995–2000), Wolfson Research Merit Award holder (2017–2022) and was awarded the Daiwa-Adrian Prize (2013), the CASE Prize (2015), the MSMLG Czarnik Award (2018) and Frontiers in Chemistry Diversity Award (2020).*



**Juyoung Yoon**

*Juyoung Yoon is a distinguished professor at the Department of Chemistry and Nanoscience, Ewha Womans University. His research interests include investigations of fluorescent chemosensors, activatable photosensitizers theranostics, and organic functional materials. He was listed as a highly cited researcher in chemistry for 2014–2021.*



**Eric V. Anslyn**

*Eric V. Anslyn is the Welch Regents Chair of Chemistry at the University of Texas at Austin. His research spans the areas of sensor development, functional materials, and mechanistic organic chemistry. He has won several research awards in the areas of supramolecular chemistry and physical organic chemistry, as well as many teaching awards from The University of Texas at Austin.*



### 1.1 Chemical weapons convention (CWC) and organization for the prohibition of chemical weapons (OPCW)

Production, stockpiling, transfer, and use of chemical weapons and their precursors are completely prohibited under the arms control treaty, as per the CWC established by the OPCW.<sup>10</sup> The treaty entered into force on 29 April 1997 with the mandate to eliminate an entire category of weapons of WMD within a fixed time frame. At present, 193 States are committed to abiding by the regulation set by the OPCW. The production for research, medical, pharmaceutical, or protective purposes is still permitted but if produced in more than 100 grams, it must be reported to the OPCW.<sup>11</sup> In 2013, the organization received the Noble Peace Prize for its legislative efforts in the non-proliferation of chemical weapons. The chemicals governed under the CWC are divided into three Schedules – Schedule 1, Schedule 2, and Schedule 3 (Table 1).<sup>12</sup> Schedule 1 substances are chemicals that can be used as chemical weapons or used in the production of chemical weapons and have no or very limited additional use. Schedule 2 substances are chemicals that can be used as chemical weapons or used in the production of chemical weapons but have legitimate small-scale applications outside of CWs. Schedule 3 substances are chemicals that can be used as chemical weapons or used in the

production/manufacture of chemical weapons, but also have legitimate large-scale industrial uses.

## 2. Chemical warfare agents

The large-scale use of toxic chemicals as weapons first became possible during the First World War (1914–1918).<sup>13</sup> Initially, lachrymators (tear gases), sternutators (an agent used in chemical warfare that causes sneezing, irritation to the nose and eyes, pain in the chest, and nausea), and vomiting agents were used to harass but not kill the enemy.<sup>14</sup> During the First and Second World Wars, poisonous chemicals were screened for their potential to be used as a weapon. Between these periods, several compounds were synthesized, or isolated from natural materials such as ricin, and examined to determine their applicability as a chemical weapon. Post-1945, a major focus was on the research and development of novel CW agents, with the extensive evaluation of their biochemistry, toxicology, and pharmacology. Despite these efforts, only a few candidates were identified that satisfied requirements, including acceptable production costs as well as appropriate physical, chemical, and toxicological properties. In total, 70 different CW agents were prepared, stockpiled, and weaponized in liquid, gas, or solid form.<sup>15</sup> The stockpiling of CW agents is largely carried out in the form of unitary agents, and sometimes in binary forms.<sup>16</sup> Unitary weapons are lethal chemical munitions that produce a toxic result in their existing state, such as GA, GB, SM, *etc.* Unitary agent chemicals are produced in a plant, loaded into a missile, and stored in a ready-to-use fashion. These munitions are highly toxic, and therefore, the storage, handling, and deployment of these chemicals need to be performed with extreme caution. Agents in the active form are also highly corrosive, thus posing the risk of leakage. Unlike unitary weapons, binary weapons involve nontoxic precursors that are mixed with the nerve agents and can be loaded into munitions just before deployment.

Chemical agents are ordered into several categories according to their physiological mode of action, tactical purpose, or chemical structure.<sup>17</sup> Based on lethality, they have also been classified as lethal CWAs and non-lethal CWAs. The categories are as follows:

- i. Nerve agents
- ii. Blister agents/vesicants
- iii. Blood agents
- iv. Choking agents or pulmonary agents
- v. Riot-control agents or Harassing agents
  - (a) Tear agents
  - (b) Vomiting agents
  - (c) Malodorants
- vi. Psychomimetic agents or incapacitating agents
- vii. Toxins

Nerve agents, blister agents, and choking agents are generally electrophilic with varied reactivity and selectivity towards biological nucleophiles. They have been found to react with water to form toxic metabolites (*e.g.*, HCl) and react with SH,

**Table 1** Concise list of the CWC-related scheduled chemicals

#### Schedule 1 substances

- 1 Sarin: *O*-Isopropyl methylphosphonofluoridate
- 2 Soman: *O*-Pinacolyl methylphosphonofluoridate
- 3 Tabun: *O*-Ethyl *N,N*-dimethyl phosphoramidocyanidate
- 4 VX: *O*-Ethyl *S*-2-diisopropylaminoethyl methyl phosphonothiolate
- 5 Sulfur mustards
  - I. Mustard gas: Bis(2-chloroethyl)sulfide
  - II. 2-Chloroethylchloromethylsulfide
  - III. Bis(2-chloroethylthio)methane
  - IV. Sesquimustards:
  - V. Bis(2-chloroethylthiomethyl)ether
  - VI. Bis(2-chloroethylthiomethyl)ether
- 6 Lewisites:
  - I. Lewisite 1: 2-Chlorovinylchloroarsine
  - II. Lewisite 2: Bis(2-chlorovinyl)chloroarsine
  - III. Lewisite 3: Tris(2-chlorovinyl)arsine
- 7 Nitrogen mustards:
  - I. HN1: Bis(2-chloroethyl)ethylamine
  - II. HN2: Bis(2-chloroethyl)methylamine
  - III. HN3: Tris(2-chloroethyl)amine
- 8 Saxitoxin
- 9 Ricin
- 10 Novichok nerve agents
- 11 Carbamates (quaternaries and bisquaternaries of dimethylcarbamoyloxypyridines)

#### Schedule 2 substances

- 1 Amiton (VG): *O,O*-Diethyl *S*-[2-(diethylamino)ethyl]phosphorothiolate
- 2 PFIB: 1,1,3,3,3-Pentafluoro-2-(trifluoromethyl)-1-propene
- 3 BZ: 3-Quinuclidinyl benzilate

#### Schedule 3 substances

- 1 Phosgene: carbonyl dichloride
- 2 Cyanogen chloride
- 3 Hydrogen cyanide
- 4 Chloropicrin: trichloronitromethane





OH, NH, and CO<sub>2</sub> amino acid residues in proteins to form protein adducts and inhibit biological function. Similarly, the mustard agents, like sulfur mustard and nitrogen mustard, have been shown to react with NH and –P(O)O– residues in DNA.

## 2.1 Nerve agents

Nerve agents, also called nerve gases, are extremely toxic chemicals that act primarily by inhibiting the enzyme acetylcholinesterase (AChE) in both the peripheral and central nervous systems.<sup>18,19</sup> This leads to an excess of the neurotransmitter acetylcholine (ACh) at synaptic junctions. Ultimately, death occurs due to asphyxiation or cardiac arrest. This can happen in minutes to hours depending on the route of exposure and the amount absorbed. The primary routes of exposure are ingestion, inhalation, and absorption through the skin. After exposure, the victim may experience involuntary salivation, lacrimation, urination, defecation, gastrointestinal pain, and vomiting. There are two main classes of nerve agents. The first is G-series agents: tabun (GA), sarin (GB), soman (GD), and cyclosarin (GF) (Fig. 1(A)).<sup>20</sup> G-series was named after the German scientist Gerhard Schrader, who was the first to synthesize such agents. He is now known as ‘the father of nerve agents’.<sup>21</sup> In 1936 the first nerve agent GA (tabun) was developed. Subsequently, in 1939 Sarin was prepared, and then in 1944 GD (soman) emerged. Then in 1949 the somewhat obscure GF (cyclosarin) was developed, and in the 1950s VX came into existence.<sup>22</sup> V-series agents are the second family of nerve agents, which include VE, VG (amiton), VM, VR, and VX (Fig. 1(B)). VX is the most studied nerve agent in this series. V stands for *victory*, *venomous*, or *vicious*, and VR stands for *Russian VX*. G-series agents are known as non-persistent, whereas the V-series are persistent because of their low vapor pressure. Sarin and VX are the chemical agents that were largely fielded in ammunition, rockets, artillery shells, airplane spray tanks, and landmines during war scenarios.

Nerve agents were originally produced during the search for insecticides and because of the identified potent toxicity, they were subsequently evaluated for military use. These agents are generally identified by both, their chemical names and their two-letter NATO codes. The second letter is the specific identifier for each compound: GA (tabun), GB (sarin), GD (soman), and GF (cyclosarin).<sup>23</sup> To mimic the physico-chemical characteristics of G-series and V-series nerve agents, various nerve agents' simulants have also been identified which are presented in Fig. 1(C).

All nerve agents are colorless and volatile liquids in their pure state at standard temperature and pressure. Their high volatility makes them a powerful weapon. G-agents produce a fruity odor and V-agents an amine odor. Sarin is soluble and soman is sparingly soluble in water, whereas VX and tabun exhibit intermediate solubility. Upon nerve agent exposure, generally, a combination of drugs having a complementary mode of action are administered. The combination treatment required pre-treatment with pyridostigmine bromide (which protects against irreversible inhibition of enzymes), and the use of atropine and oximes, such as pralidoxime chloride as post-exposure therapy. Derived from animal studies, human toxicity for nerve agents is estimated to range from 80 µg kg<sup>−1</sup> (tabun) to 7 µg kg<sup>−1</sup> (VX) for the LD<sub>50</sub> by i.v. administration, percutaneous LD<sub>50</sub> values were estimated to be 1000 mg for tabun, 1700 mg for sarin, 100 mg for soman, and 10 mg for VX, respectively, for a 70 kg person (Table 2).<sup>24</sup> An additional feature that exists in all nerve agents is the presence of chirality (asymmetry) around the phosphorus atom.<sup>25</sup> Studies show that the P(–)-stereoisomers of sarin and soman inhibit AChE several orders of magnitude better than the P(+)-stereoisomers. (–)-VX is only eight times more lethal than the (+)-stereoisomer. Hence, despite the modest selectivity of (–)-tabun towards the inhibition of AChE, this isomer is substantially more toxic in mice than (+)-tabun.<sup>26</sup> Fig. 2 portrays the normal enzymatic function of the AChE enzyme, as well as the mechanism of toxicity for the nerve agent, the aging process, and reactivation of the enzyme.

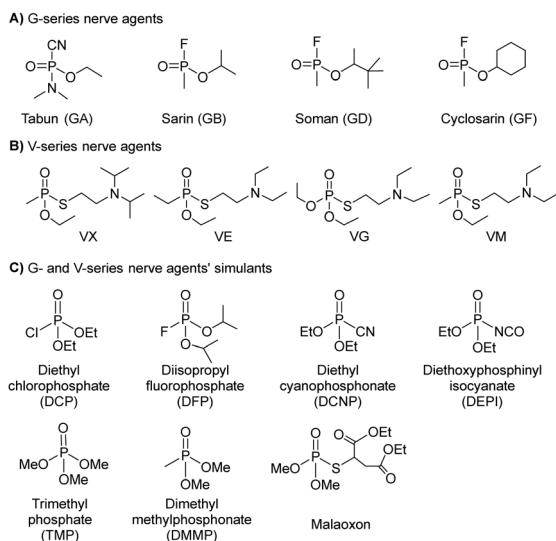


Fig. 1 Chemical structures of various G-series and V-series nerve agents and their simulants.

## 2.2 Novichok agents

The three recent assassination attempts, one on Sergei Skripal and his daughter, Yulia in the UK in the March 2018,<sup>27</sup> then three months later on Charlie Rowley and Dawn Sturgess, two UK nationals,<sup>28</sup> and very recently on Alexei Navalny of Russia in

Table 2 Toxicological data of key CW agents

Chemical agents	Toxicities in LD <sub>50</sub> (mg kg <sup>−1</sup> )	Toxicities in LCt <sub>50</sub> (mg min m <sup>−3</sup> )	IDLH (mg m <sup>−3</sup> )
Sulfur mustard (SM)	100	900	0.7
Nitrogen mustard (HN3)	10	1500	0.003
Lewisite (L)	30	1400	0.1
Tabun (GA)	21.42	70	0.1
Sarin (GB)	24.28	35	0.1
Soman (GD)	0.71	35	0.05
Cyclosarin (GF)	0.14	35	0.05
VX	0.071	15	0.003





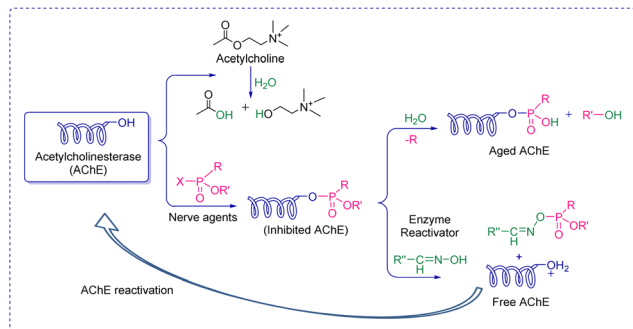


Fig. 2 Schematic presentation of acetylcholine enzyme's function, inhibition, aging, and reactivation.

2020,<sup>29</sup> have sparked significant interest from the international community to further understand the relatively new class of nerve agents known as Novichoks (the Russian word for 'new-comer'). Novichok agents (Fig. 3), also known as "N-series" agents, are organophosphorus compounds, similar to sarin and VX. They also inhibit the enzyme AChE.<sup>30</sup> It is believed that these agents were secretly developed by the former U.S.S.R in 1970 during a Cold War-era weapons program (code-named FOLIANT). The program aimed to develop nerve agents that could not be stopped by chemical protective gear. They were also intended to be safer to handle, undetectable by conventional analytical tests, and safer to store and use than previous generations of CWAs. Novichok agents are considered more potent (10 times greater) than VX and can be applied in unitary and binary forms. Unitary agents were synthesized and used much like sarin, soman, and VX; *i.e.*, the chemical structures were altered during production to have maximum potency. In general, the precursors are designed to be significantly less hazardous than the actual agents. Therefore, production, handling, and transportation are easier. A significant drawback of Novichok agents is their low stability in the environment.

The OPCW recently concluded that there was insufficient information about the chemical structure and the toxicological property of Novichok agents. Until 2020, these agents were not formally listed by the CWC, primarily out of fear that their inclusion would reveal their exact chemical structures and this knowledge might be used by some countries or terrorist

organizations to produce and use them. As of 2021, the OPCW has included them in their list of Schedule 1 chemicals.<sup>31</sup> There is no mutual consensus on the nomenclature of these mysterious agents. However, their precursors are named Novichok? Novichok-5, and Novichok-7. Their reaction products are referred to by the symbol "A" with a three-digit number (hence the name "A-series compounds"). The "Novichok" designation refers to the binary form of the agent, with the final compound being referred to by its code number (*e.g.*, A-232). The first developed agent was named Substance 33, which was very similar to VX (also known as VR; Russian VX), and it became a prototype for the series of Novichok agents. Subsequently, unitary chemical weapons were synthesized and the examples include A-230, A-232, and A-234.

From a chemistry perspective, they are organophosphorus compounds containing dihaloformamide and oxime groups (phosphorylated/phosphonylated oximes). These agents are highly toxic because the phosphorylated oximes are relatively unstable under normal conditions and the =N–O– bond readily undergoes hydrolysis, resulting in the so-called aged form of AChE. Once aging has occurred, the enzyme is irreversibly inactivated (Fig. 2). A hypothesis somewhat supported by the aging half-time of A-230 which is similar to that observed in soman, *i.e.*, 2–4 min. The treatment for poisoning by these mysterious nerve agents is similar to that of other nerve agents. The current treatment is symptomatic therapy (combination of an anticholinergic agent and anticonvulsant) or administration of so-called bioscavengers, such as butyrylcholinesterase. While drugs such as obidoxime, pralidoxime and HI-6 are designed to bind to free nerve agents in the patient's circulation and prevent the inhibition of AChE in tissue. This means detection needs to be accurate and rapid to facilitate administration of the required treatment before it is too late.

### 2.3 Carbamates

Carbamates (CBs) are another class of CW agents (fourth generation CW agents) that has recently been included in the list of Schedule 1 chemicals by the OPCW along with Novichok agents.<sup>32</sup> Carbamates are *N*-methyl carbamates derived from carbamic acid. Although, carbamic acid is unstable at room temperature, substitution using different alkyl/aryl, arylalkyl, and substituted alkyl/aryl groups at the amino as well as carboxylic groups of carbamic acid enhances the stability.<sup>33</sup> CBs are used extensively as pesticides, as tranquilizers, and in the treatment of myasthenia gravis, glaucoma, anticholinergic poisoning, and paroxysmal atrial tachycardia.<sup>34</sup>

Earlier, these agents were not covered by the CWC because they had never been used as chemical weapons, therefore they were initially omitted from the list of Schedule 1 chemicals. CBs are originally insecticides comparable to OP insecticides and exhibit similar toxicological effects to OP poisoning by causing carbamylation of acetylcholinesterase at neuronal synapses and neuromuscular junctions.<sup>35–38</sup> The agents contain one or more quaternary amine centers that help them to penetrate neuromuscular junctions. They induce toxicity typically in less than 24 hours leading to miosis and rhinorrhea as

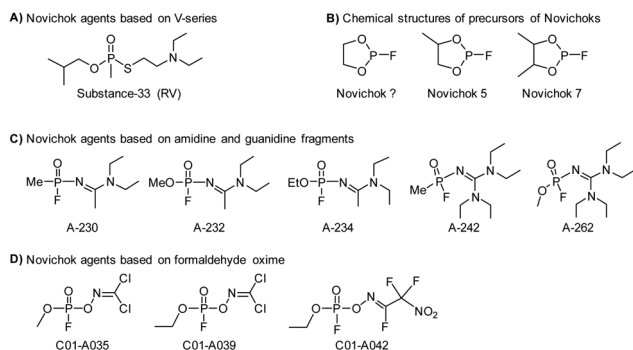
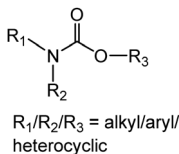
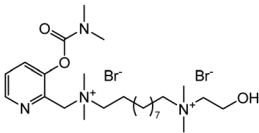
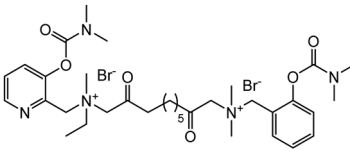


Fig. 3 Chemical structures of various Novichok agents and their precursors.



Table 3 General classification of carbamates

CW agent	Class	General nomenclature	Specific example
 <p>General structure of carbamates</p>	Quaternaries of dimethylcarbamoyloxy pyridines	1-[ <i>N,N</i> -dialkyl ( $\leq C10$ )- <i>N</i> -( <i>n</i> -(hydroxyl, cyano, acetoxy)alkyl ( $\leq C10$ )) ammonio]- <i>n</i> -[ <i>N</i> -(3-dimethyl carbamoyloxy- $\alpha$ -picolonyl)- <i>N,N</i> -dialkyl ( $\leq C10$ ) ammonio]decane dibromide ( $n = 1-8$ )	 <p>1-[<i>N,N</i>-dimethyl-<i>N</i>-(2-hydroxy)ethyl ammonio]-10-[<i>N</i>-(3-dimethylcarbamoyloxy-<math>\alpha</math>-picolonyl)-<i>N,N</i>-dimethylammonio]decane dibromide</p>
General structure of carbamates	Bisquaternaries of dimethylcarbamoyloxy pyridines	1, <i>n</i> -Bis[ <i>N</i> -(3-dimethylcarbamoyloxy- $\alpha$ -picolonyl)- <i>N,N</i> -dialkyl ( $\leq C10$ ) ammonio]-alkane-(2, ( <i>n</i> -1)-dione) dibromide ( $n = 2-12$ )	 <p>1,10-Bis[<i>N</i>-(3-dimethylcarbamoyloxy-<math>\alpha</math>-picolonyl)-<i>N</i>-ethyl-<i>N</i>-methylammonio]decane-2,9-dione dibromide</p>

primary indications of exposure at low levels. High concentrations of CBs result in vomiting, urination, or defecation, and finally loss of consciousness and convulsions in just 30 seconds, followed by cessation of breathing and flaccid paralysis. Chemically, CB nerve agents are mono- and bis-quaternaries of dimethyl carbamoyloxy pyridines which are tabulated above (Table 3). Nerve agents based on CBs are stable in water but get rapidly hydrolyzed at high pH. Furthermore, basic peroxides also rapidly detoxify CBs.

## 2.4 Blister agents

Blister agents or vesicants are substances that produce painful skin vesicles/blisters and the eyes, lungs, and mucous membranes are damaged. Symptoms can be instantaneous or can appear several hours following exposure. They have been placed in three major categories: mustard agents, *e.g.*, sulfur mustard (H, HD, HT) and nitrogen mustard (HN-1, HN-2, HN-3); arsenicals, *e.g.*, Lewisite (L); and halogenated oximes, *e.g.*, phosphine oximes (CX) (Fig. 4(A)–(C)).

**2.4.1 Sulfur mustard.** The term sulfur mustards (Fig. 4(A)) is very broad and technically exists in various forms and names. Vacuum distilled sulfur mustard with 97% purity is called distilled mustard (HD) and is chemically known as bis(2-chloroethyl) sulfide. It is popularly known as mustard gas.<sup>39</sup> It was first synthesized in 1822 by Despretz and used in World War I (1917) in the form of an artillery bombardment against the British front by the German military.<sup>40</sup> *O*-Mustard (T)/bis-(2-chloroethylthioethyl) ether and sesquimustard (Q) are the advanced forms of sulfur mustards that are three times and five times more toxic than HD, respectively. Each type of sulfur mustard has a low vapor pressure. As a result, it cannot be used in sub-zero temperatures. To use SM in cold weather or high-altitude areas, it is mixed with Lewisite (L) to lower the freezing point. This agent is referred to as Agent HL. These attributes

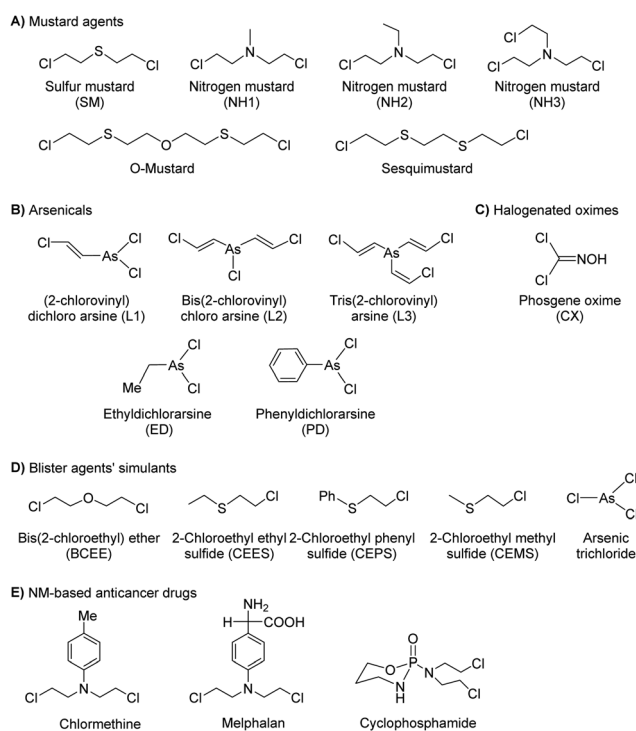


Fig. 4 Chemical structures of various blister agents, their simulants, and NM-based drugs.

make sulfur mustard a potentially dangerous chemical agent. Most of the discussion centered on sulfur mustards in this review will be focused on distilled sulfur mustard, which is conventionally abbreviated as SM.

SM has been the most extensively used blister/vesicant CWA over the past century.<sup>41</sup> Upon exposure, it causes painful blisters and vesicles, hence its name. Symptoms occur within



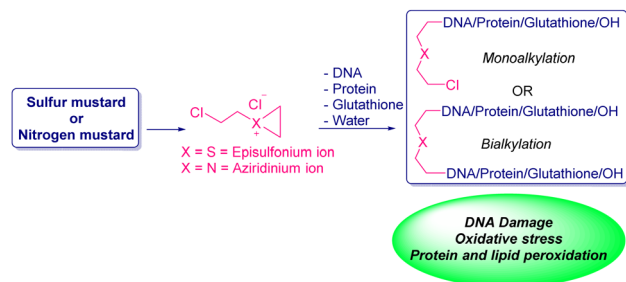


Fig. 5 Basic schematic of the mechanism for toxicity induced by blister agents, such as sulfur mustard.

2–24 h after exposure. Its toxicity lies in its ability to react with DNA, protein, and other nucleophilic biological fluids *via* the episulfonium cation, which is facilitated by the presence of water or other polarizing media.<sup>42</sup> In DNA, it acts as a bifunctional alkylator and reacts at the N7 of guanine and the N3 of adenine at a ratio of 66% and 17%, respectively. The remaining 17% reacts as a cross-linked adduct involving two guanines on the same or complementary sugar-phosphate strands (Fig. 5).<sup>43</sup> Due to the extreme toxicity, high persistence, and ease of manufacture, it was extensively used in both World Wars and has been regarded as ‘King of Warfare Gases’ with the highest military significance.<sup>44</sup>

**2.4.2 Nitrogen mustard.** Like SM, nitrogen mustard (Fig. 4(A)) is another bialkylating agent, which originated from sulfur mustard and was developed to be used as a chemical weapon.<sup>45,46</sup> However, due to its poor chemical stability and relatively low toxicity, it was repurposed and has proven as an effective anticancer agent over the last 80 years. To date, it is still used clinically and is continually being optimized with targeted modifications (Fig. 4(E)).<sup>47</sup> The toxicity of NM is the result of its ability to form an electron-deficient cyclic intermediate aminium ion (aziridinium ring) that can react *in vivo* with nucleophilic components of biologically important species. Inevitably, the covalent interactions result in the inhibition of specific processes (e.g., enzyme and DNA replication).<sup>48</sup> Cytotoxicity includes DNA binding and cross-linking, thereby preventing DNA replication and cell proliferation.<sup>49</sup> To overcome the poor selectivity and severe toxicity of the basic chlormethine scaffold, researchers have found that introducing an aromatic moiety reduces the electrophilicity/toxicity of nitrogen mustard (Fig. 4(E)). For example, chlorambucil is now used clinically for the treatment of ovarian cancer.<sup>50</sup> The timeframe of symptom development after exposure to SM and the nitrogen analogs is comparable. Available information regarding the toxicity of nitrogen mustards is less extensive than that of sulfur mustard. However, the order of relative toxicity is as follows: HN3 > HN1 > HN2. This is attributed to the fact that NH3 possesses the maximum number of chloroethyl groups (three) and NH1 is more lipophilic than NH2 (Fig. 4).

**2.4.3 Lewisite.** Lewisite (Fig. 4(B)), a powerful vesicant and sometimes called ‘Dew of Death’, was initially manufactured in 1918 by the USA and Japan to create a more effective blister agent than SM.<sup>51</sup> In the human body, the general routes of

entry of Lewisite are ocular, percutaneous, and inhalation. Additionally, the presence of an arsenic core makes it a probable carcinogen.<sup>50</sup> Lewisite is generally found as *cis*- and *trans*-isomers, with the standard ratio being 10 : 90.<sup>52</sup> As mentioned earlier, Agent HL was developed for use in the cold weather or at high-altitude and is a mixture of mustard gas (HD) and Lewisite (L), which British anti-Lewisite (BAL), regarded as dimercaprol, is a well-known antidote for Lewisite.<sup>53</sup> Lewisite is prepared by the reaction between arsenic trichloride and acetylene in the presence of a suitable catalyst (e.g., anhydrous aluminum chloride). This reaction produces a mixture of 2-chlorovinylarsonous dichloride (Lewisite 1), bis(2-chloroethenyl)arsinous chloride (Lewisite 2), and tris(2-chlorovinyl)arsine (Lewisite 3).<sup>54</sup> Lewisites are generally stable but exposure to moisture results in quick hydrolysis to 2-chlorovinylarsenious acid and a decrease in toxicity. Under mild basic conditions, hydrolysis of Lewisite results in the formation of Lewisite oxide. When exposed to a strong base, Lewisites decompose to yield acetylene and trisodium arsenate (Na<sub>3</sub>AsO<sub>4</sub>).<sup>55</sup> Using the latter reaction, the concentration of Lewisite is quantified by measuring the amount of acetylene generated.<sup>56</sup>

**2.4.4 Phosgene oxime.** Phosgene oxime (CX) (Fig. 4(C)), also known as urticant or nettle agent, was first produced in 1929 as a chemical weapon. However, it has never been used on the battlefield.<sup>57</sup> CX does not cause blisters but works as a powerful irritant that exerts instant and almost unbearable pain on exposed skin and eyes. The liquid CX is corrosive to the skin; hence, it is also known as a corrosive agent. These agents tend to incapacitate rather than kill, although, upon severe exposure, death can occur because of secondary complications, such as bacterial infections, shock, or multi-organ failure. Because the antidote for CX does not exist, the treatment consists of removing the agent from the body as early as possible and providing supportive medical aid in a hospital setting. Unfortunately, it is one of the least studied chemicals and its mechanism of action is not fully understood. Like phosgene, it interacts with sulfhydryl and amine groups to produce widespread and devastating effects. The ease of its synthetic method, devastating effects, and fast penetration through clothes and rubber make it a dangerous chemical with both military and terrorist potential. It is mostly categorized with vesicant agents but is not a true vesicant as it does not produce blisters. Despite no confirmed use of CX, an FBI investigation recently revealed its presence inside a Lawton home in Oklahoma, USA.<sup>58</sup>

## 2.5 Blood agents

The blood agents in this category are mainly hydrogen cyanide (AC), cyanogen chloride (CK), and arsine (Fig. 6(A)). They are placed on the list of Schedule 3 toxic chemicals, per the CWC.<sup>59</sup> These agents are named based on their effect on the oxygen-carrying capacity of RBCs. Hydrogen cyanide was used in World War I and II as a chemical weapon by the French, United States, and Italy. In addition to its use as a CWA, hydrogen cyanide is used in huge industrial processes for fumigation, electroplating, mining, and chemical synthesis.<sup>60</sup> Among this class





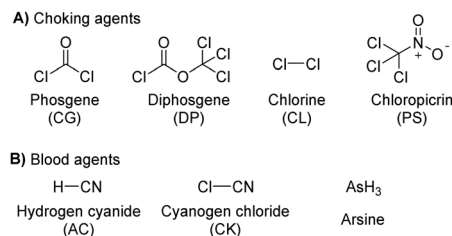


Fig. 6 Chemical structures of various (A) choking and (B) blood agents.

of CWAs, these are the least toxic agents, which mainly affect the retina and optic nerve leading to vision failure at higher doses. The toxicity of these agents is due to the affinity of the  $\text{CN}^-$  ion for the heme a3 moiety of cytochrome *c*-oxidase found in mitochondria. This inhibits the electron transfer chain and leads to cellular hypoxia.<sup>61</sup> Due to the acidity of gastric fluid ( $\text{pH} \sim 1$ ), substantial amounts of HCN can be released when cyanide salts (KCN and NaCN) are ingested.<sup>62</sup>

## 2.6 Choking agents

Choking agents are also known as lung-damaging agents or pulmonary agents that produce toxic inhalational injury as they attack lung tissue and primarily cause pulmonary edema.<sup>63</sup> These agents pose a real threat to military and civilian personnel when used as chemical weapons. Choking agents include phosgene (CG), diphosgene (DP), chlorine (CL), and chloropicrin (PS) (Fig. 6(B)).<sup>64</sup> Some of these chemicals (chlorine and phosgene) are produced in massive quantities for industrial purposes. The pulmonary agents, particularly phosgene and oxides of nitrogen, are relatively non-reactive and insoluble in aqueous solutions; hence, they readily penetrate respiratory bronchioles and alveoli. As expected, acylation reactions of biological proteins cause significant damage that ultimately leads to pulmonary edema.<sup>65</sup> The symptom occurs in 20 minutes to 24 hours depending on the exposure dose and physicochemical properties of the agent.<sup>66</sup>

## 2.7 Toxins

Toxins, such as ricin and saxitoxin (STX) (Fig. 7), are extremely toxic chemicals produced by living organisms, including animals, plants, and microbes. Therefore, these are categorized as both chemical and biological weapons.<sup>67,68</sup> Their production, stockpiling, and use are prohibited under both the CWC and BWC (Biological Weapons Convention). Toxins are highly toxic natural products found in both proteinaceous and chemical forms. Among the list of various natural bioagents, ricin and

STX have been weaponized and are included as Schedule 1 substances by the CWC.<sup>69</sup> Due to their availability from natural sources, they can be used as domestic chemical weapons for terrorist activities. However, the relative ease of accessibility for ricin (from Castor beans) as compared to STX (either from natural sources or chemical synthesis) makes ricin a greater threat.

**2.7.1 Saxitoxin.** Saxitoxin is one of the most toxic non-protein-based compounds. It acts as a potent neurotoxin and paralytic shellfish toxin.<sup>68,70</sup> Generally, it is ingested by humans through the consumption of shellfish contaminated by a variety of toxic algal species, such as cyanobacteria and dinoflagellates. When it is accumulated in the body, it leads to paralytic shellfish poisoning (PSP). The acute toxicity results from its ability to deactivate ionic conductance through the voltage-gated sodium channel.<sup>71</sup> Subsequently, action potentials are terminated and signal transmission between neurons is inhibited. This leads to respiratory paralysis and death in humans. Chemically, STX can be considered a biguanylated diamine incorporated into five- and six-membered rings with three stereocenters. STX, due to its extremely low  $\text{LD}_{50}$ , is the only marine toxin declared as a chemical weapon by the CWC.<sup>31</sup> Shellfish are regularly monitored for PSP toxins using techniques such as mouse bioassays (a benchmark technique)<sup>72</sup> and HPLC methods.<sup>73</sup> STX lacks any UV-active group; therefore, it is oxidized by  $\text{H}_2\text{O}_2$  to obtain a fluorescent derivative (oxidized-STX) (Fig. 7). This can be isolated by separation on an HPLC column.

**2.7.2 Ricin.** Ricin<sup>74</sup> is a cytotoxic protein present in the seeds of the castor bean plant *Ricinus communis*. This protein toxin consists of A and B chains joined together by a single disulfide bond.<sup>75</sup> Chain A results in ribosome inactivation. This inhibits protein synthesis, which leads to cell death. In contrast, chain B possesses cell-surface targeting galactose/*N*-acetylgalactosamine-binding lectin. Chain B is responsible for binding to galactosyl residues on the cell surface and facilitates the delivery of the ricin A chain into the cell. Both chains are mandatory for the high toxicity of ricin. Its high toxicity and ease of isolation from Castor beans make it a prominent threat as a biological weapon.<sup>76</sup>

## 2.8 Non-lethal chemical weapons

Non-lethal weapons (NLWs) or less-than-lethal weapons are designed to incapacitate personnel while minimizing fatalities, mitigating injury, and preventing any unwanted damage to structural property and the surrounding environment.<sup>77</sup> For these reasons, they may be considered appropriate for riots and civilian peacekeeping operations, which are intended to produce temporary incapacitation of an individual. NLWs should have a rapid onset of incapacitating effects, easy dissemination and decontamination, long shelf-life, low cost, and no short- or long-term adverse effects on heterogeneous populations. These agents can be grouped as riot control agents, incapacitants, calmatives, and malodorants.

**2.8.1 Riot control agents.** Riot control agents (RCAs), sometimes referred to as harassing agents, tear agents, and

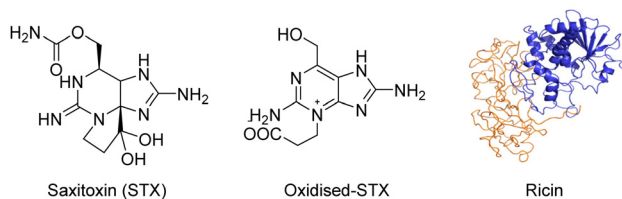


Fig. 7 Chemical structures of saxitoxin, oxidized-saxitoxin, and ricin.



lacrimators, are intended to momentarily disable victims by causing intense irritation of the mucous membranes, eyes, and skin.<sup>78</sup> This can produce sensory irritation and incapacitating physical effects that rapidly disappear within a short time. Initially, these chemicals were not listed as Schedule 1 chemicals. However, the use of riot control agents as a method of warfare is prohibited by the CWC. As a result, these compounds are now classified as CW agents by the CWC.<sup>79</sup> There are three types of RCAs: lachrymators (tear agents), sternutators, and vomiting agents.

**2.8.2 Tear gas or lachrymators.** Lachrymators are intended to cause incapacitation rather than serious injury or death.<sup>77</sup> If death does occur, it is due to pulmonary edema. These are broadly designated into four chemicals: diphenylchlorarsine (DA), diphenylcyanoarsine (DC), Adamsite (DM), and triphenylarsine (TPA) (Fig. 8).<sup>77</sup> More recently, oleoresin, a capsicum-based agent, has been used primarily by law enforcement and for personal protection.<sup>80</sup> Typically, ocular and respiratory tract irritation occurs within 20–60 seconds of exposure. The efficacy of these agents is measured by the threshold for irritation as per the falling sequence CN > CS > OC.<sup>81</sup>

**2.8.3 Vomiting agents or sternutators.** Vomiting agents or sternutators are chemical agents designed to induce vomiting. Prolonged continuous exposure can be lethal to an individual (Fig. 8).<sup>82</sup> However, individuals exposed to short-term high doses should recover in several hours. These agents were employed for the first time during WWI. They affect the mucous membranes to produce congestion, coughing, sneezing, and eventually nausea. The compounds included in this class of compounds are diphenylchlorarsine (DA), Adamsite (DM), and diphenylcyanoarsine (DC).<sup>83</sup>

**2.8.4 Incapacitating or psychotomimetic agents.** Incapacitants are also considered to be non-lethal chemical agents as they are designed to temporarily disable an individual's physical and mental capabilities.<sup>84</sup> The effect of these agents may persist for several hours or days after exposure, hindering the enemy's effectiveness in battle. Importantly, they are designed

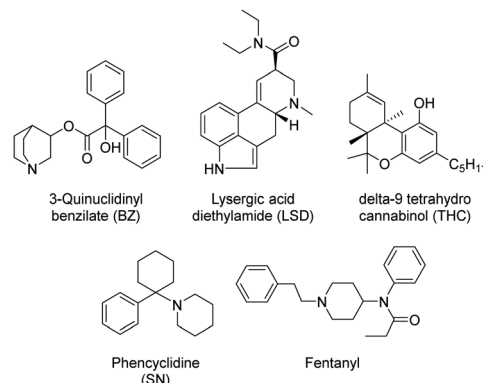


Fig. 9 Chemical structures of various psychotomimetic agents.

to not cause serious bodily harm, and the individual should recover soon after exposure. Several agents were considered for this purpose, including 3-quinuclidinyl benzilate (BZ), atropine, scopolamine, lysergic acid diethylamide (LSD), phenothiazines, and delta-9 tetrahydrocannabinol (THC) (Fig. 9).<sup>84</sup> BZ offers several advantages over atropine and scopolamine as a psychotomimetic agent because of its high safety profile and CNS anticholinergic potency.

**2.8.5 Calmative/sedative agents.** Calmative agents (a military term, not a scientific term) or sleep-inducing drugs are a class of psychoactive compounds that exert effects ranging from unconsciousness to hallucinations.<sup>82</sup> These agents are mainly used for law enforcement purposes. They have several key features, including ease of administration, fast onset of action, short duration, uniform dose-response, reversible action by antidote, and rapid metabolism. These agents also exhibit no long-lasting, toxicity-related side effects. Examples include benzodiazepines, alpha-adrenergic receptor agonists, dopamine D3 receptor agonists, selective serotonin reuptake inhibitors, opioid receptors, and neuroleptic anesthetics.<sup>85,86</sup>

**2.8.6 Malodorants.** Malodorants (obnoxious/foul-smelling compounds) are believed to be permitted under the CWC as riot control agents. These are chemicals with a very strong and intolerable odor that can influence crowds without exerting the toxic effects of tear agents and vomiting agents.<sup>87</sup> Malodorants affect behavior and act as sensory irritants, similar to other RCAs, by activating the trigeminal nerve. Popular examples are skatole and skunk spray. These compounds are usually composed of a minimum of two ingredients: the malodorant compound and a carrier liquid.

**2.8.7 Other potential chemical warfare agents.** It might come as a surprise, but several substances not included on the CWC Schedule 1 chemical list can be used as chemical weapons. This is an ongoing issue with new chemicals continually being developed each year in standard laboratory research.<sup>88</sup> Some examples are carbamates (quaternaries and bisquaternaries of dimethylcarbamoyloxypyridines), new organophosphates, dioxin, and perfluoroisobutene (PFIB) (Fig. 10). Attempts have also been made to synthesize the hybrid of OP

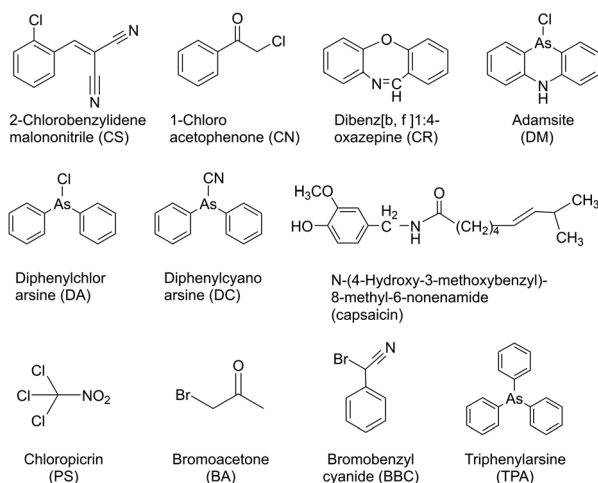


Fig. 8 Chemical structures of various riot control agents (tear and vomiting agents).



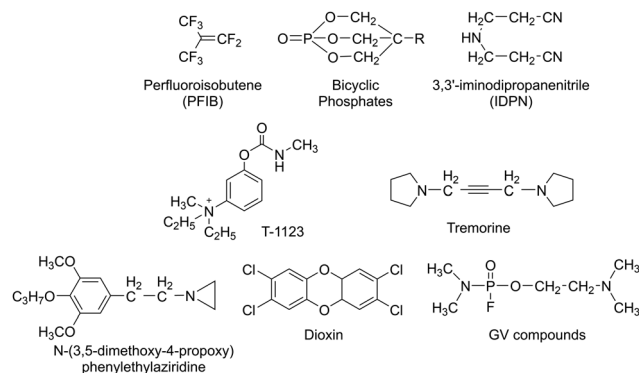


Fig. 10 Chemical structures of other probable CW agents.

compounds, described as 2-dialkylaminoalkyl-(dialkylamido)-fluorophosphates. They have structural similarities to G-series (*e.g.*, sarin, soman, tabun), V-series (*e.g.*, VX), and GV compounds (Fig. 10).<sup>89</sup> Intoxication with these chemicals has been identified to have the same effects as known nerve agents. The conventional treatment of the victims of these chemicals with atropine and reactivators (oxime-based drugs) will be difficult because of the absence of the ability to reactivate, because of the fast aging process.

### 3. Instrumental and chemical detection techniques: present status

The rapid identification of a CW agent is crucial to ensure the protection of first responders/emergency medical personnel, as well as for identifying the appropriate treatment for victims. In light of recent CW-related events (*e.g.*, Salisbury, UK),<sup>90</sup> there is increasing interest in developing new and effective instruments and chemical methods for both military and civilian purposes. This is underscored by the commonly seen spread of a CWA from the battlefield/target soldiers to civilian populations. Several types of commercially available military-based equipment exist. These require manual operation or can be fully automated.

Current technologies rely on instrumental and chemical analyses for CWA detection, which can be applied to liquid, vapor, and contaminated solids. The former techniques generally exploit the physical characteristics of the chemical agents to develop the electronic equipment/devices. Considerable progress has been made with physical-electronic systems over the last 50 years. These systems are usually faster and more adaptable, allowing for the detection of other compounds/classes of compounds. The use of wet chemistry requires detection test kits that contain various dyes and enzymatic assays. Physical-electronic (instrumental) detection differs from chemical detection which is usually rather laborious to run. Furthermore, with detection kits, extensive use of (bio)-chemicals can result in logistical difficulties. Due to the reaction design of each test, they may have a short shelf life. However, chemical detection is considered to be more reliable and cost-effective.

#### 3.1 Instrumental techniques/methods

In general, current detection technologies consist of standoff and point detectors.<sup>91</sup> Standoff detection refers to the ability of a detector to spot, evaluate, and identify an agent at a distance, while point detectors can be operated by on-site personnel who have more specific training and safety equipment. Point detectors detect chemical agents from a closer distance. The primary differences between standoff and point detectors are their size, weight, portability, and logistical support requirements. A wide variety of techniques based on standoff and point detection are commercially available and used by the armed forces. These are predominantly based on ion mobility spectrometry (IMS), flame photometry, gas chromatography (GC), and surface acoustic waves (SAW).<sup>92</sup> In addition to this, electrochemical-based detectors<sup>93</sup> and instruments based on techniques including molecularly imprinted polymer (MIP) sensors,<sup>94</sup> biosensors,<sup>95</sup> surface plasmon resonance (SPR),<sup>96</sup> and conductive polymer sensors,<sup>97</sup> *etc.*, are also in the advanced stages of development.

Flame photometry exploits the emission of light from sulfur- and phosphorus-containing compounds in a hydrogen/air flame.<sup>98</sup> These devices are therefore limited to these chemical species. Nevertheless, portable and automated detectors have been developed for on-site (in the field) detection of CW agents. These devices include AP2C, AP4C, and CHASE.<sup>99</sup> IMS is a technique that separates ionized molecules that are then distinguished based on their mass, charge, and mobility in the gas phase.<sup>100</sup> This affords a characteristic plot of the current generated over time for each type of CWA. The intensity of the peaks in the spectrum determines the relative concentration of the agent present. Chemical detectors based on this technology are GID-3, GID-2A, chemical agent monitors (CAMs), lightweight chemical detectors (LCDs), automatic chemical agent detection alarms (ACADAs or GID-4), rapid alarm identification device monitors (RAID series), individual/improved chemical agent monitors (ICAD), ChemPro 100, ICAM, M8A1 ACADA, RAID, and M-90.<sup>101</sup> A classic SAW device consists of a piezoelectric crystal plate coated with a chemically selective polymer and two interdigital transducers.<sup>91,102</sup> Light irradiation passes through a transparent medium, and the chemical species scatters the radiation beam. Differences between the incident beam and scattered radiation are measured. This difference in scattering is dependent upon the chemical structure of the molecule, which allows the identification of each type of CWA. The Joint Chemical Agent Detector (JCAD) and HAZMATCAD use SAW-based technology.<sup>103</sup> SAW devices have advantages over other methods, including their relatively low cost and high detection sensitivity. More importantly, test samples can be analyzed directly in transparent glass vials or plastic bags, which significantly reduces the danger of exposure to first responders. At present Raman-based detectors available are FirstDefender, FirstDefender XL, and Joint Contaminated Surface Detector (JCSJ).<sup>91,104</sup> Infrared-based detectors have been developed and employed for point and standoff detection of CWAs. For these devices, IR radiation





is passed through the test sample. Some radiations are absorbed whilst some are transmitted, resulting in the production of a spectrum with a unique molecular fingerprint for each CWA. The IR-based detectors most commonly used by the military are the M21 detector, Joint Service Lightweight Standoff Chemical Agent Detector (JSLSCAD), MIRAN SapphIRe, AN/KAS-1/1A, TravelIR HCl, HazMat ID, and IlluminatIR.<sup>91,101</sup> IR-based detectors offer the advantage of high sensitivity and fast detection. Additionally, no sample preparation is required. An electrochemical sensor for CWA measures the change in the electrochemical signal caused by the interaction between the agents and an electrode. These sensors show high selectivity for a CWA but have poor sensitivity. An example of a currently available detector is SensorRAE.<sup>105</sup> The CW Sentry Plus device is based on a combination of SAW arrays and electrochemical cells, which detect blood agents and choking agents along with nerve agents and blister agents.<sup>91</sup> Another approach that is similar to electrochemical detection is the use of ion-selective electrodes (ISEs). In the case of sarin and soman, nerve agent hydrolysis generates fluoride ion which is then detected using a fluoride-selective electrode, whereas GA produces a cyanide ion detected using a cyanide-selective electrode.<sup>91</sup> Gas chromatography (GC) coupled with a mass detector (GCMS) can be used to unambiguously detect most organic-based compounds, including CW agents, at very low concentrations (20–200 ng m<sup>-3</sup>).<sup>106</sup> With the advent of more sophisticated analytical capabilities, GC combined with sensitive detectors, such as nitrogen phosphorus detection (NPD), flame photometric detection (FPD), and mass selective detection (MSD), can detect extremely low concentrations of CWAs (10–100 ppb). However, these instruments require a skilled operator and need routine maintenance. Therefore, the use of this on-site has little advantage over off-site analysis, when a chemical incident occurs at a distant site where the mobile lab cannot attend. Commercially available, portable GCMS-based instruments include HAPSITE (Inficon's), the EM series (Bruker's), and MM1 or MM2.<sup>91,101</sup> In general, most of these devices/techniques have several limitations, such as low specificity and the inability to detect each type of CW agent. These detection methods are susceptible to interference and false-positive results. As a result, no single detection system can be relied upon to give an accurate result. Therefore, the recommended method is to simultaneously use two different types of detectors with different analytical techniques to obtain reliable and accurate data.

### 3.2 Chemical methods

The chemical analysis involves measuring the change in color of test materials when they are exposed to the sample in question. This color change corresponds to the detection of a CWA and usually occurs *via* a chemical reaction between the CWA and reagent. This offers good selectivity, sensitivity, speed, ease of operation, and low cost. An important aspect of this strategy is that detection can be visualized by the naked eye. No specialized instruments need to be used, making this strategy less sophisticated and less expensive. The most

common approaches use detector papers/tickets, detector tubes, and detection kits.<sup>91,101</sup> These rapid detection kits have been employed by the military for several decades owing to being the fastest, cheapest, lightest, and simplest method for field use. Suspect liquid droplets or aerosol are typically evaluated using detector papers, whereas detector tubes and kits have been developed for evaluating gaseous CWAs and water samples, respectively. Detector papers/strips that are commercially available include M8 and M9, which produce different colors on exposure to liquid CW agents. Commercial examples of detection tubes, include Dräger tubes and residual vapor detection (RVD) kits. Where the detection reagents are impregnated into silica gel, which is supported on a glass tube. The test sample is passed through the dyes' impregnated silica using a handheld suction pump. If a CWA is present, a color change is observed.<sup>107</sup> Various types of M256 and Agentase chemical agent detection kits for military use are commercially available. The U.S. Army recognized Agentase sensors in 2004 as one of the greatest army inventions of 2003. In these kits, nerve agents impart a blue color by inhibiting a butyrylcholinesterase-mediated reaction cascade (Fig. 11(A)).<sup>108</sup> For SM detection, the reaction between 4-(4-nitrobenzyl) pyridine, **3** and SM is exploited. Heating the sample at 80 °C followed by treatment with sodium hydroxide results in a change from colorless to blue, which enables the identification of SM (Fig. 11(B)).<sup>109</sup> In the case of blood agents, the analyte reacts with mercury chloride to yield hydrogen chloride (HCl). This induces a color change for pH-sensitive dyes, such as methyl red or thymol blue.<sup>110</sup> For the detection of cyanogen chloride, silica gel is impregnated with 4-benzylpyridine, **4**, and barbituric acid (yellow). The presence of cyanogen chloride causes a cascade of reactions that affords a final pink-colored product (Fig. 11(C)).<sup>111</sup> Choking agents, such as phosgene, are also detected using 4-(4-nitrobenzyl) pyridine to generate a brick red color from its original yellow color (Fig. 11(D)).<sup>112,113</sup> Based on similar chemical reactions, a testing kit consisting of test bottles and test reagents was constructed to analyze the chemical agent present in aqueous media. A major limitation to chemical analysis is that the test is only as specific as the dyes used. Each dye can only react with one class of agent at one time.<sup>107</sup>

As mentioned briefly, currently used chemical technologies have several limitations, such as low specificity, poor sensitivity, and the inability to detect and differentiate all CW agents. Excellent selectivity is a key design criterion for CWA detection. However, achieving this feature is exceptionally challenging due to the electrophilic nature of most CWAs. Several non-toxic species have the potential to interfere with testing and afford false-positive results. Moreover, regulatory bodies are continuously imposing new stringent requirements for CWA analysis; while current detection systems may work, they may fall short of new selectivity and sensitivity requirements. Therefore, the continued advancement of chemical sensors is essential for ensuring vigilance against the threat of CWAs. As will be seen throughout this review, new methods are being developed and the potential of chemical probes is emerging as a



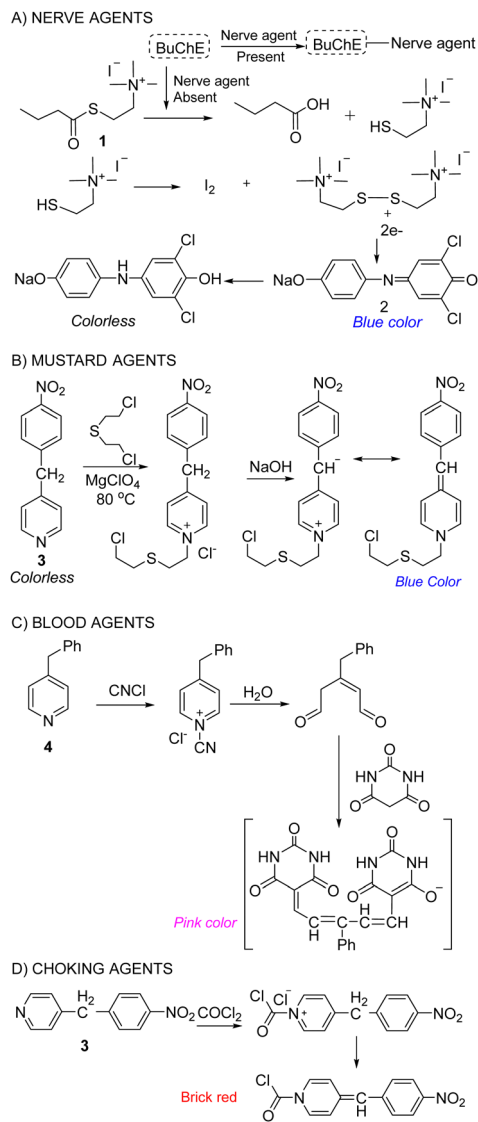


Fig. 11 Classic chemical reactions used in the detection of (A) nerve agents, (B) mustard agents, (C) blood agents, and (D) choking agents.

promising option for use in CW detection in practical applications. The development of chemical sensors is attractive not only in terms of specificity and economic reasons but also for their significantly lower logistical and operational burden on military forces and civilians.

## 4. Fluorescent and colorimetric chemosensors: design and development

The term “chemical sensor” or “chemosensor” refers to a molecule of abiotic origin that signals the presence of matter or energy. Therefore, a chemosensor can be defined as a molecule that interacts reversibly with an analyte and transforms chemical information into analytically useful and measurable signals.<sup>114–116</sup> The measurable signal is the result of

two different processes occurring during host molecule/receptor and analyte/guest interaction *i.e.*, molecular recognition and signal transduction.<sup>110</sup> The molecular recognition is based on size, shape, geometry complementarity, and the presence of specific physical and chemical interactions. The signal transduction occurs with a concomitant change in one or more properties of the system such as absorption, fluorescence, and redox potentials. Sometimes, spacers are placed between the receptor and reporting units which can establish the geometry of the system and tune the electronic interaction between the two active moieties. When the binding interaction between the receptor and indicator is irreversible, the chemosensor is then termed a “chemodosimeter”.<sup>117</sup>

Most chemosensors fit in either of three main approaches in supramolecular chemistry, namely (i) indicator-spacer-receptor (ISR)<sup>118</sup> (ii) indicator displacement assay (IDA)<sup>119</sup> (iii) a chemodosimeter approach or activity-based sensing.<sup>115,120</sup> Typically, there are three approaches invariably used by supramolecular chemists while developing chemosensors for the detection of an analyte *via* various modes of sensing mechanism. Important sensing mechanisms include photoinduced electron transfer (PeT), intramolecular charge transfer (ICT), excimer formation, fluorescence resonance energy transfer (FRET), and excited-state intramolecular proton transfer (ESIPT). Two main types of optical chemosensors *i.e.*, fluorescent and colorimetric are utilizing these sensing mechanisms. In the colorimetric sensors, there is a change in the electronic absorption spectra of the receptor, and the changes can be seen with the naked eye.<sup>121</sup> Fluorescent chemosensors can change their fluorescence after the interaction with the analyte.<sup>122</sup> Fluorescent and colorimetric chemosensors are widely used in organic, biological, and medicinal chemistry and environmental sciences for monitoring cations and anions. Fluorescent sensors are much more sensitive than the colorimetric ones and allow measurements *in situ* and *in vivo*.

### 4.1 Fluorescent and colorimetric chemosensors for the detection of nerve agents: an update

Over the preceding several decades the importance of the design and development of colorimetric and fluorescence based chemosensors for CWA detection is becoming increasingly important. Nowadays, detection is achieved using two main tactics: (i) reaction-based or activity-based sensing and (ii) receptor-based sensing. The covalent approach exploits the reactivity of the analyte with a functional group on the chemical sensor. The reaction leads to a measurable optical response. This strategy is usually irreversible, meaning the developed sensor cannot be reused. On the other hand, CWAs can also be recognized *via* non-covalent reversible interactions (supramolecular approach), providing the ability to reuse chemical sensors. However, the supramolecular approach often displays poor selectivity and sensitivity, which can lead to frequent false-positive responses.

The detection of nerve agents is accomplished by exploiting the reactions of the nucleophilic functionalities on a probe with the electrophilic phosphate ester. The resultant product leads



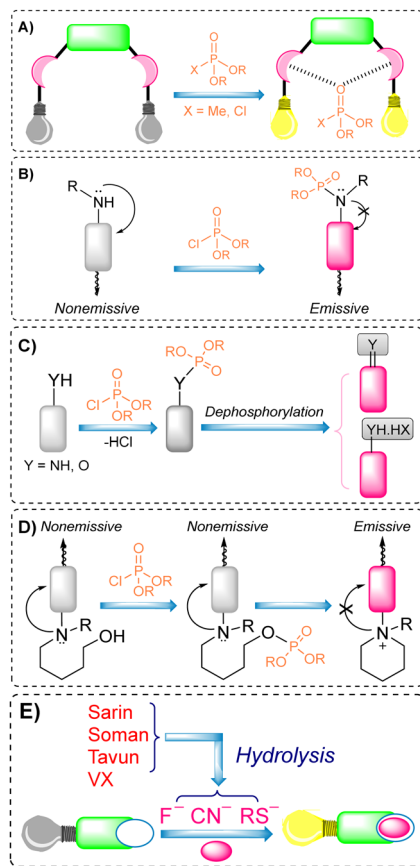


**Fig. 12** Basic schematics for various detection mechanisms for nerve agents. (A) Indicator-spacer-receptor. (B) Amino phosphorylation of sensors results in PeT inhibition leading to a turn-on fluorescence response. (C) Phosphorylation and dephosphorylation of nerve agents lead to the restoration of fluorescence emission. (D) Phosphorylation of a proximal hydroxyl unit leads to intramolecular cyclization, which affords a fluorescent cyclic product. (E) Optical detection of the hydrolyzed products from nerve agents; these are F<sup>-</sup>, CN<sup>-</sup>, and thiols.

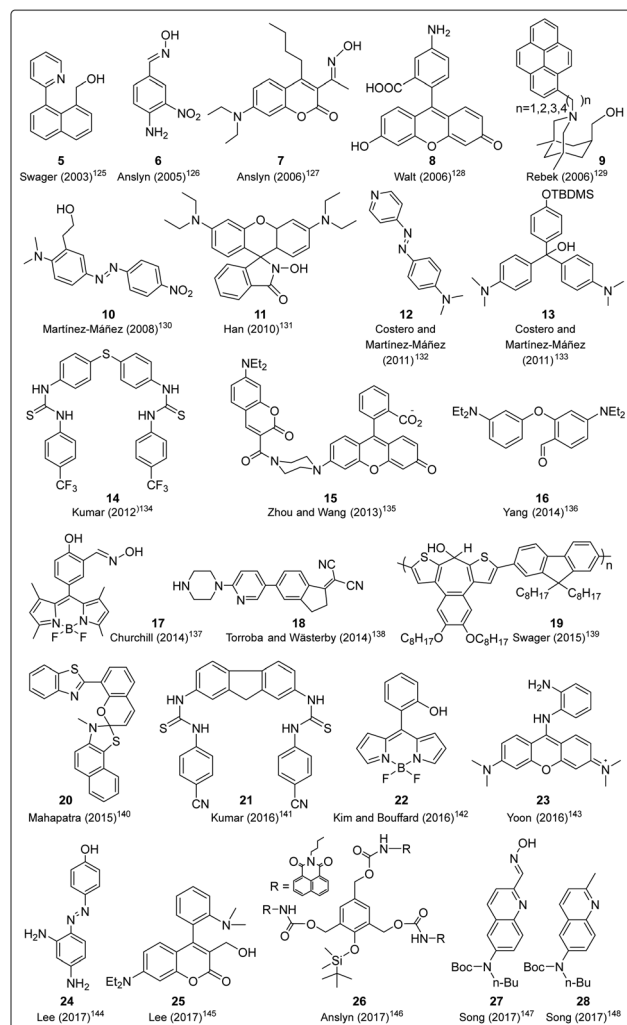


**Fig. 13** Chemical structures of the molecular probes designed for the detection of nerve agents that were previously discussed by Martínez-Mañez<sup>123</sup> and Yoon.<sup>124</sup>

to a detectable optical signal (colorimetric and/or fluorescence) (Fig. 12), either by suppression of photo-induced electron transfer (PeT), change in internal charge transfer (ICT), or an intramolecular cyclization reaction. A recent strategy includes the detection of hydrolyzed products from the nerve agents. These include fluoride ions, CN ions, and thiols (Fig. 12(E)). Various research groups around the world are continually devoting considerable attention to the design and development of new and alternative strategies. The development of chemical probes for nerve agents' detection has been covered in the literature by Martínez-Mañez<sup>123</sup> and Yoon.<sup>124</sup> The structures of these chemical sensors (5–28) can be found in Fig. 13.<sup>125–148</sup> Since they have previously been discussed, we have focused on reports that enable nerve agent detection from August 2017 to date.<sup>124</sup>

Mondal and co-workers constructed a triphenylamine-benzimidazole-based chemosensor (29) that provides a specific colorimetric and fluorescence change for the detection of diethyl chlorophosphate (DCP) in a THF/H<sub>2</sub>O (4/1, v/v) solution (Fig. 14).<sup>149</sup> The triphenylamine moiety acts as the electron-

donor group while the benzimidazole is an electron-acceptor. First, the phosphoryl unit adds to the benzimidazole moiety, which is then hydrolyzed to form protonated species (30). The overall process essentially increases the ICT efficiency of the network and generates dramatic changes in both the absorbance and emission profiles. The authors further used probe 29 by immobilizing it on a TLC plate for the vapor phase detection of DCP.

Following an unconventional strategy, Kumar *et al.* developed a system containing a single molecular probe that enables the simultaneous detection of three nerve agents: sarin, tabun, and VX (Fig. 15).<sup>150</sup> In this approach, oxime (31) was used to react with each nerve agent and afford the corresponding nucleophilic hydrolyzed species (F<sup>-</sup>, CN<sup>-</sup>, and thiols). Each species reacted with electrophilic dye 32 to change its photo-physical properties. As shown in Fig. 15, 32 interacts with cyanide and affords the new chemical species 33. This protocol showed no interference from close competitors, such as electrophilic agents and blister agents.



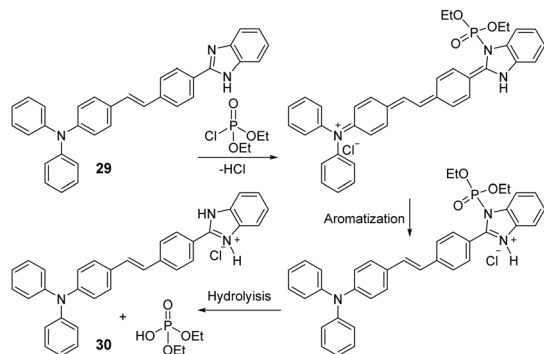


Fig. 14 The mechanism of detection of **29** for DCP in a THF/H<sub>2</sub>O (4/1, v/v) solution.

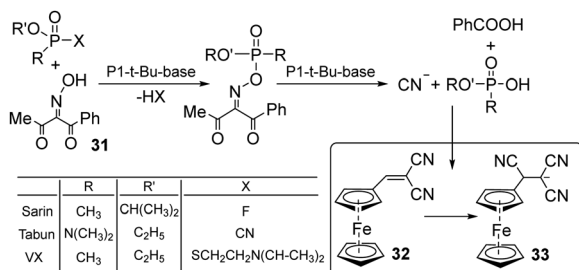


Fig. 15 The indirect sensing mechanism of **32** for DCP using oxime (**31**) in chloroform.

Exploiting the well-known chemistry used in the RVD kit for the detection of nerve agents, Wang and co-workers used the combination of bovine serum protein and gold nanoclusters to afford **34**, which enabled the detection of organophosphorus pesticides in water (Fig. 16).<sup>151</sup> **34** was prepared using gold nanoclusters protected by bovine serum protein (BSA-AuNCs) and a fluorescent substrate, thereby making the complete ensemble fluorescent. This ensemble was found to undergo fluorescence quenching when thiocholine (TC) was released by AChE-mediated enzymatic hydrolysis of acetylthiocholine iodide (ATCI). As expected, the hydrolysis of ATCI is inhibited in the presence of nerve agents (parathion methyl), thus

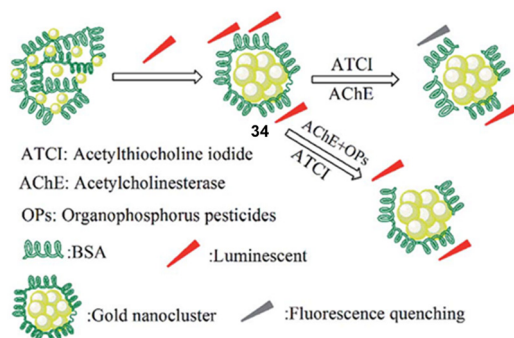


Fig. 16 The sensing mechanism of **34** for parathion methyl in water. Reproduced with permission from ref. 151 Copyright (2017) Royal Society of Chemistry.

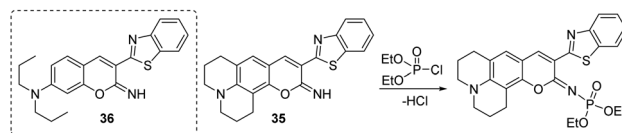


Fig. 17 The sensing mechanism of **35** and **36** for DCP in DMF.

preventing the production of TC and any change in fluorescence at 630 nm. This method was also implemented for the detection of OP pesticides in food samples.

Peng and co-workers developed two on-off chemosensors that contained a nucleophilic imine moiety for the rapid detection of DCP in DMF (Fig. 17).<sup>152</sup> The iminocoumarin-benzothiazole-based probes (**35** and **36**) demonstrated a notable decrease in their fluorescence emission at 526 nm and 531 nm, respectively, within 10 seconds of the addition of DCP. The fluorescence color of **35** changed from green-emissive to light-yellow-emissive, while for **36** a change from green to pink-yellow was observed. The mechanism of detection involves the nucleophilic addition of imine with DCP and the elimination of HCl.

There is no difference in terms of the reactivity of probes **35** and **36**. However, **35** displayed a high fluorescent quantum yield, which is ascribed to the increased co-planarity and rigidity of the scaffold from the quinolizidine ring. The present method was also applied for the recognition of DCP in the gaseous state, with significant color changes that are easily observed by the naked eye.

The immobilization of chemical sensors onto inorganic materials (e.g., silica) affords new smart materials with improved attributes. Silica-based hybrid materials demonstrate numerous benefits, such as high selectivity, sensitivity, recyclability, and robustness compared to discrete probes.<sup>153</sup> The Ruracka group developed a silica-based material that contained the BODIPY chemical probe **37**, which is designed to undergo intramolecular cyclization in the presence of nerve agents.<sup>154</sup> **37** was immobilized on the walls of mesoporous silica materials (SBA-15) to prevent aggregation-caused quenching (ACQ) in water. On interaction with nerve agents (sarin, soman, and tabun), phosphorylation of the hydroxyl group occurred. This was followed by intramolecular cyclization with the pyrrolidine nitrogen to afford the cyclic product **38**. This cyclization gave rise to changes in color and fluorescence (Fig. 18).

The direct incorporation of a chemical sensor into the polymer backbone is one of the most attractive ways to develop a reversible supramolecular sensor (Fig. 19).<sup>155,156</sup> Lee *et al.* reported a pyrene-based polymeric probe (**39**) for the off-on sensing of DCNP in THF/H<sub>2</sub>O (3 : 1, v/v) mixed solutions and in the vapor phase.<sup>157</sup> The polymer sensor (**39**) contains 2-(2-((pyren-1-ylmethyl)-amino)-ethoxy)-ethanol (38), in which pyrene is used as the fluorophore and the hydroxyl group is the nerve-agent-recognition unit. The reaction between the hydroxyl arm and DCNP resulted in phosphorylation, followed by intramolecular cyclization which led to the formation of the morpholino cation, **40**. Initially, **39** was found to



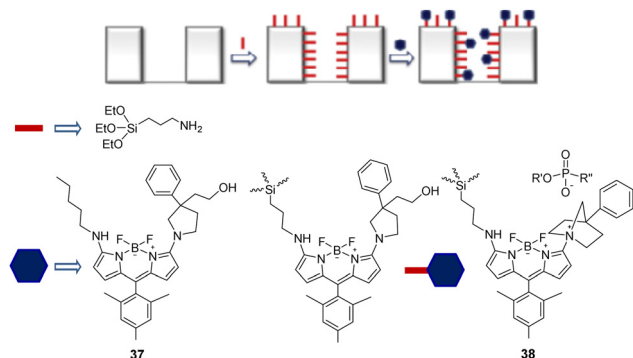


Fig. 18 The sensing mechanism of SBA-15-bound **37** for sarin, soman, and tabun in water. Reproduced with permission from ref. 154. Copyright (2017) Elsevier B.V.

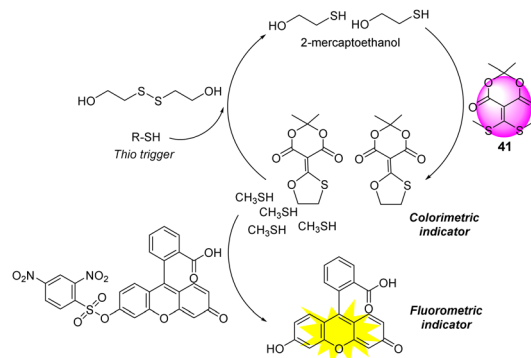


Fig. 20 The sensing mechanism of **41** for DCP.

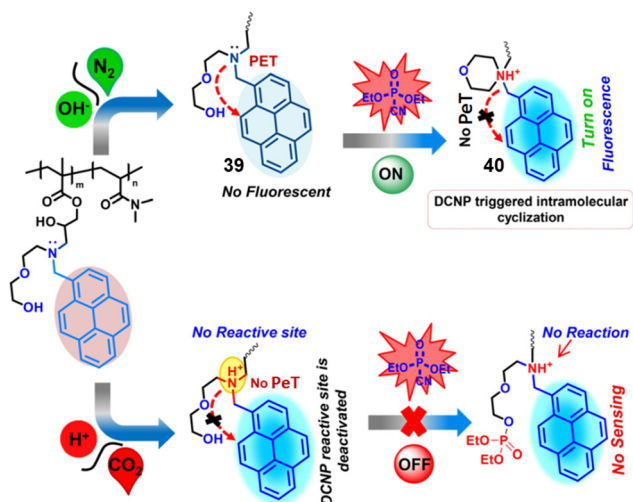


Fig. 19 The sensing mechanism of **39** for DCNP. Reproduced with permission from ref. 157. Copyright (2017) American Chemical Society.

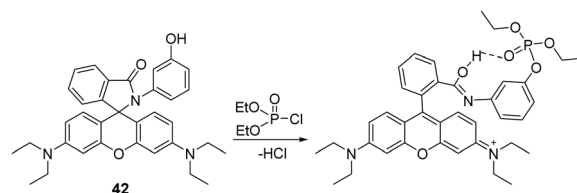


Fig. 21 The sensing mechanism of **42** for DCP in the  $\text{H}_2\text{O}/\text{CH}_3\text{CN}$  (10 : 1, v/v) solution.

be nonfluorescent due to PeT. However, upon DCNP-mediated cyclization and formation of **40**, PeT is inhibited and a significant increase in the fluorescence emission at 395 nm was observed. Probe **39** is tunable *via*  $\text{CO}_2$  and pH for the detection of DCNP, and the sensing system is reversible without any build-up of by-products. The tertiary amine groups of the polymer can be protonated to form quaternary ammonium salt upon exposure to  $\text{CO}_2$  gas, and the resulting protonated amine reverted to the original tertiary amine units in the presence of  $\text{N}_2$  or the absence of  $\text{CO}_2$ .

Auto inductive cascades can amplify the signal response and allow for the detection of a single analyte with ultra-high sensitivity.<sup>158,159</sup> Anslyn and co-workers reported a unique auto inductive cascade strategy for the detection of V-type nerve agents (Fig. 20).<sup>160</sup> This protocol was designed for the optical detection of thiols, which are the hydrolyzed products of V-type agents. Meldrum's acid-based conjugate acceptor (**41**) was used as an additional thiol source for signal amplification. The autoinduction is initiated by a thiol-disulfide exchange with the release of  $\beta$ -mercaptoethanol, which in turn reacts with **41**

to release two equivalents of methyl sulfide. As shown in Fig. 20, this results in a self-propagating cycle that continues until all of **41** is consumed. As a result, this two-step integrated protocol produces a precise diagnostic assay for ultra-trace quantitation of V-type nerve agent detection.

A rhodamine-based chemosensor (**42**) (Fig. 21) was developed by Sahoo and co-workers for the successful *in vivo* and *in vitro* imaging of DCP of DCP in catfish brains.<sup>161</sup> **42** was initially colorless and non-fluorescent. However, the addition of DCP into the  $\text{H}_2\text{O}/\text{CH}_3\text{CN}$  (10 : 1, v/v) solution led to gas-phase-induced ring-opening of the spirolactam ring. This resulted in a 100-fold increase in the emission intensity and a color change from colorless to pink. **42** was used to image DCP in the A549 human cell line and study the distribution of DCP *in vivo*. This demonstration shows chemosensors can be used to study the effects of nerve agents in living systems, providing opportunities to identify therapeutic countermeasures.

Che and co-workers reported a unique self-assembly approach for the selective and highly sensitive detection (15 ppb) of DCP in the vapor phase using a fluorescent nanofiber (Fig. 22).<sup>162</sup> The fluorescent perylene diimide (PDI) derivative, functionalized with the 4-(hydroxymethyl)benzyl group and a dodecyl chain, was found to self-assemble through light-sensitive internanofiber hydrogen-bonding interactions. In this study, it was found that 4-(hydroxymethyl)benzyl was crucial to the formation of the hierarchical nanofiber, and this structure gave rise to a greater fluorescent quantum yield with respect to its monomeric unit, thereby amplifying the sensing signal. Light irradiation of the internanofiber hydrogen bonds weakened the interactions, resulting in a decrease in the fluorescence emission intensity. The exposure of DCP to the light-irradiated



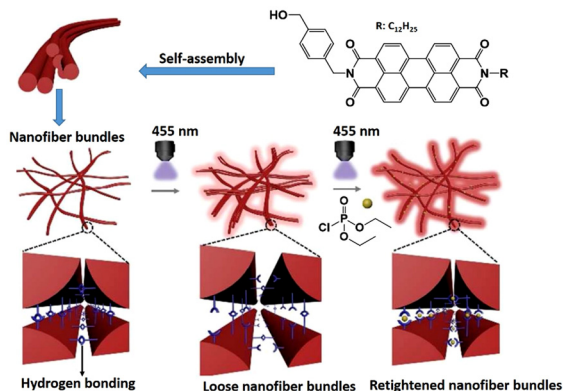


Fig. 22 The sensing mechanism of perylene diimide (PDI) derivative-based nanofibers for DCP. Reproduced with permission from ref. 162. Copyright (2018) American Chemical Society.

system resulted in the retightening of the nanofibers, enhancing the fluorescence emission intensity.

Yoon and co-workers reported the benzothiazole-based chemosensor (**43**), which is functionalized with an oxime unit, for the selective detection of the nerve agent surrogate DCNP (Fig. 23).<sup>163</sup> The new ESIPT (excited-state intramolecular proton transfer) fluorescent probe 2-(2'-hydroxyphenyl)-benzothiazole (**43**) demonstrated that the hydroxyl group in the oxime moiety undergoes nucleophilic reaction with DCNP, followed by ring-closing and ring-opening to afford the highly fluorescent nitrile derivative **45** via the benzisoxazole intermediate **44**. An overall 60-fold enhancement in the fluorescence emission intensity at 480 nm was observed. The electron-withdrawing cyano group present in **43** results in strong fluorescence because it inhibits the PeT quenching process responsible for inefficient emission from the probe. Demonstrating its real-life application, the authors used an electrospinning technique to develop **43**-containing nanofibers, which were used for vapor detection.

Wang and co-workers established a similar oxime-based chemosensor (**46**) for the detection of DCP in methanol (Fig. 24).<sup>164</sup> In the presence of DCP, a notable fluorescence

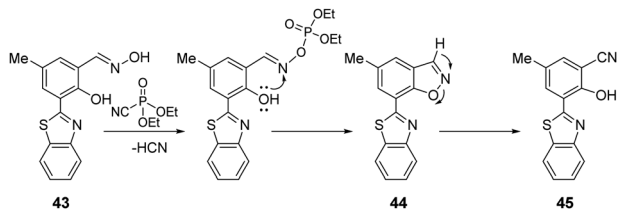


Fig. 23 The sensing mechanism of **43** for DCNP.

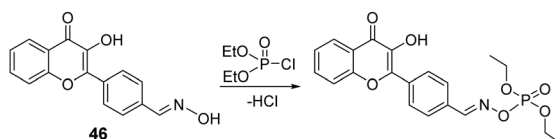


Fig. 24 The sensing mechanism of **46** for DCP.

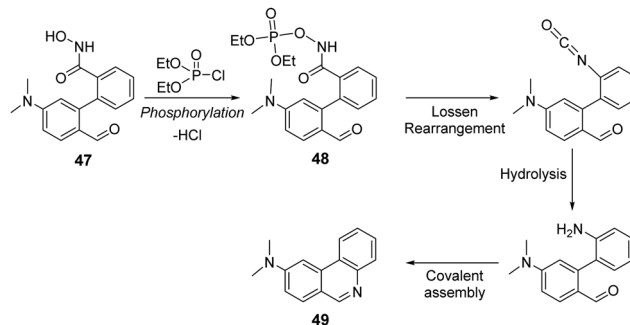


Fig. 25 The sensing mechanism of **47** for DCP in acetonitrile.

enhancement accompanied by an emission color change was observed within 90 s by the naked eye in the solution. This is attributed to the fact that the addition of the phosphate group suppresses the intramolecular rotation, thereby increasing the fluorescence of the probe. Dye-coated test strips were constructed for the detection of DCP vapor.

Yang and co-workers reported a “covalent-assembly-based” fluorescent probe (**47**) for the detection of DCP in acetonitrile (Fig. 25).<sup>165</sup> This strategy exploits the Lossen rearrangement with DCP to form cyclic fluorescent product **49** ( $\lambda_{em} = 418$  nm). As seen in Fig. 25, the hydroxamic acid group of **47** was shown to react with DCP to form a phosphoryl intermediate **48** that quickly undergoes Lossen rearrangement to produce an isocyanate intermediate. Since this reaction occurs in water, isocyanate transforms into an aniline intermediate that condenses to form a fluorescent phenanthridine system (**49**). This sensor featured excellent selectivity, fast response (within 100 s), and a low limit of detection (10.4 nM) toward DCP, even in the gas state.

Similar to previous reports,<sup>118,122</sup> Son and co-workers reported a rhodamine-deoxylactum-based colorimetric and fluorometric sensor (**50**) for the instantaneous detection of DCP in DMF (Fig. 26).<sup>166</sup> The phosphorylation of hydroxy-arm and the subsequent intramolecular-cyclization-induced ring-opening of the deoxylactum afforded the observed fluorimetric (564 nm) and colorimetric response. **50** was applied to the development of a gas sensing device in the form of polyurethane-based test strips, which were able to detect DCP at a concentration of  $9.66 \times 10^{-9}$  M.

Using a smartphone and an easily assembled LEGO box, Anslyn, Marcotte, and co-workers developed a technique for the simultaneous detection and differentiation of G- and V-series nerve agent mimics for real-world applications (Fig. 27).<sup>167</sup> Since fluoride and thiolate are the key constituents of these agents, the detection of these anions can serve as a way to indirectly detect the respective nerve agents. In this study,

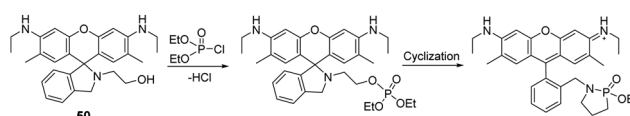


Fig. 26 The sensing mechanism of **50** for DCP in DMF.





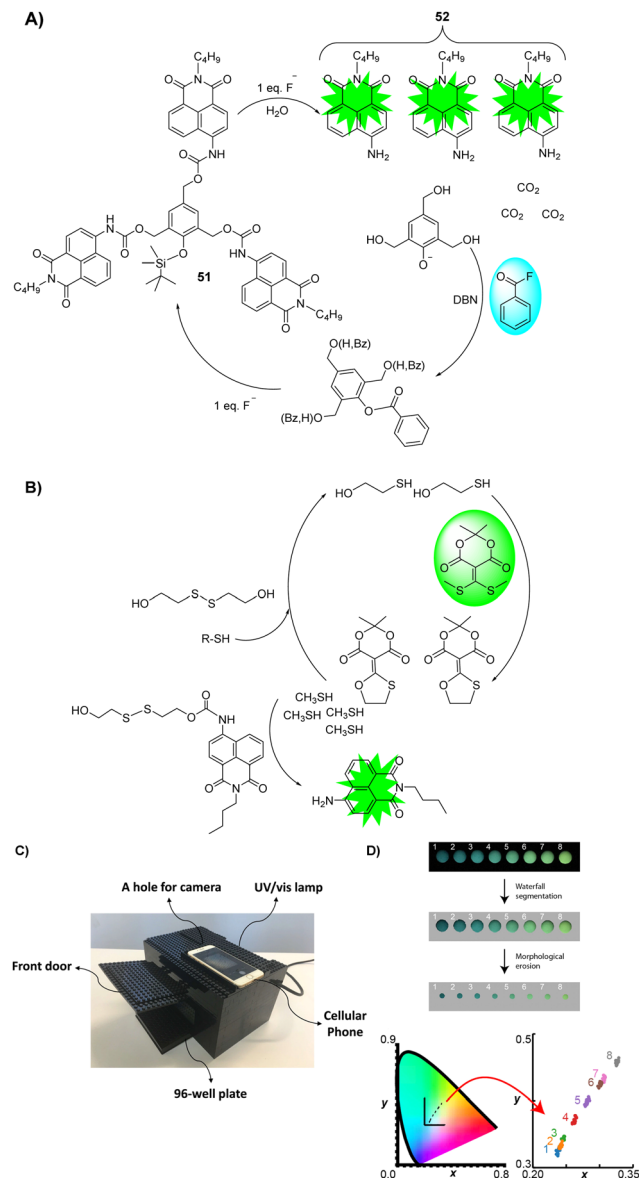


Fig. 27 (A) Self-propagating cascade employing benzoyl fluoride as a latent source of fluoride for signal amplification. (B) Self-propagating protocol employs a Meldrum's acid-based conjugate acceptor as a latent source of thiol for signal amplification. (C) A homemade LEGO dark-box for imaging using a cell phone. (D) Fluorescent cascade reaction chromatography corresponds to the analyte concentration quantitatively, and processing of the image using a watershed and morphological erosion algorithm. Reproduced with permission from ref. 167. Copyright (2018) American Chemical Society.

fluoride anions and thiols (Fig. 27) were used to initiate a self-propagating cascade reaction that amplifies fluorescence signals drastically in a ratiometric manner. It was shown that only one equivalent of fluoride or thiol was needed to activate the cascade reaction of 51 and produce further equivalents of fluoride or thiol. This caused the fluorescent signal to grow exponentially. In both self-propagating cascade reactions, 4-aminonaphthalimide (52) was used as the fluorophore. For signal amplification, benzoyl fluoride and Meldrum's acid-based conjugate acceptor were employed as the latent

source of fluoride and thiol, respectively. Using the chromatography and LEGO approach, concentrations of the analytes were accurately determined and differentiated. To accomplish this, the images were digitally processed using a watershed and morphological erosion algorithm. Watershed and morphological erosion algorithms are used in image processing to generate boundaries between objects, and to remove pixels on that object's boundaries, respectively.

Zhao and co-workers reported the ratiometric fluorescence detection of DCP vapors using a carbazole-based self-assembled nanofiber (53).<sup>168</sup> In this super-fast and ultrasensitive detection method, the exposure of DCP to the nanofibers resulted in the phosphorylation of pyridine, leading to fluorescent quenching within the diffusion length of the nanofibers. This amplified the fluorescence quenching (Fig. 28). At the same time, nanofibers amplified the intramolecular charge transfer emission by harvesting excitons within the diffusion length. The most likely interferents, in this case, could be DCNP; however, these did not interfere because of the relatively weak electrophilic ability of DCNP to form a pyridine-phosphorylated complex. Unfortunately, acidic interference showed an equal response, as in the case of DCP, thereby making acids a major interferent.

Reaction-based sensing methods are one of the best approaches for the development of colorimetric biosensors. As discussed in the introduction, commercial biosensors for nerve agent detection consist of the substrates acetyl(thio)choline or butyryl(thio)choline, which are hydrolyzed by AChE to afford choline and the corresponding acid. The hydrolyzed product is then detected *via* color change by using a pH indicator, redox indicator, or chromogenic reporter.<sup>169–171</sup> In an attempt to improve upon existing biosensing technologies, Matěvský explored the combination of two triphenylmethane dyes, Guinea Green B and Fuchsin, for the visual detection of G and V agents *via* the indirect detection of thiocholine (Fig. 29) in water.<sup>172</sup> Both dyes are sensitive to thiolate attack *via* Michael-type addition, which changes the optical properties in the form of a blue–red transition (*i.e.*, from  $\lambda_{\max}$  620 nm and 540 nm). The authors have also examined the stability of the sensing system by impregnating the reagents/substrates and dye into

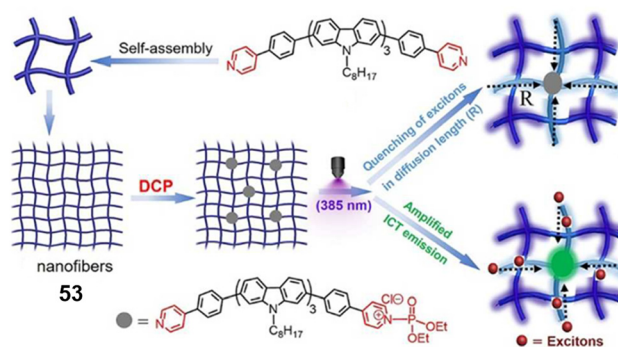


Fig. 28 The sensing mechanism of self-assembled nanofibers (53) for DCP. Reproduced with permission from ref. 168. Copyright (2018) American Chemical Society.



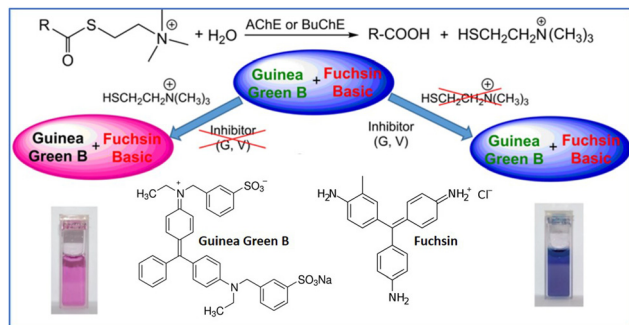


Fig. 29 The combination of Guinea Green B and Fuchsin for G- and V-series nerve agents. Reproduced with permission from ref. 172. Copyright (2019) American Chemical Society.

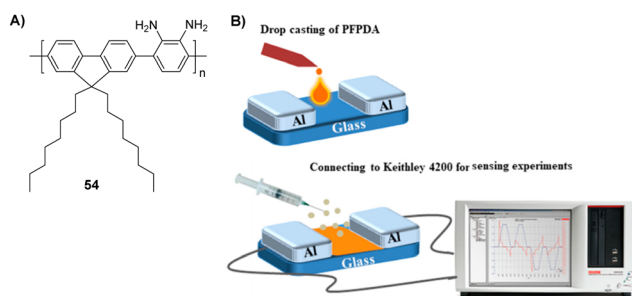


Fig. 30 (A) Structure of PFPDA (**54**). (B) The sensing mechanism of an amine-functionalized conjugated polymer for G- and V-series nerve agents. Reproduced with permission from ref. 173. Copyright (2019) American Chemical Society.

the glass nanofiber filter paper for NA detection to successfully demonstrate field applications.

The Iyer group reported a portable sensor device for DCP detection using an amine-functionalized conjugated polymer (Fig. 30).<sup>173</sup> Poly(3-(9,9-dioctyl-9H-fluorene-2-yl)benzene-1,2-diamine) (PFPDA) (**54**) was used as a sensory channel material for a two-terminal sensor, which provided the detection of the analyte with good selectivity and sensitivity (LOD: 5.88 ppb). The amplified current signal was obtained due to the redox interaction between the semiconducting polymer and DCP. Furthermore, the sensing response of the fabricated sensor was fast (3 s), reversible, and reproducible, demonstrating its enormous potential as a portable device for the on-site detection of nerve agents.

Koning and co-workers reported a chromophore-functionalized metal-organic framework (NU-1000) for the effective degradation and visual detection of VX (Fig. 31).<sup>174</sup> The MOF was functionalized with Ellman's reagent (5,5'-dithiobis-(2-nitrobenzoic acid) or DTNB), which is a quantitative reporter for measuring thiol concentrations. The reaction between thiol and Ellman's reagent affords 5-mercapto-2-nitrobenzoic acid (TNB) with a bright yellow absorption ( $\lambda_{\text{abs}} = 412 \text{ nm}$ ).<sup>175</sup> This functional MOF-based material (DTNB@NU-1000) in neutral buffer degraded VX and afforded a visual response. This degradation showed a linear correlation with the concentration of VX, which allows for quantification.

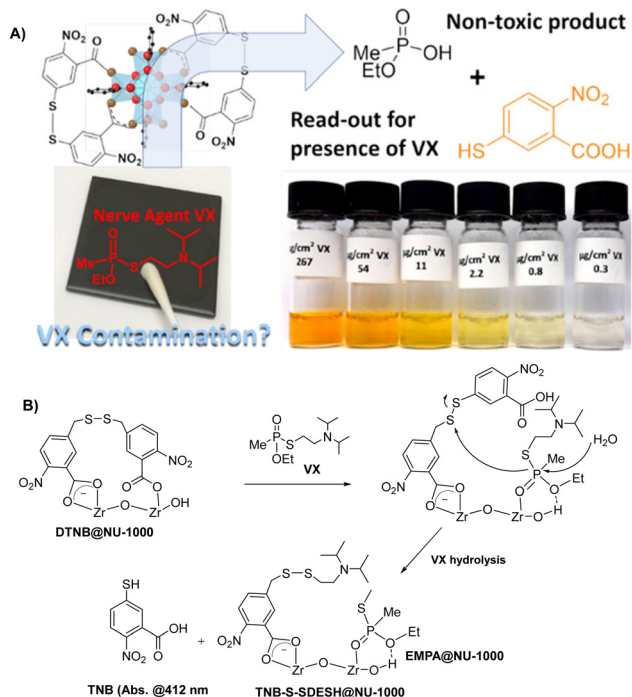


Fig. 31 The sensing mechanism of DTNB@NU-1000 for VX. Reproduced with permission from ref. 174. Copyright (2019) American Chemical Society.

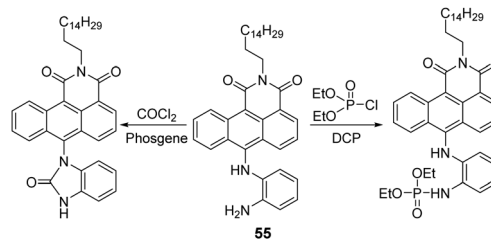


Fig. 32 The sensing mechanism of **55** for DCP and phosgene in chloroform. Reproduced with permission from ref. 176. Copyright (2019) American Chemical Society.

Yoon and co-workers developed a fluorescent chemosensor (**55**), consisting of the anthracene carboximide fluorophore and a phosphorylative-reactive *o*-phenylenediamine unit (Fig. 32).<sup>176</sup> The reaction between **55** and DCP in chloroform afforded a large emission enhancement of **55** at 588 nm with a fluorescence quantum yield of 3.2% within a minute. The calculated LOD was 88 nM. This turn-on response was attributed to the phosphorylation of *o*-phenylenediamine and the inhibition of PeT. Additionally, the **55**-coated membrane was constructed for its potential for on-site analysis. Interestingly, **55** was also found to be selective and sensitive to choking agents, such as phosgene.

The boron dipyrromethene (BODIPY) scaffold has attracted significant interest in the realm of chemical biology for its use in fluorescent dyes<sup>177</sup> and tags.<sup>178</sup> Over the years, the BODIPY core has also been used to develop several chemical probes due to its ease of modification, good photostability, and



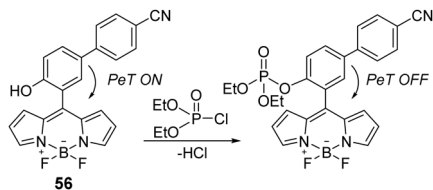


Fig. 33 The sensing mechanism of **53** for DCP in DMF.

environment-dependent fluorescence quantum yield.<sup>179</sup> Attracted by these properties, Lu and co-workers developed a BODIPY-based sensor (**56**) for the detection of DCP in DMF.<sup>180</sup> Probe **56** enabled the rapid ( $\sim 1$  min) selective and sensitive detection of DCP (Fig. 33). This mechanism of detection was believed to be based on the inhibition of PeT upon phosphorylation of the hydroxyl unit found on **56**. Encouraged by the performance of probe **56**, the authors evaluated it for the detection of DCP using testing paper and investigated its practical applicability for on-site analysis.

Another example of a BODIPY-based fluorescent sensor (**57**) for nerve agents' detection was reported by Zhao and co-workers. In this design, the authors introduced the NA-reactive 2-salicylaldoxime unit onto the BODIPY scaffold *via* an ethynyl spacer (Fig. 34).<sup>181</sup> **57** in acetonitrile solution was initially treated with the base triethylamine ( $\text{NEt}_3$ ), which led to a decrease in the fluorescence emission intensity at 520 nm. Subsequent phosphorylation of the phenol unit through treatment with DCNP resulted in a significant fluorescence enhancement at 560 nm. Probe **57** demonstrated an excellent LOD for DCNP (34 nM), fast response times ( $t_{1/2} = 175$  s), and excellent selectivity (better than other OP compounds, such as DCP, DMMP, TPP, and TMP). They also investigated the detection of DCNP vapor using test strips with **57** immobilized.

Sfrazzetto *et al.* demonstrated the ability to detect dimethyl methylphosphonate (DMMP) (a nerve agent simulant, Fig. 1(C)) by exploiting the metal coordination properties of phosphate esters with metal-salen complexes ( $\text{Zn}^{2+}$  and  $\text{UO}_2^{2+}$ ) (**58**) (Fig. 35).<sup>182</sup> The interaction studies revealed that the coordination of DMMP with Zn-salen resulted in the complex adopting a square-based pyramidal geometry with molecular recognition occurring in a pseudo-axial position. In contrast, the  $\text{UO}_2$ -salen complex adopted a bipyramidal geometry with DMMP coordinated to the fifth equatorial position.<sup>183</sup> Additionally, the binding constant values of the coordination to the complex were further enhanced due to hydrogen bonding interactions

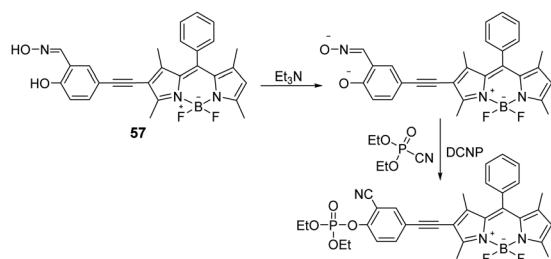


Fig. 34 The sensing mechanism of **57** for DCNP in acetonitrile.

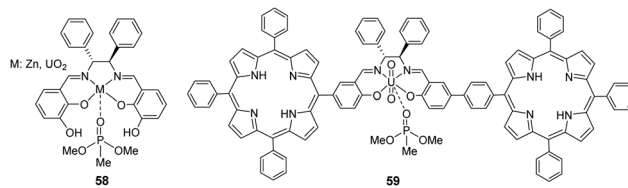


Fig. 35 The structures of metal-salen-based complexes (**58** and **59**) with DMMP.

between hydroxyl groups of **58** and DMMP. The recognition between Zn-salen and DMMP was performed in chloroform, which resulted in the rise of fluorescence emission at 430 nm. In an attempt to generate a colorimetric response, Pappalardo *et al.* developed the bis-porphyrin-salen- $\text{UO}_2$  complex (**59**) for the detection of DMMP.<sup>184</sup> The same coordination event led to significant color changes from light blue to purple in  $\text{CHCl}_3$ . The presence of the porphyrin units was crucial for gaining these absorption properties owing to their extensive conjugation and photophysical properties. Since this coordination event is reversible, this sensor is particularly attractive for real-world applications as the device has the potential to be recycled.

Bao and co-workers reported the ESIPT-based fluorescent chemosensor (**60**) for the detection of DCP in acetonitrile. Initially, **60** displayed fluorescence emission due to keto-/enol-form conversion. The phosphorylation of **60** by DCP resulted in the inhibition of the ESIPT mechanism, leading to a concomitant change in fluorescence emission intensity at 453 nm (Fig. 36).<sup>185</sup> This could lead to turn-on fluorescence within six seconds, with high sensitivity and selectivity. The nucleophilicity of the phenol group is greatly enhanced by the proton transfer from the phenol group to the benzothiazole group to form the phosphorylated product (**61**), leading to a strong fluorescence response. **61** was immobilized in a polystyrene-based membrane for on the spot analysis of DCP vapor with the naked eye. This approach provides a practical, real-time detection kit for DCP environmental samples.

Khatua and co-workers synthesized the organometallic complex (**62**) for the detection of a nerve agent mimic in acetonitrile (Fig. 37).<sup>186</sup> The reaction between **62** and DCP resulted in a ratiometric change in the fluorescence emission intensity from 518 nm to 565 nm in an acetonitrile solution at nanomolar concentrations. This change in luminescence was attributed to an increase in steric hindrance upon phosphorylation, which restricted intramolecular rotation. This led to the optical changes. **62**-coated paper strips and PEO films which were prepared for visual detection of DCP vapor.

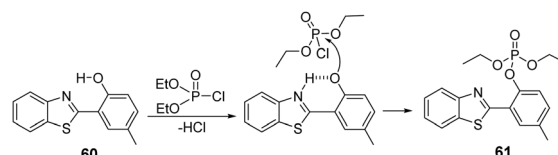


Fig. 36 The sensing mechanism of **57** for DCP in acetonitrile.





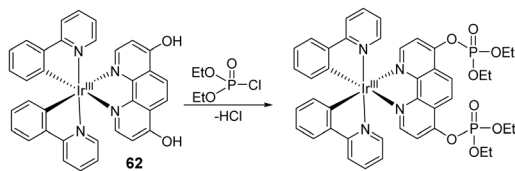


Fig. 37 The sensing mechanism of **62** for DCP in acetonitrile.

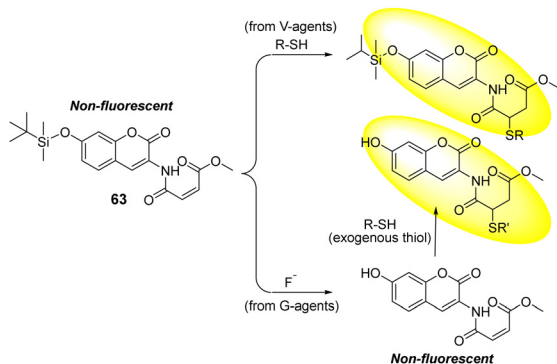


Fig. 38 The sensing mechanism of **63** for DCP in an EtOH-HEPES buffer.

In an attempt to distinguish between G- and V-series nerve agents, Zhigang's group designed the coumarin-based fluorescent probe **63**, which contained two different reactive units for fluoride anions ( $F^-$ ) and thiols, respectively. Fluoride is the hydrolyzed product of sarin and soman nerve agents and thiol is the hydrolyzed product of the VX nerve agent (Fig. 38).<sup>187</sup> The two reactive groups are maleimide and silyl, which are specific for thiols. These react *via* conjugate addition and fluoride-mediated silyl deprotection, respectively. Distinct fluorescence responses were obtained in both cases. The reaction of **63** with thiols in an EtOH-HEPES buffer solution produces a clear peak in the fluorescence emission at 404 nm within 1 min. In the case of fluoride detection, the reaction of **63** with  $F^-$  in the EtOH-HEPES solution initially led to no fluorescence change due to the formation of the desilylation product of **63**. This desilylation product develops a response upon the addition of exogenous thiols, showing a new fluorescence emission peak at 460 nm.

$Ln(III)$ -based luminescent sensors are routinely developed for the detection of analytes due to their strong luminescence and reversible properties.<sup>188</sup> The strong Lewis acidity and oxophilic nature of  $Ln(III)$  ions allow the selective coordination-mediated detection of phosphate-based nerve agents. The terpyridine-dicarboxylate-based  $Eu(III)$  probe, **64**, was recently reported by Patra and co-workers as a turn-on luminescent sensor for the selective detection of nerve agent simulants, *e.g.*, DCP, in acetonitrile (Fig. 39).<sup>189</sup> Upon gradual addition of DCP, a subtle decrease was observed initially, followed by a rapid enhancement of the emission intensity of **64**. This could be attributed to the fact that the nucleophilic attack at the electron-deficient phosphoryl-chloride bond of DCP by the peripheral phenolic  $-OH$  group of the antenna is known to be

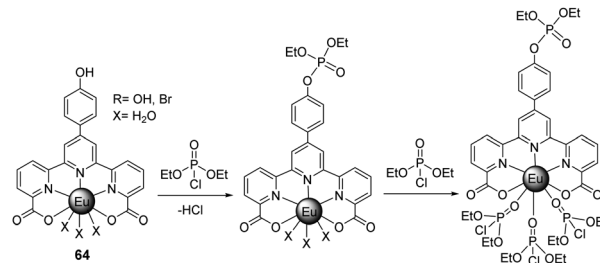


Fig. 39 The sensing mechanism of **64** for DCP in acetonitrile.

facile. This results in a minor decrease in the luminescence intensity, originating from  $f \rightarrow f$  transitions. However, after the subsequent addition of DCP to **64**, a notable increase in the luminescence intensity was observed, especially for the hypersensitive  $^5D_0 \rightarrow ^7F_2$  transition band at 614 nm. This is due to the subsequent displacement of the labile water molecules from the coordination sphere.

Thiagarajan and co-workers evaluated the photophysical and aggregation-induced emissive (AIE) properties of the azine-based donor- $\pi$ -acceptor probe (**65**) in different solvents with varying polarity (toluene, DCM, THF, MeOH, ACN, and DMF) (Fig. 40).<sup>190</sup> **65** was shown to detect DCP in both its monomeric form and aggregated forms. In THF (Fig. 40(A)), the imine nitrogen of **65** was found to undergo phosphorylation, resulting in a red-shift in absorption (460 nm) and strong orange fluorescence with maximum emission at 513 nm. In a THF/water mixture (30 : 70) (Fig. 40(B)), DCP undergoes hydrolysis to form a diethyl phosphate and release hydrochloric acid. Subsequent protonation of the amine nitrogen of **65** resulted in changes in the absorption and emission spectra, with a absorption band shift from 417 nm to 350 nm and a emission shift from 570 nm to 406 nm.

As shown in Fig. 41, naphthalimide-based fluorescent probe **66** was developed by Cheng's group for the detection of DCP in DMF.<sup>191</sup> Initially, **66** was found to be weakly emissive, owing to PeT quenching from the piperazine nitrogen. The DCP-mediated phosphorylation of **66** resulted in the inhibition of PeT, which resulted in a significant fluorescence enhancement

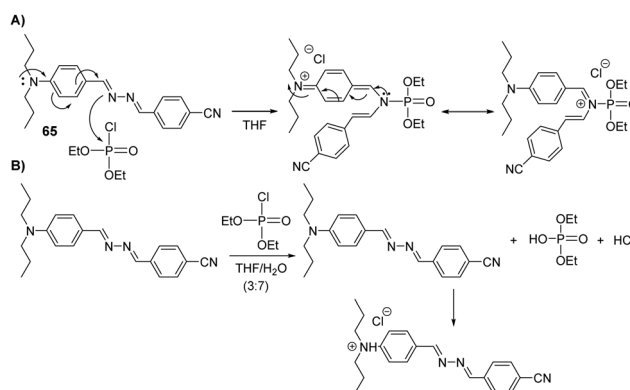


Fig. 40 (A) The sensing mechanism of **65** for DCP in THF. (B) The sensing mechanism of **65** for DCP in a THF/water mixture (30 : 70).





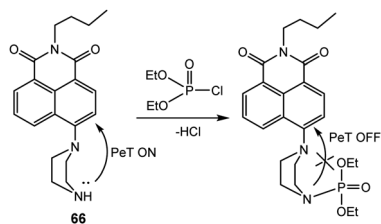


Fig. 41 The sensing mechanism of **66** for DCP in DMF.

(150-fold) at 510 nm. In an attempt to explore practical applications for the vapor phase detection of DCP, probe **66** was also coated on filter paper; the desired response was observed, as expected.

Bag and co-workers, reported the rhodamine-based chemical probe, **67**, for the fluorimetric and colorimetric detection of DCP in ethanol (Fig. 42).<sup>192</sup> The mechanism of detection was believed to be based on the phosphorylation of the carbonyl of the spirolactam unit, which induced ring-opening and afforded both an increase in absorption at 533 nm and a fluorescence increase at 553 nm ( $\lambda_{\text{ex}}$  480 nm).

In 2020, the functional polymer **68** containing (*E*)-2-(methyl(4-(pyridine-4-ylidiazene)phenyl)amino)ethyl acrylate, *N*-(4-benzoylphenyl)acrylamide, and *N,N*-dimethyl acrylamide as polymer subunits was developed by Lee's group for the selective and visual detection of DCP in water (Fig. 43).<sup>193</sup> An instant optical change from yellow to red was observed when **68** was treated with DCP in water. Quaternization of the pyridine groups of **68** was accompanied by a color change from yellow to pink due to strong interactions between electron-donating nitrogen atoms and electron-withdrawing quaternary ammonium (pyridinium) salts. Demonstrating the reusability

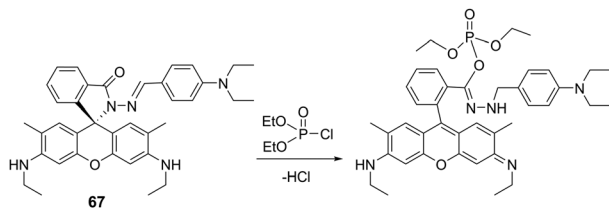


Fig. 42 The sensing mechanism of **67** for DCP in ethanol.

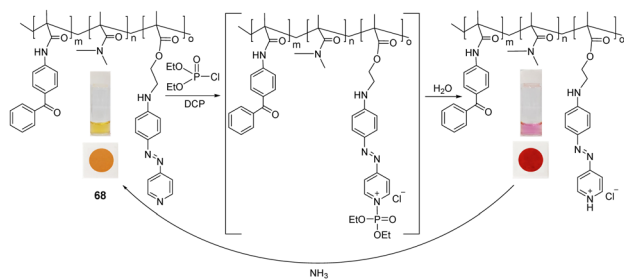


Fig. 43 The sensing mechanism of colorimetric polymer **68** for DCP in water. Adapted with permission from ref. 193. Copyright (2019) American Chemical Society.

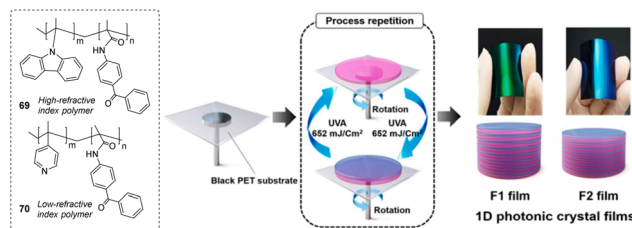


Fig. 44 Pictorial representation of the sensing ensemble based on one-dimensional photonic crystal films of high and low refractive index polymers (**69** and **70**) for DCP in the vapor phase. Reproduced with permission from ref. 194. Copyright (2020) Elsevier B.V.

of this polymeric system, a 2.0 M ammonia solution in ethanol was used to regenerate DCP-exposed films *via* deprotonation of the pyridine moiety. This was accompanied by a color change from pink back to yellow. This repeatability was shown in four successive cycles, which confirmed this system could provide an ideal solution for the detection of these analytes in a pure aqueous medium.

Lee and his group developed one-dimensional photonic crystal films for the colorimetric detection of a nerve agent mimic (DCP) (Fig. 44) in the vapor phase.<sup>194</sup> The films were constructed *via* sequential, alternating layer deposition of polymers with high and low refractive indexes (**69** and **70**) containing poly(*N*-vinyl carbazole-*co*-benzophenone acrylate) and poly(4-vinyl pyridine-*co*-benzophenone acrylate) as photo-crosslinkable units onto a black polyethylene terephthalate substrate. This was achieved *via* the spin-coating of each layer, followed by chemical immobilization onto the surface *via* UV-light irradiation. The polymers contained 7–15 mol% of photo-active benzophenone acrylate to promote film stability with high crosslinking density. The initial colors of the F1 and F2 films were green and cyan with maximum reflectance wavelengths of 540 and 490 nm, respectively. The color of the F1 film changed from green to yellow and finally to red when exposed to increasing DCP concentrations. F1 was chosen because it exhibited more diverse color transitions than F2 with increasing DCP concentrations. No response was observed when the films were treated with DMMP, TEP, TBP, or DCNP. The quaternary pyridinium salts generated by DCP detection can be dequaternized in the presence of an ammonium hydroxide solution. The sensitivity and visibility were enhanced with an increase in the relative humidity, and the detection process was reversible and repeatable over three cycles.

Takahashi and co-workers developed a gold nanoparticle (AuNPs) approach that could be used for the naked-eye detection of VX in a buffer solution (pH 9.0) (Fig. 45).<sup>195</sup> The authors' strategy focused on the detection of 2-(diisopropylamino)ethanethiol (DAET), *i.e.*, the hydrolyzed product of VX. In this study,

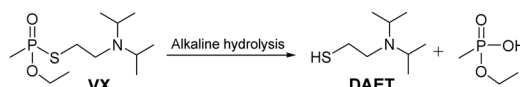


Fig. 45 Chemical reaction showing alkaline hydrolysis of VX.



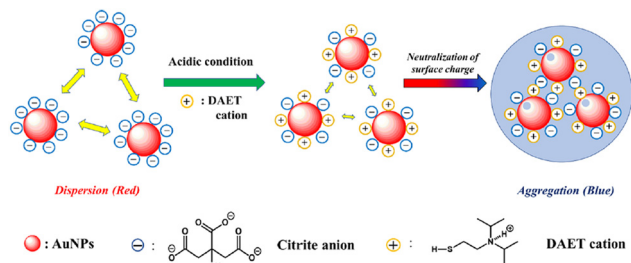


Fig. 46 The sensing mechanism of AuNPs capped with citric acid for DAET in a buffer solution (pH 9.0). Reproduced with permission from ref. 195. Copyright (2021) Elsevier B.V.

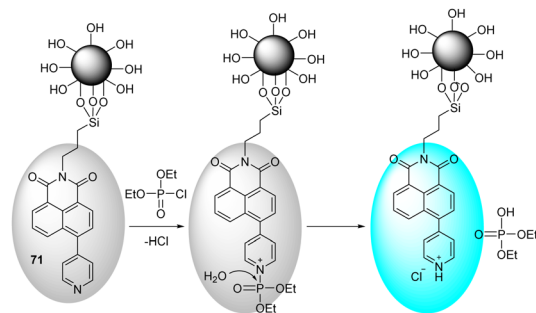


Fig. 47 The sensing mechanism of **71** for DCP in THF.

protonated DAET was found to interact with anionic-based AuNPs (capped with citric acid). As illustrated in Fig. 46, the electrostatic interaction between cationic DAET and anionic AuNPs promoted aggregation, leading to a color change from red to blue with a bathochromic shift from 520 nm to 680 nm (Fig. 46). This optical change is attributed to dipole coupling between the plasmons of neighboring aggregated particles.

Zhang and co-workers exploited 1,8-naphthalimide-pyridine-functionalized hybrid SiO<sub>2</sub> nanoparticles (**71**) for DCP detection in THF (Fig. 47).<sup>196</sup> 1,8-naphthalimide was used as the fluorescent reporter with the pyridine moieties used to react with DCP and DCNP. The addition of both DCP and DCNP resulted in phosphorylation of the pyridine moieties, followed by hydrolysis and their subsequent protonation. This mechanism resulted in a large enhancement in the fluorescence emission at 427 nm. Interference from mineral acids (e.g., HCl, HBr) is commonly observed for pyridine-based strategies. However, immobilizing **71** on the hydrophilic silica overcame this issue. This was attributed to mineral acids having a greater affinity for the surface of SiO<sub>2</sub> NPs.

## 4.2 Fluorescent and colorimetric chemosensors for the detection of blister agents

The development of chemical sensors for the optical detection of blister agents has primarily focused on SM, rather than NM or Lewisite. This is believed to be due to the lack of appropriate molecular recognition units. In general, the design of chemosensors for the detection of SM targets the electrophilic alkylhalides or the electrophilic episulfonium ions that form in a

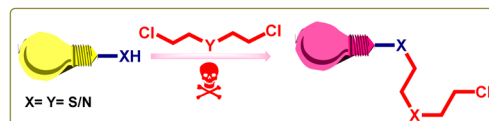


Fig. 48 The general sensing mechanism for SM.

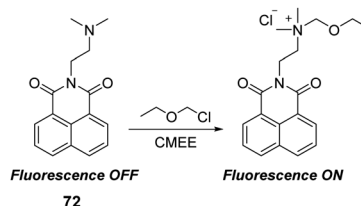


Fig. 49 The sensing mechanism of **72** for CME in acetonitrile.

polar medium (Fig. 48).<sup>197</sup> However, this nucleophilic strategy often leads to poor selectivity against other electrophilic CWA analytes (*i.e.*, nerve agents). Therefore, fine-tuning of the chemosensor and experimental conditions are needed. Over the years, extensive efforts have been devoted by several research groups to develop SM-responsive probes with high selectivity and sensitivity. The reported approaches for SM detection must use the mimic CEES, which is far more reactive: SM ( $t_{1/2}$ , 8.5 min at 25 °C in H<sub>2</sub>O) vs. CEES ( $t_{1/2}$ , 44 s at 25 °C in H<sub>2</sub>O).<sup>198</sup> The instant and accurate detection of SM is imperative for medical countermeasures. Current technologies require around a week to a month for analysis in dedicated laboratories.<sup>199</sup>

**4.2.1 Detection of sulfur mustard.** The initial report that demonstrated the optical detection of chloromethyl ethyl ether (CME) was reported by Eichen and co-workers in 2006 (Fig. 49).<sup>200</sup> The developed sensor 2-(2-dimethylaminoethyl)-benzo[de]isoquinoline-1,3-dione (**72**) was assessed against alkylating agents (CME) in acetonitrile. As shown in Fig. 49, the tertiary amine serves as both a PeT quencher and reactive unit for CME. **72** saturates with CME at a ratio of 1:1, yielding luminescence at 382 nm which is about 130 times stronger than that of the free probe. Unfortunately, a major flaw with this approach was that the presence of any species with similar electrophilicity or acids (Lewis and Brønsted) are likely to cause interference and lead to a false-positive signal.

Using their expertise in indicator displacement assays (IDAs), Anslyn and Kumar reported the first-ever selective and sensitive fluorescent sensor for the detection of CEES<sup>201</sup> and then again for SM (Fig. 50).<sup>202</sup> In this design, a dithiol (**73**) was first allowed to react with CEES at 80 °C under pH 9 to form podand (**74**). **74** was then able to interact with the metal-indicator complex (**75**), resulting in the release of an indicator (coumarin fluorophore, **ME**) by forming metal-podand complex **76** with a concomitant turn-on fluorescence response at 460 nm. This strategy took advantage of the greater binding affinity of podand for Cd<sup>2+</sup> ions. By taking advantage of the molecular design and reaction conditions, interference from nerve agents and other electrophilic agents was not observed.



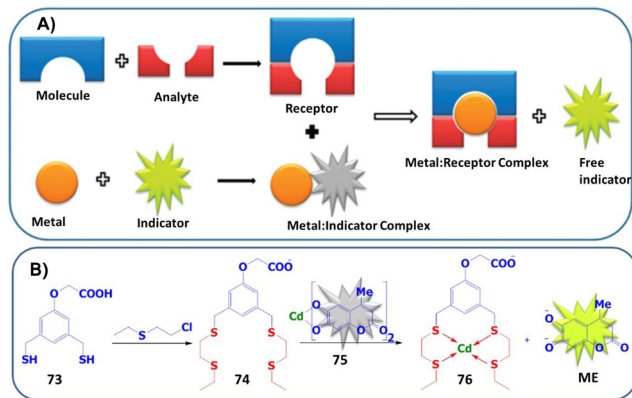


Fig. 50 (A) Pictorial presentation of the IDA approach for SM detection. (B) Schematic illustration of chemical sensor components for CEES detection. Reproduced with permission from ref. 201. Copyright (2013) American Chemical Society.

This is because nerve agents were rapidly hydrolyzed under these alkaline conditions (pH 9), and the less-reactive species, such as benzyl bromide and the bis-(2-chloroethyl)ether (BCEE), could not react under sensing conditions. The sensing ensemble was designed in such a way that it was directly implemented on bialkylating SM. Kumar *et al.* applied this same protocol to realize the selective and sensitive detection of SM.<sup>200</sup> However, in the present case, it is necessary to use capping agents to tame the ligating properties of thiolate anions of 73, particularly when SM is absent. As a result, it is necessary to cap the thiol before performing experimental analysis. This process makes this method somewhat cumbersome.<sup>201</sup>

Ongoing efforts by Anslyn and Kumar resulted in the exploitation of squaraine (SQ) dyes for the colorimetric and fluorescent detection of CEES<sup>203</sup> and SM in a basic methanolic solution.<sup>204</sup> Squaraine dyes are a class of organic dyes that have an intense blue color with an absorption maxima between 630–670 nm and a fluorescence emission between 650–700 nm. The central, electron-deficient, four-membered ring is well-known to be susceptible to nucleophilic attack, which leads to its decolorization (Fig. 51(B)). In this approach, dithiol 73

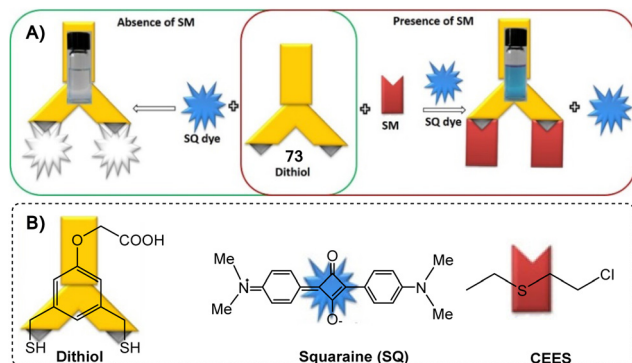


Fig. 51 (A) Pictorial representation of a chemodosimeter approach for SM detection. (B) Chemical structure of the species involved in CEES sensing. Reproduced with permission from ref. 203. Copyright (2017) Royal Society of Chemistry.

was again used to react with CEES (and SM) and then exposed to SQ. If the blue color from SQ persists, this indicates the presence of SM. Alternatively, in the absence of CEES, 73 reacts with SQ, resulting in a color change from blue to colorless (Fig. 51). This sensing scheme was further extended by Kumar and co-workers for SM detection.<sup>202</sup> Taking advantage of the visual detection of SM, the method was further explored for on-site detection by analyzing the sample in various matrices (soil and surface).

Pardasani and co-workers reported the rhodamine-6 G-based chemosensor, 77, for the detection of SM and NM in methanol/chloroform (4 : 1). In this design, thioamide functionality was used for the selective recognition of SM and NM (Fig. 52).<sup>205</sup> The *S*-alkylation of the thioamide functional group induced ring-opening of spirolactam, affording a simultaneous increase in absorption at 520 nm and fluorescence emission at 566 nm. This fluorescence response was observed between 15–60 min at room temperature and within 3 min at 60 °C. The selectivity of 77 was demonstrated against various alkyl halides, such as butyl iodide, butyl bromide, and BCEE.

Using a similar design concept, Wang and co-workers reported a benzothiazole-functionalized rhodol with SM-reactive thioamide functionality (78) for the chromo-fluorogenic detection of SM in methanol (Fig. 53).<sup>206</sup> Rhodol can be seen as a hybrid between rhodamine and fluorescein.<sup>207</sup> Similar to rhodamine and fluorescein, rhodol (in the presence of appropriate external stimuli) can undergo spirocyclic ring-opening to form the highly fluorescent quinoid form. In the presence of SM, the solution of 78 changed from colorless to fuchsia. The reaction between SM and 78 was shown to induce ring-opening, which was found to be faster than the rhodamine-based sensor (20 min vs. 60 min). The authors attributed this rapid response to the benzothiazole-mediated ESIPT, where intramolecular proton transfer generated the photoinduced structural transformation of rhodol from the

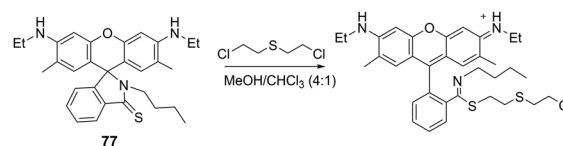


Fig. 52 The sensing mechanism of 77 for SM in methanol/chloroform (4 : 1).

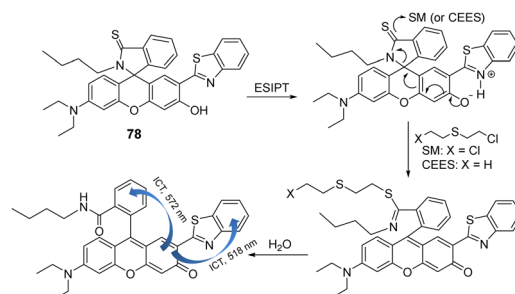


Fig. 53 The sensing mechanism of 78 for CEES and SM in methanol.



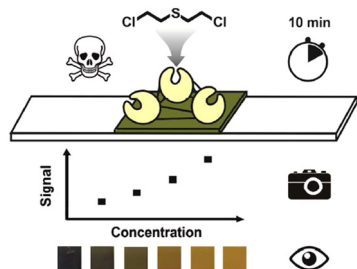


Fig. 54 Pictorial representation of photographic detection and quantitation of SM in the vapor phase. Reproduced with permission from ref. 208. Copyright (2016) American Chemical Society.

phenol form to the quinoid form. At room temperature and 60 °C, optical responses were observed within 25 min and 3 min, respectively. The selectivity was superior over alkyl halide, an oxygen analog of SM, and strong electrophiles (such as benzoyl chloride). Probe **78** was further used for the detection of SM in solution, soil, and air at ambient temperature, indicating its potential application for the on-site detection of SM.

Wolfbeis and co-workers developed enzyme-based test strips for the visual/photographic detection and quantification of SM vapor (Fig. 54).<sup>208</sup> This strategy relies on the use of the enzyme haloalkane dehalogenase as a biorecognition element. This enzyme is known to degrade SM spontaneously into non-toxic thiodiglycol, chloride ions, and a proton. Using pH indicators present in the test strips, this change can be directly visualized from a color change of blue-green to yellow within 10 min. A quantitative readout was achieved using a conventional digital camera based on red-green-blue data acquisition. Selectivity was seen over 1,2-dichloroethane and ethyl bromoacetate, and excellent sensitivity was observed, especially at 0.01 ppm (for visual detection) and at 0.003 ppm (for red-green-blue readout). These results make this approach extremely valuable as the strips are disposable, fairly rapid, and cost-effective for field use.

In 2017, the mercaptomethylphenyl-modified tetraphenylethene (TPE) probe **79** was developed by Wang and co-workers for CEES detection in an aqueous solution (Fig. 55).<sup>209</sup>

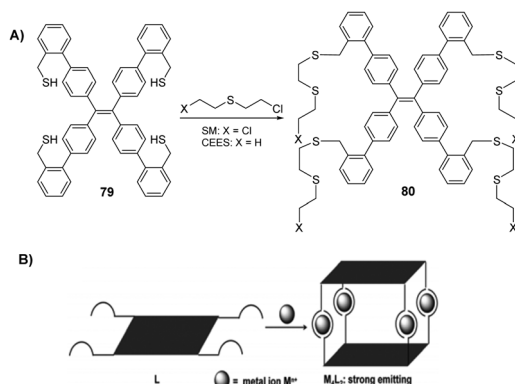


Fig. 55 (A) The sensing mechanism of **79** for CEES and SM in an aqueous solution. (B) Its schematic presentation. Reproduced with permission from ref. 209. Copyright (2017) Royal Society of Chemistry.

The authors developed a mercaptomethylphenyl-modified tetraphenylethene probe that was allowed to react with CEES to form a sulfur-based podand with four open chains, *i.e.*, 1,1,2,2-tetrakis(20-(ethylthio)propyl-[1,10-biphenyl]-4-yl)-ethene (**80**). These two staggered sulfur-based chains ligate with thiophilic metal ions, such as ( $\text{Hg}^{2+}$  and  $\text{Cd}^{2+}$  ions, form sandwiched structures). Such face-to-face molecular stacking eventually restricts the rotation of the phenyl rings of TPE. This process results in a fluorescence enhancement, leading to a selective fluorescence turn-on detection of SM simulants like CEES. The procedure shows high sensitivity (1.10  $\mu\text{M}$ ) and good selectivity over butyl iodide, butyl bromide, BCEE, and 2-chloroethyl ether.

Kumar and co-workers developed probe **81** for the detection of SM in methanol. In this design, **81** incorporated the nucleophilic thioketone (thione) unit to interrupt the conjugation of the acridine orange (AO) dye scaffold (Fig. 56).<sup>210</sup> **81** reacted with SM *via* the thione unit to afford the conjugated AO derivative with a change in turn-on response. The selectivity for SM over sarin, soman, tabun, VX, oxygen mustard, benzyl bromide, ethyl iodide, and HCl was achieved by fine-tuning the reaction conditions where methanolic potassium hydroxide acts as a base and was used to destroy any additional reactive interference. The detection is achieved within one minute, affording a color change from yellow to orange (443 nm to 502 nm) and a fluorescence change from green to yellow (518 nm to 555 nm) in less than a minute at 60 °C.<sup>210</sup> To assess the feasibility of using **81** for real-time analysis of SM, soil samples, swab samples, and a kit for on spot the detection were used. **81**-coated test strips displayed no response, even with organic solvents, acids, and bases. This method was highly sensitive when using chromogenic and fluorogenic techniques with calculated LODs of 0.02 mg (0.3 mM) and 0.005 mg (7.5  $\mu\text{M}$ ), respectively, which is the safe value (0.02 mg) to cause any blister on human skin.

A similar approach was developed by Tian and co-workers, in which the pyronin-based fluorescent probe **82** was capable of detecting an SM simulant with concentrations as low as 0.6  $\mu\text{M}$  (in solution phase) and 0.25 ppm (in gaseous phase); these are below the AGEL-1 level of SM (Fig. 57).<sup>211</sup> The *S*-alkylation of **82** with CEES was shown in DCM, which resulted in the formation of a highly fluorescent thiopyronin derivative ( $\lambda_{\text{em}} = 570 \text{ nm}$ ,

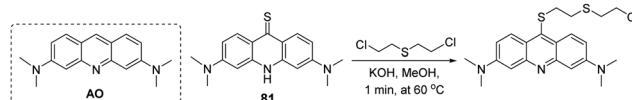


Fig. 56 The sensing mechanism of **81** for SM in methanol.

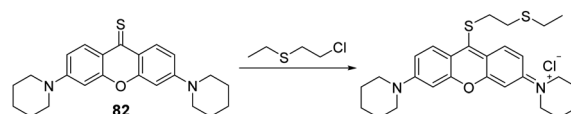


Fig. 57 The sensing mechanism of **82** for CEES in DCM.





850-fold turn-on) with a marked shift in absorption from 445 nm to 567 nm. Excellent selectivity was seen for CEES over other interfering substances with similar reactivities, such as nerve agent's simulants (DCP and DCNP), acylating agents, an alkylating agent (ethyl iodide), and sulfur-containing compounds. An **82**-treated TLC plate was developed and exposed to the vapor of CEES, which showed marked contrast in the color and fluorescence brightness (under illumination with 365 nm UV light) to those of the plate before the 2-CEES vapor treatment.

Broome and co-workers reported a new strategy that uses a pyrene functionalized with a salicylic acid tether (**83**) to enable the selective detection of alkylating agents, such as methyl iodide (MeI), in a mixed PBS (phosphate-buffered saline) buffer (9 : 1 PBS/DMSO (v/v)) (Fig. 58).<sup>212</sup> Initially, **83** was found to be weakly emissive. However, upon alkylation of the carboxylic acid with MeI, a 1000-fold increase in the fluorescence emission at 475 nm was observed. The mechanism of detection was proposed to be FRET-based, in which salicylic acid and pyrene act as FRET acceptors and FRET donors, respectively. The esterification resulting from alkylation by MeI turns on the fluorescence at 475 nm. The sensing is realized within 48 h (at 40 °C) or within 30 min at 90 °C using tetrabutylammonium iodide (Bu<sub>4</sub>NI) as a phase-transfer catalyst. Along with CW detection, the protocol was also implemented for the analysis of alkyl bromides and iodides, diazomethane, and their derivatives, as well as for pharmaceutical compounds like anticancer drugs, busulfan, and pipobroman (Fig. 59). Interestingly, **83** was the first probe of its kind to use oxygen as the nucleophile recognition unit; most sensors rely on either tertiary nitrogen or sulfur nucleophiles.

Fluorescent probes with absorption and emission in the near-infrared region (650–900 nm) are more attractive for biological applications, as it permits deeper tissue penetration, low background interference, and low phototoxicity.<sup>213</sup> One of the most notable reports on the NIR detection of SM was developed by Cao, Li, and Xiao. Among the series of reported fluorescent probes (**84–87**) (Fig. 60), **87** afforded the best response for SM combined with excellent selectivity.<sup>214</sup> The

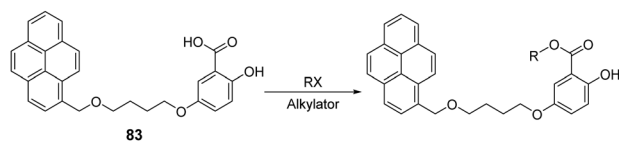


Fig. 58 The sensing mechanism of **83** for alkylating agents, such as methyl iodide, in a mixed phosphate-buffered saline buffer (9 : 1 PBS/DMSO (v/v)).

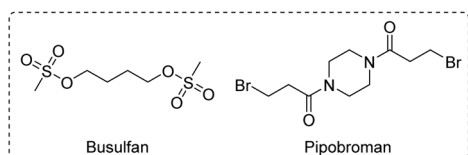


Fig. 59 Chemical structure of anticancer drugs.

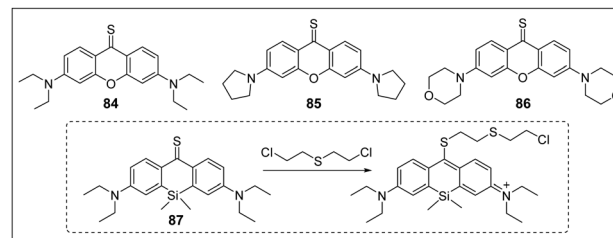


Fig. 60 The sensing mechanisms of **84–87** for SM.

reaction of **84–86** and **87** with SM produced fluorescence responses at 600 nm and 690 nm in 25–60 min and 10 min, respectively. The developed sensing systems were tested for SM selectivity against other interfering substances, such as nerve gas mimics, sulfur-containing compounds, inorganic compounds, alkylating agents, and hydrochloric acid, all of which did not lead to a change in fluorescence intensity. To provide new insights into SM-mediated injury, **87** was successfully applied to image SM distribution in live cells (HaCaT cells), and SM was found to accumulate in the mitochondria (Fig. 61). Examples like **87** can be used as tools for the study of SM in biological samples.

Che and co-workers reported the chemical sensor **88** for the simultaneous detection and differentiation of a sulfur mustard simulant (CEES) and DCP in the vapor phase (Fig. 62). This approach used nanofibers that were co-assembled with **88** and **89**; through FRET, the photostability and fluorescence emission at 466 nm were enhanced.<sup>215</sup> Upon exposure to DCP and CEES, fluorescence quenching occurred due to the formation of a complex between DCP or CEES and **88**. This acts as an exciton trap to compete with FRET, thereby decreasing the emission. Additionally, combining **88** with **89** in nanofibers results in competitive CEES binding providing distinct fluorescence response, thereby facilitating the detection of DCP and CEES. The probes exhibited excellent selectivity for DCP and CEES against other test substrates, including DCNP, HCl, DMMP, common organic solvents, and water. The LOD for CEES was 0.3 ppm, which is among the lowest values ever reported.

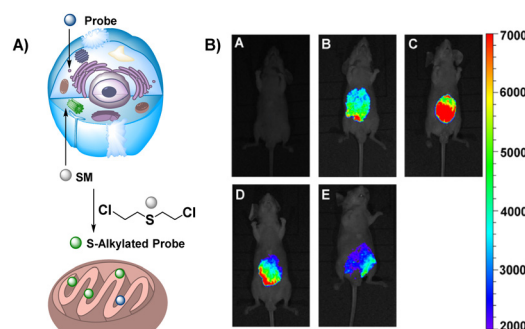


Fig. 61 (A) Possible fluorescence mechanism of **87** concentrated in the mitochondria. (B) Representative fluorescent images for visualizing sulfur mustard levels in living SKH-1 mice using SiNIR-SM. Reproduced with permission from ref. 214. Copyright (2019) American Chemical Society.



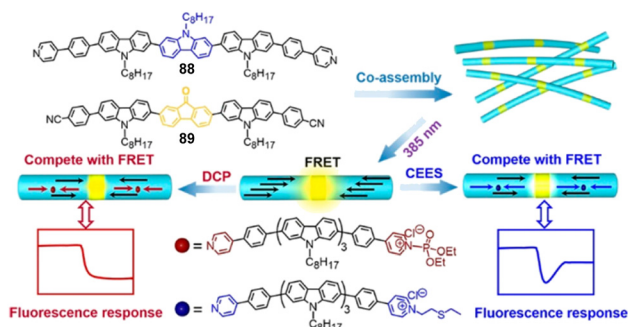


Fig. 62 Schematic representation of the fluorescence detection and discrimination of DCP and CEES using the coassembled nanofibers with **88** and **89** in the vapor phase. Reproduced with permission from ref. 215. Copyright (2019) American Chemical Society.

In an important development, rather than using a nucleophilic reaction for SM detection, Che and co-workers reported the ability to detect SM based on noncovalent interactions (sulfur- $\pi$  and dipole-dipole interactions), thus affording desirable reversibility.<sup>216</sup> The systems include hierarchical microspheres assembled from fluorene-based oligomer **90** or two fluorene-based oligomers (**90** and **91**) resulting in sensitive fluorescence detection of SM vapor (30 ppb) (Fig. 63). The responses of the systems were evaluated in terms of their fluorescence response with SM and interferences.

Recently, Gall and co-workers explored a different approach using a FRET-based fluorescent probe (**92**) for the detection of reactive alkylating agents, such as CEES and alkyl halides, in DMSO/H<sub>2</sub>O (9:1) (Fig. 64).<sup>217</sup> The chemosensor contains a fluorophore and a quencher linked using a reactive spacer; upon reaction with CEES, the sample degrades to release the coumarin fluorophore, leading to an increase in the fluorescence signal at 477 nm. In probe **92**, a nucleophilic tertiary amine reacts with electrophilic alkylating agents, to generate a tetraalkylammonium cation. In water elimination and

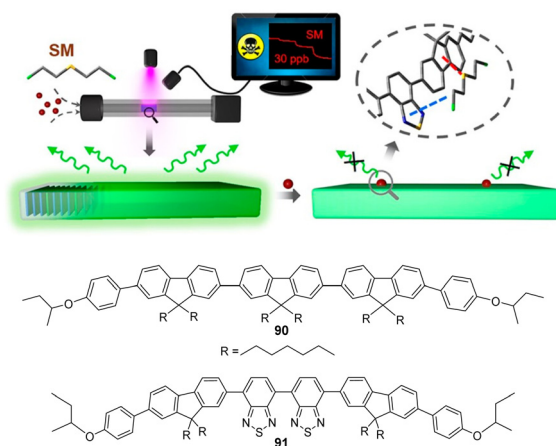


Fig. 63 Schematic representation of the fluorescence detection of SM using hierarchical microspheres of fluorene-based oligomers (**90**) and (**91**) in the vapor phase. Reproduced with permission from ref. 216. Copyright (2019) American Chemical Society.

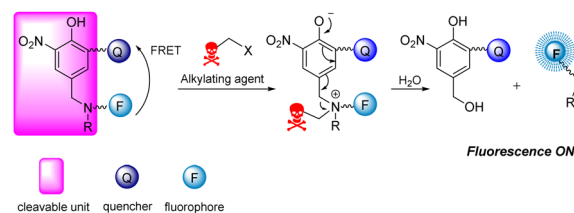


Fig. 64 General presentation of FRET-based fluorescent sensing of alkylating agents.

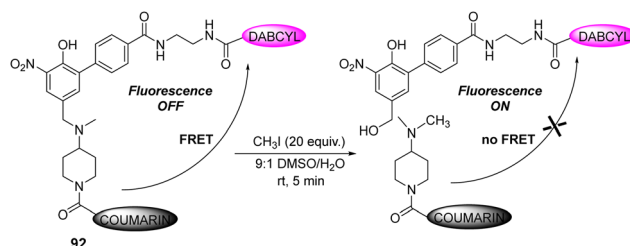


Fig. 65 The FRET-based sensing mechanism of **92** for methyl iodide.

separation of the quencher and fluorophore occurs (Fig. 65). In the probe, coumarin is employed as a fluorophore whose fluorescence is quenched by DABCYL (4-(dimethylaminoazo)-benzene-4-carboxylic acid) (*i.e.*, a quencher). The beauty of these techniques lies in their ability to detect not only SM simulants but also nitrogen mustard. Turn-on fluorescence was demonstrated with several alkyl halides over related interfering substances, like epoxides. The limit of detection for CEES was calculated to be 2.3 mM.

In 2021, Kumar's group designed and developed an innovative protocol that employed luminol as a receptor and a fluorescence reporter for the detection of SM in a bicarbonate buffer (pH = 8.5) (Fig. 66).<sup>218</sup> The identified reaction conditions needed to afford a response between **93** and SM used ionic liquid and water in an optimized concentration (0.31 M). The ionic liquid *viz.* 1-ethyl-3-methylimidazolium dicyanamide ([emim][DCA]) not only enhanced the nucleophilicity of **93** by abstracting its enolic proton using a dicyanamide fragment but

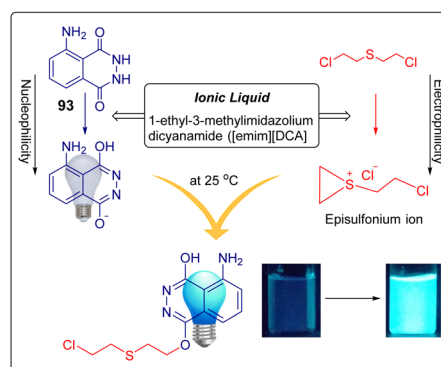


Fig. 66 Schematic illustration of chemical sensing based on luminol (**93**) for SM. Reproduced with permission from ref. 218. Copyright (2021) American Chemical Society.



also stabilized the intermediate ion (episulfonium ion) of SM with the help of its positive counterpart, *i.e.*, 1-ethyl-3-methylimidazolium. The combination of luminol and the ionic liquid in water exhibited a turn-on fluorescence response at 420 nm for SM within seconds with a sensitivity of 6 ppm. No interferences from reactive and non-reactive species were observed; these included nerve agents, reactive electrophilic agents, BCEE, benzyl bromide, and diethyl sulfide. In order to make the method field-deployable, a chromogenic response was attained by using a high concentration of **93**. Significantly, the analysis of environmental samples, swab samples, and vapor phase detection can pave the way for the development of miniaturized, portable, and cost-effective chemosensor kits that can be used in the field and at strategic locations, such as airports and subways.

Based on an IDA 'proof of concept' approach, Beer and co-workers developed and evaluated a turn-on fluorescent sensor for SM detection (Fig. 67). In this study, a dansyl fluorophore was ligated to gold nanoparticles (AuNPs) *via* imidazole and amine groups.<sup>219</sup> The authors hypothesized that the displacement of the nitrogen of imidazole or amine, with the relatively soft sulfur donors present in SM/CEMS, release the dansyl fluorophore and affords a fluorescent response. The initial non-fluorescent conjugate is the result of an energy transfer process due to the proximity of functionalized fluorophores to a gold nanoparticle; this is attributed to through-space relaxation by nano surface energy transfer (NSET). Both AuNPs exhibited a weak fluorescence from the ligated dansyl group with emission maxima around 500 nm. The addition of the CEMS or SM produced a significant increase in the fluorescence intensity, which is due to the distance, dependent nature of the non-radiative processes. The response between both nanoparticles and analytes was almost instant and was complete within five minutes. Notably, analogous interfering agents, such as octanol and di-*n*-butyl ether, gave no significant fluorescence increase. Based on the SPECFIT analysis, the association constants between the host and guest were  $\log K = 4.65 \pm 0.06$  and  $\log K = 4.19 \pm 0.05$  for CEMS and SM, respectively.

Dubey and co-workers exploited microfluidic paper-based analytical devices, *i.e.*,  $\mu$ -PADs, for the detection of blister

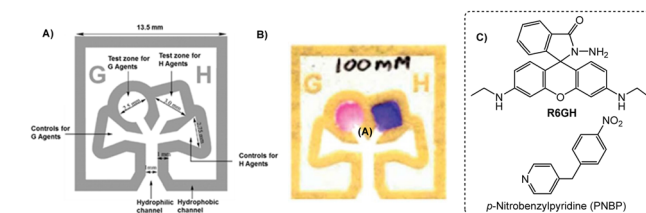


Fig. 68 (A) Design of  $\mu$ -PAD for the simultaneous detection of nerve agents and blister agents. (B) Colorimetric responses with sarin and SM (100 mM) on the  $\mu$ -PAD. (C) Chemical structures of the dyes used. Reproduced with permission from ref. 220. Copyright (2012) Royal Society of Chemistry.

agents along with nerve mimics by utilizing well-established chemistry (Fig. 68).<sup>220</sup>  $\mu$ -PADs are cellulose fiber networks possessing several advantages, such as very low cost, power-free application, portability and disposability, compatibility with a small volume of samples, and easy operation and construction. They are generally used for point-of-care diagnosis, biosensing, environmental monitoring, biomedical and pharmaceutical analysis, clinical diagnosis, and forensic investigations. In this study, a tree-shaped  $\mu$ -PAD with one central channel and four test zones was designed. Out of the four test zones, two test zones were used for blister agents and nerve agents, respectively, and two were used for their respective controls. The detection of blister agents was based upon their reaction with para-nitrobenzyl pyridine in the presence of a base, which generates an intense purple/blue ionic product. The reaction of R6GH with nerve agents generated a fluorescent red/pink color. SM, NM, and nerve agents exhibited LOD values of 100  $\mu$ M, 1 mM, and 2.5 mM, respectively.

Suryanarayana and co-workers developed molecularly imprinted polymers (MIPs) and evaluated them for the recognition of SM.<sup>221</sup> Methacrylic acid, ethylene glycol dimethacrylate, and 2,2-azobisisobutyronitrile were polymerized in the presence of SM (Fig. 69). After the formation of SM-bonded polymers, SM was removed with the help of methanol, which formed an SM-imprinted site that is very specific to SM binding. A non-imprinted polymer (NIP) was similarly synthesized in the absence of SM. The SM-imprinted polymer exhibited a higher surface area than the control NIP. Enhanced SM binding to the MIP, when compared to the NIP, was observed with an

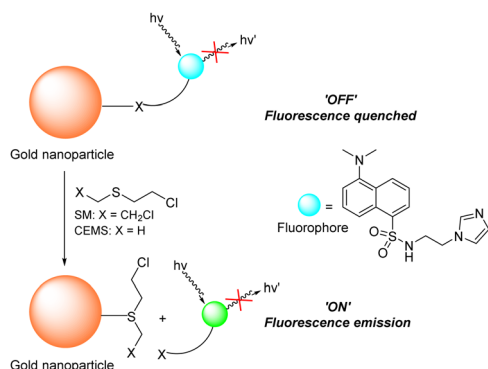


Fig. 67 The sensing mechanism of dansyl-fluorophore-ligated gold nanoparticles for SM/CEMS.

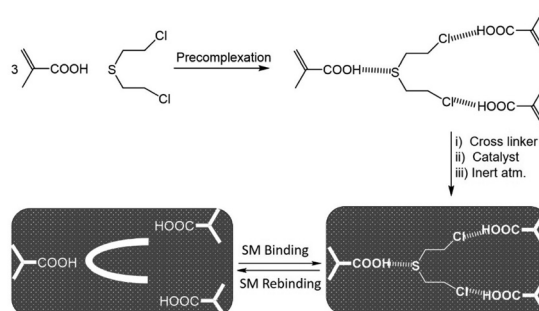


Fig. 69 The schematic representation of MIP-based sensing of SM.



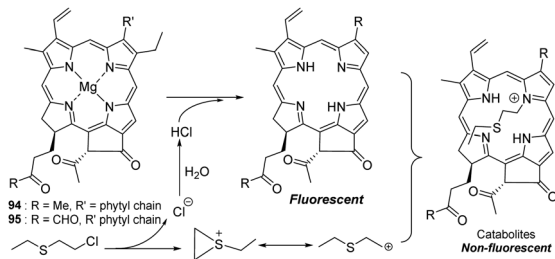


Fig. 70 The sensing mechanism of a fluorimetric biosensor for CEES.

imprinting efficiency ( $\alpha$ ) of 1.3. No interference was observed with SM MIP from BCEE.

Singh and co-workers reported an ultrasensitive fluorimetric biosensor for CEES using chlorophyll derivatives **94** and **95** (Fig. 70).<sup>222</sup> In the presence of CEES, the chlorophyll fluorescence at 673 nm was quenched, which was attributed to the conversion of chlorophyll into its degradation products (as suggested by high-performance liquid chromatography profiles).<sup>222</sup> This biosensor was found to be ultrasensitive with a LOD of  $7.68 \times 10^{-10}$  M.

Li and co-workers demonstrated the efficient encapsulation of SM and its simulants by per-ethylated pillar[5]arene (**96**) for the recognition of SM (Fig. 71).<sup>223</sup> **96** exhibited strong binding affinity toward analytes in solution, as well as in the solid-state. The interaction between the host and guest was established using NMR spectroscopy. It was determined that the binding constant ( $K_a$ ) between SM and the host was  $(6.2 \pm 0.6) \times 10^3$  M. In the complex,  $\text{CH}_2\text{-Cl}$  protons of SM provide a very large upfield shift ( $\delta$ : 0.42 ppm), while protons from **96** exhibit downfield shifts ( $\Delta\delta$  = 0.26–0.30 ppm) due to de-shielding effects. XRD studies revealed the 1 : 1 inclusion complex, which is driven by multiple  $\text{C-H} \cdots \pi\text{Cl/S}$  and  $\text{S} \cdots \pi$ -interactions. The complex was found to be stable for more than six months in an exposed environment. This type of encapsulation of SM would be extremely beneficial in designing and developing materials for the detection and decontamination of CW agents and other toxicants.

Bowman-James and co-workers studied a series of amide-based palladium(II) pincer complexes (**97**) coordinated with a solvent ( $\text{CH}_3\text{CN}$ ) for the recognition of CEES (Fig. 72).<sup>224</sup>  $^1\text{H}$  NMR spectroscopy and X-ray crystallography confirmed the binding of CEES with palladium(II) pincer complexes, replacing the  $\text{CH}_3\text{CN}$  with CEES. The soft nature of the palladium and sulfur atoms may account for the high affinity of the

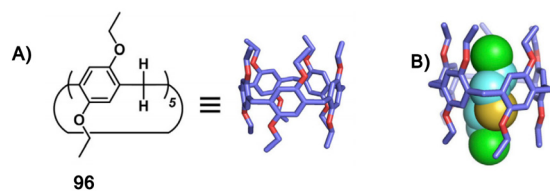


Fig. 71 Schematic illustration of (A) the per-ethylated pillar[5]arene host (**96**) and (B) single-crystal structures of host–SM complexes. Reproduced with permission from ref. 223. Copyright (2020) The Author(s).

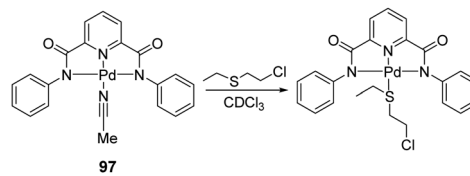


Fig. 72 Scheme for the sensing mechanism of **97** for SM.

palladium complexes for CEES, as compared to the solvent. The crystal structure analysis revealed that the CEES molecule is shielded by aromatic walls of the aromatic ring, and data suggest that Pd–N1 distances are longer for the mustard structures by about 0.02 Å compared to the acetonitrile complexes. The effect of phenyl rings with various substitutions and with larger aromatic rings was systematically studied, revealing that substitution at the phenyl ring does not significantly affect the binding interaction. However, larger aromatic rings produced a significant increase in binding, possibly due to increased steric and electronic interactions. An NMR investigation revealed that the coexistence of *cis*- and *trans*-stereoisomers, corresponding with the two sides of the naphthalene rings oriented in the same (*cis*) or opposite (*trans*) direction. It is believed that the molecular wall effect due to the presence of aromatic rings appended perpendicular to the pincer plane observed with the mustard surrogate may lead to new applications, such as chemosensing, separation applications, and molecule/ion transport.

Astruc and co-workers reported bifunctional 1,2,3-triazole derivatives with polyethylene glycol (PEG) (**98**) chain and a fluorescent dye (coumarin), which exhibit fluorescence in the presence of CEMS (2-chloroethyl methyl sulfide).<sup>225</sup> When combined with AuNPs, this ensemble (containing 1,2,3-triazole derivatives, the polyethylene glycol (PEG) (**98**) chain, and a fluorescent dye) loses fluorescence due to the formation of triazole–AuNPs. Through a ligand-displacement process, CEMS was able to turn on the fluorescence ( $\lambda_{\text{max}}$  = 472 nm) by displacing the AuNPs from a quenched complex of triazole–AuNPs, indicating the presence of the analyte (Fig. 73).

A pyridine-appended Mg–porphyrine complex (**99**) was designed by Gupta and co-workers to perform molecular logic operations for the optical detection of CEES in  $\text{CHCl}_3/\text{CH}_3\text{OH}$  (5 : 1, v/v) (Fig. 74).<sup>226</sup> The interaction of **99** with CEES leads to the perturbation/reduction in absorbance of the Q-band of **99**.

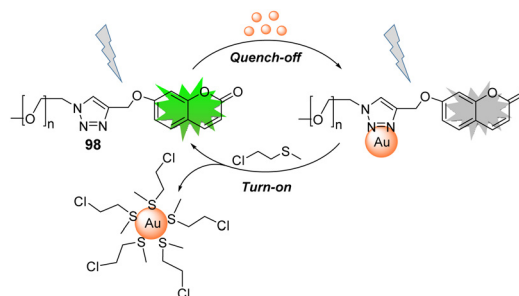


Fig. 73 The sensing mechanism of sensing ensemble **98** for CEES.





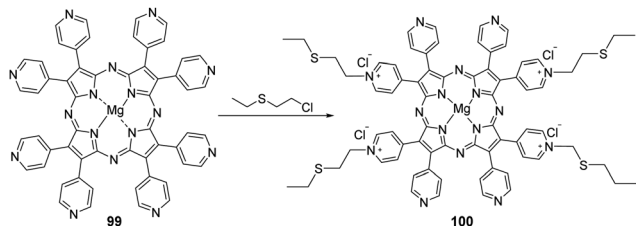


Fig. 74 The sensing mechanism of **99** for CEES in  $\text{CHCl}_3/\text{CH}_3\text{OH}$  (5 : 1, v/v).

Treatment of the probe-CEES complex (**100**) with  $\text{KMnO}_4$  solution resulted in the reappearance of the Q-band (634 nm) of **99** and allowed the probe to be reused after a simple filtration step. This reversible sensing setup allowed for the creation of a platform that can generate different input-based combinatorial and sequential molecular logic gate(s).

Xi and co-workers developed the chemical probe *N*-(rhodamine-B)-thiolactam-2-*n*-butane (**101**), in which rhodamine and thiourea moieties played the roles of chromogenic and reactive groups, respectively (Fig. 75).<sup>227</sup> The sensing ensemble with an SM simulant generated a chromo-fluorogenic response with the emergence of new absorption peaks at 560 nm and new emission peaks at 583 nm in the presence of the ionic liquid 1-butyl-3-methylimidazolium dicyandiamide ([BMIm]DCA). Owing to the better solubility of CEES in the ionic liquid (132.5%, w/w), the reaction between the probe and CEES was very rapid; it took place in 1 min at room temperature. Generally, this reaction takes place at an elevated temperature.

In the next development, Li and co-workers described the design, synthesis, and application of a selective and sensitive turn-on fluorescent probe (**102**) (Fig. 76) for SM detection in living cells (HT-22 cells) and whole animals (*Aurelia coerulea* polyps).<sup>228</sup> A simple alkylation of the **102** by SM in the natural environment ( $\text{H}_2\text{O}$ ) leads to the formation of the fluorescent product with the emergence of an emission peak at 525 nm that indicates the presence of SM. The basic objective of the present study was to visualize the presence of intact SM in living cells and whole animals.

In 2021, Song *et al.* reported a similar fluorescent probe **103** that undergoes *S*-alkylation with CEES in ethanol. 4-Mercaptocoumarin-based chemical probes can detect blister agents (CEES, SM, and NH1) in both solution and vapor forms within five minutes (Fig. 77).<sup>229</sup>

The next development was by Abuzalat and Kim's group who demonstrated the facile and trace-level detection of CEES using a fluorescein-encapsulated metal-organic framework (F@Zr-BTC) sensory material (Fig. 78).<sup>230</sup> The fluorescein dye was

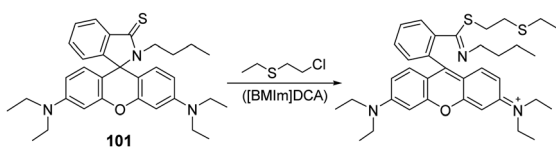


Fig. 75 The sensing mechanism of **101** for CEES in 1-butyl-3-methylimidazolium dicyandiamide as an ionic liquid.

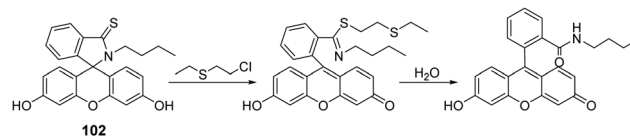


Fig. 76 The sensing mechanism of **102** for CEES.

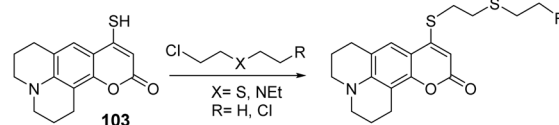


Fig. 77 The sensing mechanism of **103** for CEES (X = S; R = H), SM (X = S; R = Cl), and NH1 (X = S; R = H).

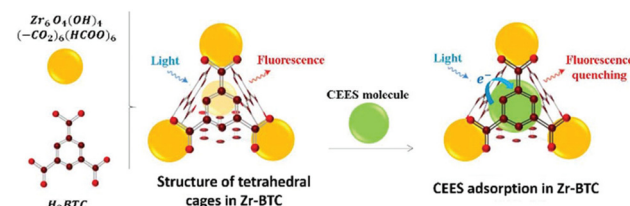


Fig. 78 The sensing mechanism of the fluorescein-encapsulated metal-organic framework for CEES in ethanol. Reproduced with permission from ref. 230. Copyright (2021) Royal Society of Chemistry.

encapsulated within the internal voids (with aperture diameters of 14 and 18 Å, respectively) of a Zr-based MOF using an *in situ* guest encapsulation method, resulting in enhanced fluorescence. When F@Zr-BTC was exposed to CEES, drastic fluorescence quenching at an emission wavelength of 534 nm occurred. This was attributed to the fact that the electron-deficient properties of the fluorescein affects the electronic interaction between CEES and F@Zr-BTC. Through an adsorptive phenomenon, there is a donor-acceptor electron transfer mechanism between CEES (electron donor) and F@Zr-BTC (electron acceptor), lowering the fluorescence intensity. The fluorescein present inside the Zr-BTC voids accepts the electrons from CEES. This sensing material also shows good selectivity to CEES, as compared to other analytes containing sulfur-like 2-mercapto ethanol, and  $\text{H}_2\text{S}$  and DMMP.

In recent years, wearable electrochemical sensors have received great attention owing to their applicability, flexibility, portability, and biocompatibility. They also offer clinical monitoring of a patient at hospitals and personalized care at home.<sup>231</sup> Arduini and co-workers realized the first wearable electrochemical biosensor for the on-site detection of SM and NM by exploiting paper-based, origami-like devices (Fig. 79).<sup>232</sup> The detection was performed by monitoring the inhibitory effects of each agent on choline oxidase enzyme (ChOx), through the amperometric measurement of hydrogen peroxide (*i.e.*, the enzymatic by-product). A nanocomposite of carbon black/Prussian blue (CB/PBNP) was used as a bulk modifier for conductive graphite ink, which constituted the working



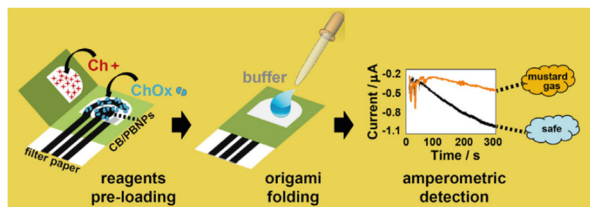


Fig. 79 Pictorial representation of origami-like devices based on an electrochemical sensor for SM and NM. Reproduced with permission from ref. 232. Copyright (2019) Elsevier B.V.

electrode. The sensing tool represents a critical point within the security field to provide early alarm systems.

**4.2.2 Detection of nitrogen mustard.** They may not be a separate method for the optical detection of NM. However, it has been chromo-fluorogenically detected along with SM. Pardasani's group described the detection of NM using a rhodamine 6G-based chemodosimeter.<sup>205</sup> Gall<sup>217</sup> and co-workers also utilized a FRET-based fluorescent probe for the detection of NM along with SM. Song *et al.* demonstrated NM detection using 4-mercaptocoumarin-based chemical probes.<sup>229</sup> In their SM sensing strategy, Arduini and co-workers also implemented a wearable biosensing technique for NM detection (as described previously).<sup>232</sup>

**4.2.3 Detection of Lewisite.** The first approach developed for the optical detection of a Lewisite simulant, *i.e.*, AsCl<sub>3</sub>, occurred in 2016. Taking advantage of the thiophilic characteristics of arsenic species, Hong and co-workers established a fluorescence sensor using a coumarin-based probe appended with bis(2-mercaptoethyl)amine (**104**) (Fig. 80).<sup>233</sup> **104** was shown to bind with AsCl<sub>3</sub>. This resulted in fluorescence quenching at  $\lambda_{\text{max}} = 445 \text{ nm}$ , which was attributed to the heavy atom effect. Other metal ions, including thiophilic metals such as Hg<sup>2+</sup>, Ag<sup>+</sup>, Cu<sup>2+</sup>, Fe<sup>2+</sup>, Zn<sup>2+</sup>, Pb<sup>2+</sup>, and Cd<sup>2+</sup> (in large excess), did not induce any optical change in the probe, thus showing good selectivity. The estimated limit of detection using  $3\sigma/\text{slope}$  was  $1.34 \times 10^{-6} \text{ M}$  ( $1.34 \mu\text{mol kg}^{-1}$ ), which is much less than the LD<sub>50</sub> of Lewisite ( $145 \mu\text{mol kg}^{-1}$ ). This method is effective from pH 4 to 9. Therefore, HCl being produced as a by-product of AsCl<sub>3</sub> detection did not significantly influence the fluorescence change.

### 4.3 Fluorescent and colorimetric chemosensors for detection of blood agents

**4.3.1 Detection of hydrogen cyanide.** Blood agents are mainly cyanogen chloride and hydrogen cyanide. To the best of our knowledge, there is no optical sensing method reported

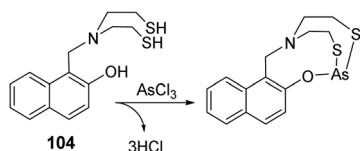


Fig. 80 The sensing mechanism of **104** for a Lewisite simulant, such as arsenic trichloride.

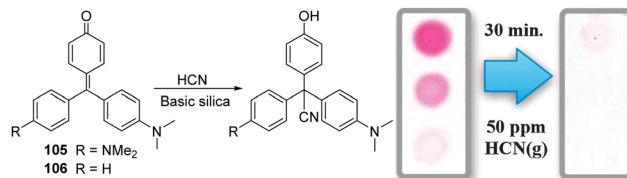


Fig. 81 The sensing mechanism of **105** and **106** for HCN. Reproduced with permission from ref. 234. Copyright (2013) Royal Society of Chemistry.

thus far for the detection of cyanogen chloride. However, hydrogen cyanide has been detected by several chromo-fluorogenic strategies. Martínez-Máñez explored triphenyl-methane-based chemodosimeters (**105** and **106**) for the visual detection of HCN gas (Fig. 81).<sup>234</sup> The nucleophilic addition of cyanide to the electron-deficient carbon atom of the probe results in a colorimetric response. The authors observed a similar color response with CN<sup>−</sup> and HS<sup>−</sup> for **105** and **106**. The probes displayed reasonably good selectivity over H<sub>2</sub>S, NH<sub>3</sub>, and HCl in the gas phase with a limit of detection of 2 ppm. Pre-adsorption of probe **105** with aminated basic silica test strips resulted in color changes when placed in a box containing HCN. Spots containing 5.00, 0.50, and 0.05 nM of **105** with HCN (50 ppm) after 20 min as shown in Fig. 81.

The detection of hydrogen cyanide gas along with the detection of cyanide in solution was realized by Song and co-workers using diethylaminoquinoline derivatives possessing dicyanovinyl substituents (Fig. 82).<sup>235</sup> The chemodosimeter (**107**) was allowed to react with HCN *via* a Michael addition reaction. A polyethylene oxide-based test strip loaded with **107** was used to selectively detect HCN gas at 60 ppm.

A paper-based sensor was fabricated using a cobinamide-based indicator for the detection of HCN gas (Fig. 83).<sup>236</sup> A piece of filter paper was impregnated with monocyanocobinamide [CN(H<sub>2</sub>O)Cbi]<sup>236</sup> (**108**) facilitating the detection of HCN within 10 s of exposure at concentrations as low as 5.0 ppm. Cobinamide (Cbi), a cobalt-centered hydroxocobalamin, has the ability to bind up to two cyanide (CN<sup>−</sup>) ions. At neutral pH in water, it exists as the mixed hydroxy-aquo complex, known as aquohydroxocobinamide. Upon interaction with HCN, it forms monocyanocobinamide (CN(H<sub>2</sub>O)Cbi) and then diacyanocobinamide [(CN)<sub>2</sub>Cbi]. The change from CN(H<sub>2</sub>O)Cbi to diacyanocobinamide [(CN)<sub>2</sub>Cbi] produces a significant color change from orange (510 nm) to violet (583 nm).<sup>236</sup> In the extension of the above studies, Greenawald *et al.* recently developed an RGB (red, green, blue) color sensor for HCN detection. A glass fiber filter paper was impregnated with

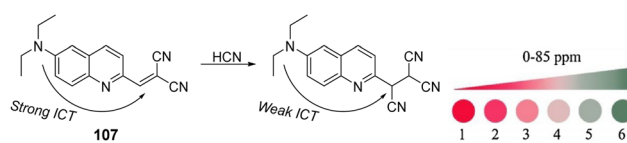


Fig. 82 The sensing mechanism of **107** for HCN. Reproduced with permission from ref. 235. Copyright (2018) Elsevier B.V.



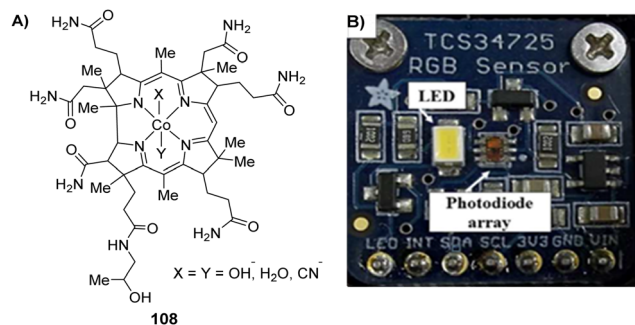


Fig. 83 (A) Chemical structure of probe **108** used for HCN detection. (B) RGB color sensor for HCN detection. Reproduced with permission from ref. 237. Copyright (2017) American Chemical Society.

CN(H<sub>2</sub>O)Cbi and placed above the RGB color sensor with on chip LED.<sup>237</sup> Exposing the paper circle to HCN gas, resulted in a rapid color change. The device is controlled by a microcontroller, which transforms data into real-time RGB readouts, thereby permitting rapid color change analysis.

Gupta's group reported a chemodosimeter (**109**) that showed a notable chromo-fluorogenic response to HCN gas, as well as to cyanide in solution and on a solid surface (Fig. 84).<sup>238</sup> The color response is generated due to the formation of an oxazole derivative from the reaction of **109** with HCN under slightly basic conditions (pH 8.5). The chemodosimeter detected HCN gas with a detection limit of 7 ppm, which is far below the dangerous limit.

#### 4.4 Fluorescent and colorimetric chemosensors for the detection of choking agents

**4.4.1 Detection of phosgene.** Apart from classical methods based on instrumentation and chemical techniques (see above), the detection of phosgene has also been achieved recently using electrochemical assays, enzyme-based methods, nanoparticles, carbon nanotubes, and other techniques. Exploiting the sensing strategies that are presented in Fig. 85, several groups have reported selective and sensitive chromo-fluorogenic sensors for phosgene detection. Broadly, these probes use ethylenediamine, *o*-phenylenediamine, oxime, *ortho*-aminophenols, or cinnamic acids recognition moieties that are connected to the fluorophore/chromophore covalently. Resulting in fluorescence quenching by blocking PeT or changes in the ICT characteristics.

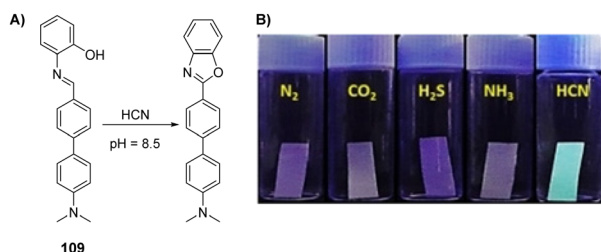


Fig. 84 (A) The sensing mechanism of **109** for HCN. (B) Sensing of gases (i.e., N<sub>2</sub>, CO<sub>2</sub>, H<sub>2</sub>S, NH<sub>3</sub>, and HCN) on cellulose paper strips containing **109**. Reproduced with permission from ref. 238. Copyright (2018) Wiley-VCH Verlag GmbH & Co. KGaA, Weinheim.

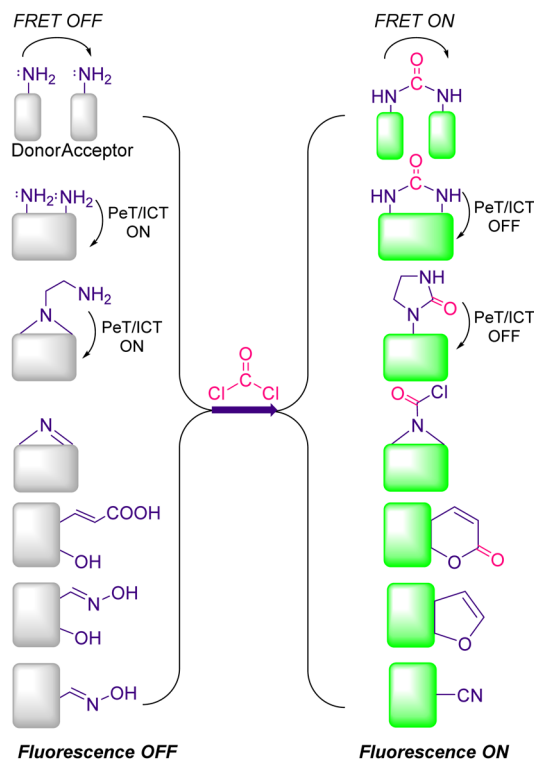


Fig. 85 General sensing mechanisms for phosgene.

After interaction with phosgene and intramolecular cyclization, the chemical probes impart a fluorescent response by converting non-fluorescent molecules into a highly fluorescent products. However, since Yoon<sup>124</sup> and Zheng<sup>239</sup> have recently summarized the literature on choking agent-responsive chemical probes, we will not discuss these reports in this review.

#### 4.5 Fluorescent and colorimetric chemosensors for the detection of toxins

**4.5.1 Detection of saxitoxin.** A strategy for the detection of saxitoxin (STX) was initially developed and popularized by the Gawley group. This strategy can be seen as analogous to fluorescent sensors for the detection of cations, where a fluorophore is linked to a recognition unit (e.g., crown ethers) *via* spacers (Fig. 86).<sup>240</sup> Similarly, STX inhibits PeT when bisguanidinium ions bind to crown ethers *via* ion-dipole interactions. Molecular probes (**110–116**) based on several fluorophores (anthracene, coumarin, acridine, and aza-BODIPY) and crown

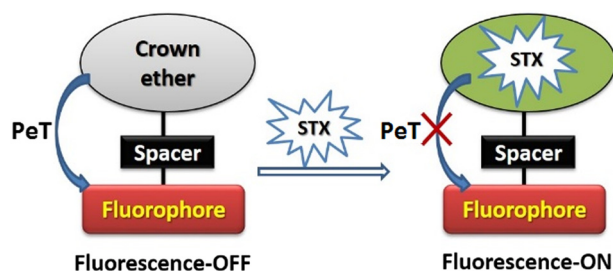


Fig. 86 General design of a PeT-based chemosensor for saxitoxin.



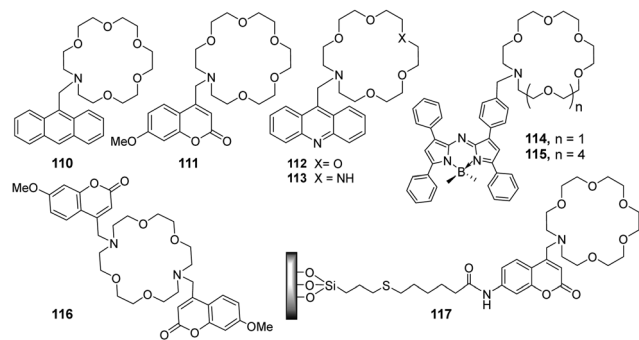


Fig. 87 Various chemical probes (**110–117**) used for the detection of saxitoxin.

ethers were designed and exploited for the detection of STX (Fig. 87).

Exploiting the fact that guanidiniums are known to bind with crown ethers, Gawley initially designed an anthracene-based crown ether (**110**) that was used for the fluorescence detection of STX with a binding constant of  $3.88 \times 10^3 \text{ M}^{-1}$  in ethanol.<sup>241</sup> This work was further advanced by evaluating a series of anthracene-based crown ethers (eleven derivatives) to analyze the effect of structural variations on binding and developing host derivatives that are suitable for incorporation into combinatorial libraries. The crown ethers exhibited good binding constant and higher selectivity over closely related interferents such as arginine, adenine, guanidinium ions, and *o*-bromophenol. In subsequent improvement, various sizes of crown ethers, *e.g.*, 15-crown-5, 18-crown-6, 21-crown-7, 24-crown-8, and 27-crown-9 were evaluated.<sup>242</sup> The study indicated that chemosensors with large crown ethers like 27-crown-9 are superior to previous probes for STX detection in terms of selectivity, sensitivity, and binding constant ( $2.29 \times 10^5 \text{ M}^{-1}$ ). Changing indicators from anthracenyl to a coumarin fluorophore leads to the selectivity of STX over  $\text{Na}^+$ ,  $\text{K}^+$ , and  $\text{Ca}^{2+}$  in aza crown ether-based chemosensors (**111**).<sup>243</sup> The main drive of the present research was to incorporate the spectral features of coumarin, such as large Stokes shifts (70–100 nm) and high quantum yields, into the STX chemosensor.

Tetrodotoxin (TTX), which is a guanidine-based neurotoxin, is another sodium channel blocker that binds with voltage-gated sodium channels and blocks the passage of sodium ions into the neuron.<sup>244</sup> The mouse bioassay failed to distinguish between STX and TTX due to similarities in the clinical symptoms of the two toxins.<sup>245</sup> The selectivity of STX over TTX was demonstrated by Gawley *et al.* using acridine-based crown ether chemosensors (**112–113**).<sup>246</sup> However, the binding constant was similar to that of the anthracenyl derivative, suggesting a similar interaction between the host and guest. Two chemosensors with 18-crown-6 (**114**) and 27-crown-9 rings (**115**) containing a boron azadipyrrin (a chromophore) were synthesized and evaluated by Gawley *et al.* for visual detection of STX.<sup>247</sup> The use of boron azadipyrrin dye was justified by the authors due to the fact that the azadipyrrin dye with absorption  $\lambda_{\text{ex}} = 650 \text{ nm}$  is remote from any absorption bands due to STX

(330 nm), thus reducing interference from the analyte. This is an improvement compared to previously developed probes based on coumarin (328 nm), acridine (350 nm), or anthracene (three bands from 360 to 390 nm). The visible sensor exhibits excellent sensitivity with LOD of  $40 \mu\text{M}$  for STX and 100% fluorescence enhancement, displaying 1:1 toxin/crown stoichiometry and binding constant at  $3\text{--}9 \times 10^5 \text{ M}^{-1}$ .

Similarly, Leblanc's group placed two coumarin moieties in a single crown ether chemosensor (**116**) and observed a slight blue shift (7 nm) that was attributed to the destabilization of the excited state of the fluorophore by the analyte.<sup>248</sup> The fluorescence spectroscopic results indicated two emission bands at 420 nm and 550 nm. The latter band is the result of the charge transfer (CT) process between two fluorophores, which are at a distance of about 8–10 Å. Hence, charge transfer occurs resulting in the red-shifted CT band (550 nm). In their next development, they further functionalized the surface of quartz with a coumaryl-aza-crown-6 derivative (**117**).<sup>249</sup> The chemically modified quartz slide was placed under a bifurcated optical fiber and in the presence of STX a fluorescence enhancement ( $E_{\text{x}} = 332 \text{ nm}$ ,  $E_{\text{m}} = 415 \text{ nm}$ ) was observed with a detection limit of  $10^{-5} \text{ M}$  for STX. As a substitute to the currently used mouse bioassay technique, the development of this functionalized material would be beneficial to fabricate an inexpensive and reusable nanosensor device.

In a fascinating approach, the authors integrated the major attributes of two approaches, *i.e.*, MIPs and quantum dots (QDs). MIPs and QDs were utilized as the recognition elements and signal transducers, respectively, to design a new type of molecularly imprinted silica appended to quantum dots (MIP-QDs) for the detection of STX. The developed selective fluorescence nanosensor exhibited excellent fluorescence quenching in the presence of the analytes because of the complementary imprinted cavities on the surface of MIP-QDs (Fig. 88).<sup>250</sup> The fluorescence on-off takes place in the presence/absence of STX. Using a surface-grafting technique, STX-imprinted sites were generated *via* the hydrolysis and condensation reaction of tetraethyl orthosilicate (TEOS) and 3-aminopropyl triethoxysilane (APTES) to provide  $-\text{NH}_2$  surface binding sites on the QD surface. The morphological data revealed that MIP-QDs have a larger external surface area and total pore volume than the non-imprinted polymer, thus providing more specific recognition sites

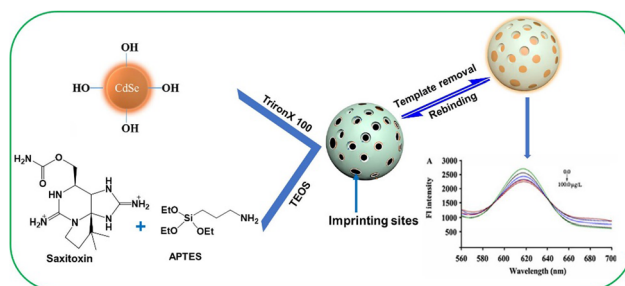


Fig. 88 Pictorial representation of MIP-QD-based chemical sensing for the detection of saxitoxin. Reproduced with permission from ref. 250. Copyright (2017) Elsevier B.V.





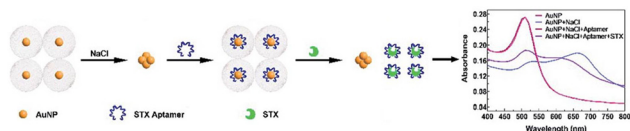


Fig. 89 Schematic representation of an AuNP-based sensing ensemble for saxitoxin. Reproduced with permission from ref. 251. Copyright (2020) Royal Society of Chemistry.

to the STX than the NIPs. Structural analogs of STX, such as okadaic acid, gonyautoxin, anatoxin-a, and neosaxitoxin, were applied to assess the selectivity of MIP-QDs, the results confirmed that the imprinted cavities were only complementary for STX.

More recently, an ultrasensitive colorimetric biosensor based on gold nanoparticles (AuNPs) and an aptamer (AuNPs-aptamer biosensor) for specific detection of STX were reported by Zhang and Han (Fig. 89).<sup>251</sup> The chromogenic response is the result of the aggregation of AuNPs (from AuNP functionalized with the aptamer) caused by the interaction between STX and the aptamer. The absorbance peak changes are attributed to the surface plasmon resonance absorption peak leading to a quantitative determination of the analyte. The present biosensor achieves the lowest STX detection limit of 10 fM within 30 min.

**4.5.2 Detection of ricin.** Currently, ricin detection is mainly achieved by various instrumental techniques and bioassays.<sup>252</sup> Recently, colorimetric aptasensors using modified AuNPs have attracted more attention due to their high sensitivity. Li's group recently introduced a simple, sensitive, and selective colorimetric biosensor for the detection of ricin where AuNPs act as the probe and a ricin-binding aptamer acts as the recognition element.<sup>253</sup> Fig. 90 shows that ricin specifically binds with the ricin-binding aptamer. This induces the aggregation of AuNPs by NaCl, resulting in a color change from red to blue.

Employing the unique feature of gold nanoparticles possessing peroxidase-like activity, Li *et al.* demonstrated a simple and sensitive naked-eye detection technique for ricin (Fig. 91).<sup>254</sup> 3,3',5,5'-Tetramethylbenzidine (TMB), a chromogenic substrate used in immunohistochemistry, exhibits strong affinity toward a negatively charged nanoparticle surface and gets oxidized in the presence of H<sub>2</sub>O<sub>2</sub>, leading to the enhancement of TMB

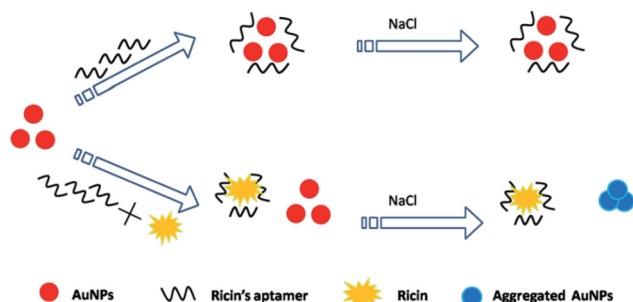


Fig. 90 Schematic representation of an aptasensor based on modified AuNPs for ricin. Reproduced with permission from ref. 253 Copyright (2014) Royal Society of Chemistry.

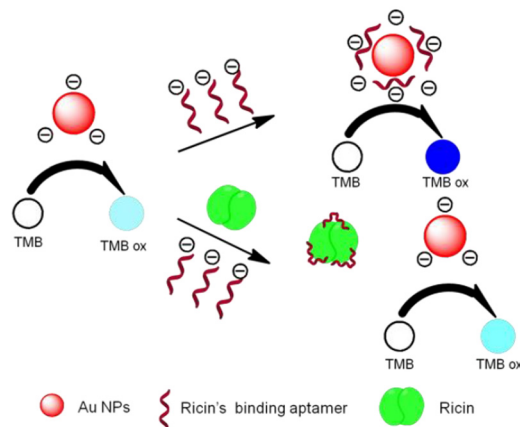


Fig. 91 The sensing mechanism of the colorimetric aptasensor for ricin. Reproduced with permission from ref. 254. Copyright (2015) Royal Society of Chemistry.

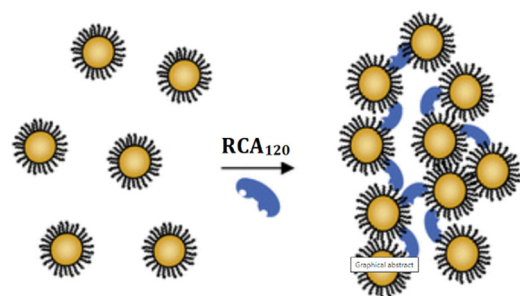


Fig. 92 The sensing mechanism of the galactose-stabilized nanoparticles for the ricin mimic (RCA120). Reproduced with permission from ref. 255. Copyright (2008) Royal Society of Chemistry.

absorbance (from light blue to deep blue). In this report, the authors established that the peroxidase-like activity of AuNPs can be enhanced by surface activation with a ricin-specific aptamer. In the presence of ricin, the aptamer is desorbed from the AuNPs' surface, resulting in a decrease in the catalytic abilities of the AuNPs and the absorbance of TMB. The protein-like thrombin (Th), glucose oxidase (GOx), and bovine albumin (BSA) did not interfere in the determination of ricin.

Russell's group presented a biosensing assay for the detection of a ricin mimic, Ricinus communis agglutinin 120 (RCA120) (Fig. 92).<sup>255</sup> The approach is based on the aggregation of carbohydrate-stabilized AuNPs to generate a visual response, which was also monitored by UV-vis spectroscopy. To develop a bioassay, both long-chain 9-mercapto-3,6-dioxaoctyl-β-D-galactoside and short-chain 2-mercaptoethyl-β-D-galactoside derivatives were assembled onto gold nanoparticles, where RCA120 induced aggregation. The LOD for the toxin was 9 nM using the optimally presented galactose-stabilized nanoparticles.

Boopathi and co-workers developed a MIP for the recognition of ricin by adopting a two-step, procedure-based soft silane polymerization technique on a silica gel matrix using 3-amino-propyl triethoxysilane as a monomer and tetraethoxysilane as a crosslinker (Fig. 93).<sup>256</sup> This technique does not require harsh



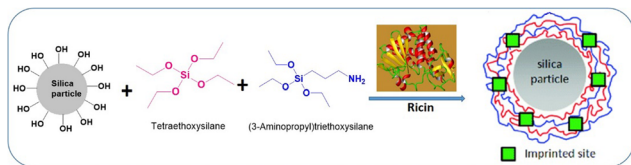


Fig. 93 Schematic presentation of MIP-based ricin detection.

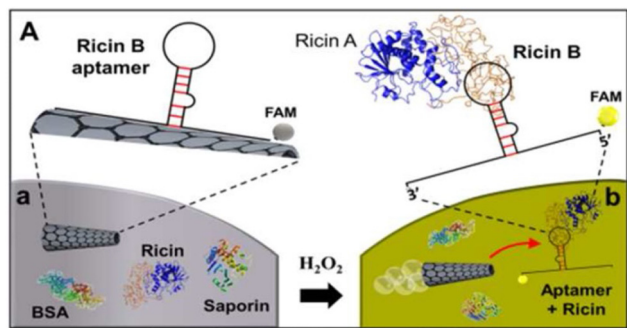


Fig. 94 The sensing mechanism of the aptamer-modified micromotor-based fluorescence detection of ricin B. Reproduced with permission from ref. 257. Copyright (2016) American Chemical Society.

reaction conditions and free radicals, which may affect the 3D structure of the protein during the imprinting process. The ricin-MIP exhibited nanopatterns, and it was found to be entirely different from the non-imprinted polymer (based on SEM imaging). The ricin-MIP exhibited an imprinting efficiency of 1.76, and it exhibited 10% interference from the structurally similar protein abrin.

Wang *et al.* reported the aptamer-modified micromotor-based turn-on fluorescence detection of ricin B toxin (Fig. 94).<sup>257</sup> This concept is based on self-propelled chemically-powered micro motors consisting of reduced graphene oxide (rGO)/platinum (Pt) micromotors, which are modified with a specific ricin B aptamer tagged with fluorescein amidine dye. The aptamer displays a stable folding conformation under harsh environments, including wide pH (2–7) and temperature (4–63 °C) ranges. This approach exhibits rapid ‘on-the-fly’ binding of the toxin with a visual ‘‘off-on’’ fluorescent response that enables rapid detection of ricin at the ng mL<sup>−1</sup> level and selective real-time measurements in diverse samples, which makes it attractive for defense applications.

## 5. Selectivity issues

Selectivity is the capability of a chemosensor to exclusively detect the target analyte in the presence of other species. This is one of the most challenging aspects during the design and development of the chemosensor as many molecular substances with similar structure, size, and charge can co-exist in complex media. Therefore, the incorporation of selectivity within the molecular receptor, requires elegant design of finely-tuned artificial receptors with optimized affinity for the analyte is of paramount importance. As such, the development

of selective chemosensors is still one of the main frontiers in supramolecular chemistry. In order to impart selectivity into a chemosensor, a complete understanding of the target analyte and possible interferences is required.<sup>2</sup>

Given the concern regarding the lethal nature of CW agents, selectivity become far more significant in the case of fluorescent and colorimetric chemosensors for the detection of CW Agents. Both blister agents and nerve agents are electrophilic in nature, and consequently all the developed molecular sensors are most likely to possess nitrogen, oxygen, and sulfur as a nucleophilic site in order to react with electrophilic agents, thus inducing the observed optical changes in the chemosensor. Obviously, this will lead to interference from other less toxic or non-toxic electrophilic agents such as sulfonyl chlorides, thionyl chloride, anhydrides and acid chlorides. Furthermore, in the case of chemosensors based on a nucleophilic center such as nitrogen, inferences from acids (organic/inorganic) is almost certain. In the presence of moisture, G- and V-series are susceptible to hydrolysis thus forming an organophosphoric acid and hydrofluoric/thio acid. Significantly, in many cases, the response of the sensing material to DCP and hydrochloric acid/hydrogen chloride is the same.<sup>258</sup> Therefore, while detecting the real agents the presence of small amount of hydrolyzed product invariably occurs in the chemical agents and can interfere with the detection of CWAs. However, this situation can be avoided by removing the acid contaminants prior to measurement or by performing the detection studies in the presence of acid scavengers such as hexamethylenetetramine.

A literature survey indicates that in most cases, detection of CW agents were reported using DCP (in case of nerve agents) or CEES (in case of blister agents). In both the cases, the rate of reaction with chemosensors are different when compared to the respective real agents *i.e.* DCP or CEES react more quickly due to the weaker P–F or C–Cl bond.<sup>198,259</sup> The specific detection of individual agents is highly desirable not only to reduce false positive signals but in addition from point of view of medical countermeasures. Since, in a war scenario, a specific antidote must be provided rapidly to the victim of a CWA attack. The different oximes (reactivators) are effective against different chemical agents, for example, pralidoxime chloride (PAM-Cl) is effective against GB and VX while HI-6 and HIO-7 provide better protection against GA and GD. Furthermore, in war-like situations, interference with acids could pose challenges for first responders or law enforcement agencies. Since these acidic gases may produce false positive signals that can cheat the detection device developed based on these chemosensors.

## 6. Conclusions and outlook

For more than a century, CW agents have constantly been posing serious threats to mankind, national security, and the environment. Broadly, the first half of the century was largely occupied with the development of various CW agents and their



exploitation as weapons of mass destruction. In the second half of the century, efforts were made to improve detection, protection, and decontamination technologies against CW agents. In this review, we briefly introduced the long and unfortunate history of lethal and non-lethal chemical weapons in an attempt to provide an in-depth account of their chemistries and toxicities on a single platform. Here, we have pointed out the latest developments in CW detection technologies, and subsequently summarized currently used technologies in the military and peace-keeping operations. The past few decades have witnessed tremendous progress in the development of detection methods based on instrumental techniques and chemical detection principles. This has resulted in several technologies in the form of electronic devices and kits, which are currently being used by several nations.

Ideally, to explore practical solutions to the existing problems related to selectivity, sensitivity, speed, portability, and cost, chemical sensors/detection are considered to be the more promising solution, particularly when exploring approaches based on supramolecular tools.<sup>260</sup> Due to the diverse chemical nature of each class of CW agents (*i.e.*, nerve agents, blister agents, blood agents, choking agents, and toxins), different chemical approaches have been exploited in each case.

Fluorescent and colorimetric chemosensors are among the most broadly discussed, researched, and applied synthetic chemical sensors. The structural diversity of these probes provides a range of exceptional electronic and optical properties. When combined with their robust chemistry and ease of manipulation, these probes have become attractive candidates for sensor applications. In most cases, optical detection systems rely on a suitable interaction between chemical probes and chemical agents.

The field of chemosensors for CW agents has seen tremendous progress in the past 20 years with the evolution of, probably, the first fluorescent chemosensor for CW agent mimics reported by Swager. This was followed by studies conducted by many groups,<sup>261</sup> who have inspired countless researchers through their seminal contributions to the field of chemosensors. Most of these reports reveal different combinations of binding or reactive sites and signaling units coupled in different ways to develop selective and sensitive detection systems for diverse CWAs. Each segment was classified according to the signaling paradigm used. For example, (a) the binding site–signaling unit, (b) the displacement assay, and (c) chemodosimeters exhibiting “turn-off” or “turn-on” responses mediated by various sensing mechanisms, such as PeT, ITC, RET, and ESIPT. In most of the examples of chemosensors for the detection of nerve agents, blister agents, choking agents (phosgene), and blood agents (HCN), their electrophilic ability was utilized by incorporating a nucleophilic site in the chemical probe that eventually lead to the signal transduction. With the success of using a discrete molecular-like sensor, further attempts were undertaken to utilize the already developed science for the fabrication of technologies using polymers, hybrid materials, and nanomaterial—even for gas-phase detection—with much greater selectivity and

sensitivity. In some cases, sensory materials have been integrated into devices that can be used to detect a diverse range of CW agents.

From the literature, it is evident that many innovative and sophisticated approaches have been explored for the detection of nerve agents and choking agents (phosgene). However, very few have been proposed for blister agents, blood agents (HCN), and toxins like saxitoxin and ricin. The last decade has seen an exponential growth in the development of chromo-fluorogenic probes for sulfur mustard after a report by the Anslyn group. Unfortunately, due to the high toxicity and unavailability of these chemical agents in academic environments, the majority of these approaches have been tested with simulants for nerve and blister agents, such as DCP and CEES, respectively. Both surrogates differ in chemical reactivity, which may lead to changes in the experimental settings while dealing with real agents in real-life scenarios. In addition, many of the chemical probes encounter challenges like interference, even with other non-toxic electrophilic species. These two major challenges were partially addressed by developing a strategy based on the detection of hydrolyzed products of nerve agents, which not only resolved these issues to some extent but also provided methods that can discriminate these compounds from one another.

Regardless of the notable progress, these emerging instrumental techniques are still confronting many difficulties owing to the inherent limitations of false-positive signals, operation complexity, and high cost. Chemical detection techniques have partly resolved the latter two problems, but selectivity is still a major concern. Given the challenges associated with CW detection—and because this is an opportunity for the scientific community to develop ‘ideal’ chemical sensor and detection systems—advanced, innovative, and more selective fluorescent and colorimetric chemosensors are of vital importance. Despite recent exciting reports, there are still only a small number of specific chemical probes, and this remains a largely unexplored area. Further efforts are needed to make advancements for the next-generation of responsive probes in terms of specificity. Furthermore, integrating different sensing approaches and designing and developing ‘single probes’ for the specific detection of various classes of CW agents will be a growing trend in the upcoming years. Additionally, superior performance can be achieved by developing efficient sensor materials that can be incorporated into conjugated/non-conjugated polymers, organic–inorganic hybrids, and nanomaterials. The merits of these smart and advanced materials include high sensitivity, simplicity, signal amplification, easy fabrication into devices, processability, stability, and reusability. The developed materials can further be transformed into responsive luminescent films, which in turn can be integrated with other technologies (*e.g.*, electronics and imaging instruments) to fabricate prototype devices and kits.

In summary, we present a comprehensive review of various aspects of CW agents and the development of state-of-the-art detection techniques to protect the global community. Recent developments in the field of optical chemical sensors for CWAs



are a new area that has been extensively discussed, covering each class of CW agents. Innovative advances in the chemistry of fluorescent and colorimetric probes continue to be carried out within the field of CW sensing, and we expect that chemosensor research will continue to expand and develop in the near future. We predict that new developments will address major challenges related to selectivity, sensitivity, and simplicity. These novel concepts and innovative ideas give us great hope that global security will be improved with CW chemosensors through the close collaboration between chemists, electronic engineers, and industrial partners. The national and international collaboration of these stakeholders should lead to exciting discoveries and commercial technologies in the field of chemical sensing for CWAs over the decades to come.

## Abbreviations

AC	Hydrogen cyanide
ACADA	Automatic chemical agent detection alarm
AChE	Acetylcholinesterase
AGEL	Acute exposure guideline level
AO	Acridine orange
APTES3	Aminopropyl triethoxysilane
ATCI	Acetylthiocholine iodide
AuNP	Gold nanoparticle
BA	Blister agent
BCEE	Bis-2-chloroethylether
BMIDC	1-Butyl-3-methylimidazolium dicyandiamide
BODIPY	Boron dipyrromethene
BSA	Bovine albumin
BSA	Bovine serum albumin
BWC	Biological weapon convention
BZ	3-Quinuclidinyl benzilate atropine scopolamine
CAM	Chemical agent monitor
CB	Carbon black
Cbi	Cobinamide
C-CX	Chinese VX
CEES	2 Chloroethyl ethyl sulfide
CG	Phosgene
ChO	Choline oxidase enzyme
CK	Cyanogen chloride
CL	Chlorine
CNS	Central nervous system
CT	Charge transfer
CWA	Chemical warfare agent
CWC	Chemical weapon convention
CX	Phosgene oxime
DA	Diphenylchlorarsine
DABCYL	4-Dimethylaminoazobenzene-4-carboxylic acid
DAET	2-Diisopropylaminoethanethiol
DC	Diphenylcyanoarsine
DCNP	Diethyl cyanophosphonate
DCP	Diethyl chlorophosphate

DEPI	Diethoxyphosphinyl isocyanate
DFP	Diisopropyl fluorophosphate
DMMP	Dimethyl methylphosphonate
DMMP	Dimethyl methylphosphonate
DMSO	Dimethyl sulfoxide
DP	Diphosgene
DTNB	55-Dithio-bis-2-nitrobenzoic acid
[EMIM] [DCA]	1-Ethyl-3-methylimidazolium dicyanamide
ESIPT	Excited-state intramolecular proton transfer
ET	Energy transfer
FPD	Flame photometric detection
FRET	Förster resonance energy transfer
GA	Tabun
GB	Sarin
GD	Soman
GF	Cyclosarin
GOx	Glucose oxidase
HD	Highly distilled
HPLC	High-performance liquid chromatography
ICAD	Individual/improved chemical agent detector
ICT	Internal charge transfer
IDA	Indicator displacement assay
ISE	Ion-selective electrodes
JCAD	Joint chemical agent detector
LCD	Lightweight chemical detector
LOD	Limit of detection
LSD	Lysergic acid diethylamide
ME	4-Methylesculetin
MIP	Molecular imprinted polymer
MOF	Metal-organic framework
MSD	Mass selective detection
NA	Nerve agent
NATO	North atlantic treaty organization
NC	Nanocluster
NIP	Non-imprinted polymer
NIR	Near Infrared
NLW	Non-lethal weapon
NM	Nitrogen mustard
NMR	Nuclear magnetic resonance
NPD	Nitrogen phosphorus detection
NSET	Nano surface energy transfer
OP	Organophosphorus
OPCW	Organization for the prohibition of chemical weapon
PB	Prussian blue
PDI	Perylene diimide
PEG	Polyethylene glycol
PEO	Polyethylene oxide
PeT	Photo-induced electron transfer
PS	Chloropicrin
QD	Quantaum dot
RAID	Rapid alarm identification device
RCA	Riot control agent
RCA-120	Ricinuscommunis Agglutinin-120
RGB	Red green blue
rGO	Reduced graphene oxide





RVD	Residual vapor detection
R-VX	Russian VX
SAW	Surface acoustic wave
SM	Nitrogen mustard
SQ	Squaraine
STX	Saxitoxin
TC	Thiocholine
TEOS	Tetraethyl orthosilicate
Th	Thrombin
THC	Delta-9 tetrahydrocannabinol
THF	Tetrahydrofuran
TMB	3,3',5,5'-Tetramethylbenzidine
TMP	Trimethyl phosphate
TPA	Triphenylarsine
TPE	Tetraphenylethene
TTX	Tetrodotoxin
WMD	Weapon of mass destruction
XRD	X-ray diffraction

## Conflicts of interest

There are no conflicts to declare.

## Acknowledgements

V. Kumar thanks the Director, DRDE Gwalior, for his keen interest and encouragement. J. Yoon thanks to the National Research Foundation of Korea (NRF) grant funded by the Korean government (MSIT) (No. 2022R1A2C3005420). TDJ wishes to thank the Royal Society for a Wolfson Research Merit Award and the Open Research Fund of the School of Chemistry and Chemical Engineering, Henan Normal University for support (2020ZD01). EVA thanks the Welch Regents Chair for continued support (F-0046).

## References

- 1 M. Raynal, P. Ballester, A. Vidal-Ferran and P. W. N. M. van Leeuwen, *Chem. Soc. Rev.*, 2014, **43**, 1660–1733 (*Chem. Soc. Rev.*, 2014, **43**, 1734–1787).
- 2 B. Wang and Eric V. Anslyn, *Chemosensors: Principles, Strategies, and Applications*, John Wiley & Sons, Inc., 2011, ISBN:9780470592069, DOI: [10.1002/9781118019580](https://doi.org/10.1002/9781118019580).
- 3 D. Dattler, G. Fuks, J. Heiser, E. Moulin, A. Perrot, X. Yao and N. Giuseppone, *Chem. Rev.*, 2020, **120**, 310–433.
- 4 D. B. Amabilino, D. K. Smith and J. W. Steed, *Chem. Soc. Rev.*, 2017, **46**, 2404–2420.
- 5 S. Erbas-Cakmak, D. A. Leigh, C. T. McTernan and A. L. Nussbaumer, *Chem. Rev.*, 2015, **115**, 10081–10206.
- 6 J. Zhou, Y. Guocan and H. Feihe, *Chem. Soc. Rev.*, 2017, **46**, 7021–7053.
- 7 B. S. Sekhon, *Curr. Drug Targets*, 2015, **16**, 1407–1428.
- 8 *Handbook of toxicology of chemical warfare agents*, ed. R. C. Gupta, Elsevier/AP, Academic Press is an imprint of Elsevier, Amsterdam, Boston, 3rd edn, 2020.
- 9 L. D. Prockop, *J. Neurol. Sci.*, 2006, **249**, 50–54.
- 10 <https://www.opcw.org> (Accessed November 07, 2022).
- 11 <https://www.opcw.org/chemical-weapons-convention/annexes/verification-annex/part-vi-regime-schedule-1-chemicals>. (Accessed November 07, 2022).
- 12 <https://www.opcw.org/chemical-weapons-convention/annexes/annex-chemicals/annex-chemicals> (Accessed November 07, 2022).
- 13 L. Szinicz, *Toxicology*, 2005, **214**, 167–181.
- 14 J. K. Smart, History of Chemical and Biological Warfare: An American Perspective, in *Medical Aspects of Chemical and Biological Warfare*, ed. F. R. Sidell, E. T. Takafuji, D. R. Franz, Office of the Surgeon General, Washington, DC, 1997, p. 15.
- 15 K. Ganesan, S. K. Raza and R. Vijayaraghavan, *J. Pharm. BioAllied Sci.*, 2010, **2**, 166–178.
- 16 <https://web.archive.org/web/20130908034743/http://www.armscontrol.org/print/363> (Accessed November 07, 2022).
- 17 R. Black, *Development, historical use and properties of chemical warfare agents*, In book, *Chemical Warfare Toxicology*, 2016, pp. 1–28, DOI: [10.1039/9781782622413-00001](https://doi.org/10.1039/9781782622413-00001).
- 18 L. Szinicz, F. Worek, H. Thiermann, K. Kehe, S. Eckert and P. Eyer, *Toxicology*, 2007, **233**, 23.
- 19 H. Rice, *Toxicology of Organophosphorus Nerve Agents In book*, *Chemical Warfare Toxicology*, 2016, pp. 81–116, DOI: [10.1039/9781782622413-00081](https://doi.org/10.1039/9781782622413-00081).
- 20 S. M. Somani and J. A. Romano, *Chemical Warfare Agents*, CRC Press, Washington, DC, 2001, p. 447.
- 21 G. Schrader and H. Gebhardt, (Farbenfabriken Bayer AG): D. B. P. 767.830 (1939/1953).
- 22 M. A. Hayoun, M. E. Smith, C. Ausman and H. D. Swoboda, *Toxicology, V-Series Nerve Agent*, StatPearls Publishing, Treasure Island (FL), Stat Pearls, 2020.
- 23 A. Watson, L. Hall, E. Raber, V. D. Hauschild, F. Dolislager, A. H. Love and M. L. H. Hum, *Ecol Risk Assess.*, 2011, **17**, 2–56.
- 24 P. Taylor, in *Anticholinesterase agents*, In *The Pharmacological Basis of Therapeutics*, ed. A. G. Gilman, L. S. Goodman, T. W. Rall, and F. Murad, Macmillan, New York, 6th edn, 1985, p. 110.
- 25 K. Mislow and J. J. Siegel, *J. Am. Chem. Soc.*, 1984, **106**, 3319–3328.
- 26 C. E. A. M. Degenhardt, G. R. Van Den Berg, L. P. A. De Jong and H. P. Benschop, *J. Am. Chem. Soc.*, 1986, **108**, 8290–8291.
- 27 S. Lewis, Salisbury, Novichok and International Law on the Use of Force, *RUSI J.*, 2018, **163**, 10–19.
- 28 <https://www.bbc.com/news/uk-44760875>. (Accessed November 07, 2022).
- 29 <https://www.bbc.com/news/world-europe-43377698>. (Accessed November 07, 2022).
- 30 M. Kloske and Z. Witkiewicz, *Chemosphere*, 2019, **221**, 672–682.
- 31 <https://cen.acs.org/policy/chemical-weapons/New-nerve-agents-added-Chemical-Weapons-Convention/97/web/2019/12>. (Accessed November 07, 2022).



- 32 <https://www.opcw.org/chemical-weapons-convention/annexes/annex-chemicals/schedule-1> (Accessed November 07, 2022).
- 33 P. Jäger, C. N. Rentzea and H. Kieczka, Carbamates and carbamoyl chlorides, *Ullmann's encyclopedia of industrial chemistry*, 2000.
- 34 A. K. Ghosh and M. Brindisi, *J. Med. Chem.*, 2015, **58**, 2895–2940.
- 35 A. Vale and M. Lotti, Organophosphorus and carbamate insecticide poisoning, *Handbook of clinical neurology*, 2015, **131**, pp. 149–168.
- 36 A. McVicar, Carbamate Nerve Agents, *Handbook of Chemical and Biological Warfare Agents*, CRC Press, 2007, pp. 141–176.
- 37 A. M. King and K. A. Cynthia, *Emerg. Med. Clin.*, 2015, **33**, 133–151.
- 38 J. Silberman and A. Taylor, *Carbamate Toxicity*, StatPearls Publishing LLC, USA, 2019, NCBI Number: NBK482183.
- 39 J. A. Romano, Jr., B. J. Lukey and H. Salem, *Chemical Warfare Agents: Chemistry, Pharmacology, Toxicology, and Therapeutics*, CRC Press, London, 2007.
- 40 H. Q. Le and S. J. Knudsen, *Emerg. Med. J.*, 2006, **23**, 296–299.
- 41 M. Balali-Mood and M. Hefazi, *Fundam. Clin. Pharmacol.*, 2005, **19**, 297–315.
- 42 K. Kehe and L. Szinicz, *Toxicology*, 2005, **214**, 198–209.
- 43 J. Jenner, *Toxicology of Vesicants In book*, Chemical Warfare Toxicology, 2016, pp. 29–80, DOI: [10.1039/9781782622413-00029](https://doi.org/10.1039/9781782622413-00029).
- 44 M. Shohrati, M. Davoudi, M. Ghanei, M. Peyman and A. Peyman, *Cutaneous Ocul. Toxicol.*, 2007, **26**, 73–81.
- 45 A. Gilman, *Am. J. Surg.*, 1963, **105**, 574–578.
- 46 S. M. Somani, Toxicokinetics and toxicodynamics of mustard, in *Chemical Warfare Agents*, ed. S. M. Somani, Academic Press, New York, NY, 1992.
- 47 R. K. Singh, S. Kumar, D. N. Prasad and T. R. Bhardwaj, *Eur. J. Med. Chem.*, 2018, **151**, 401–433.
- 48 K. W. Kohn, J. A. Hartley and W. B. Mattes, *Nucleic Acids Res.*, 1987, **15**, 10531–10549.
- 49 A. Polavarapu, J. A. Stillabower, S. G. W. Stubblefield, W. M. Taylor and M. H. Baik, *J. Org. Chem.*, 2012, **77**, 5914–5921.
- 50 C. Descoteaux, K. Brasseur, V. Leblanc, S. Parent, E. Asselin and G. Berube, *Steroids*, 2012, **77**, 403–412.
- 51 D. C. Keyes, J. L. Burstein, R. B. Schwartz and R. E. Swienton, *Medical Response to Terrorism: Preparedness and Clinical Practice*, Lippincott Williams & Wilkins, 2004, p. 16.
- 52 D. H. Rosenblatt, T. A. Miller and J. C. Dacre, *Problem definition studies on potential environmental pollutants. II. Physical, chemical, toxicological, and biological properties of 16 substances. Technical Report 7509, U.S. Army Medical Bioengineering Research and Development Laboratory, Fort Detrick, Frederick, MD*, 1975.
- 53 J. A. Vilensky and K. Redman, *Ann. Emerg. Med.*, 2003, **41**, 378–383.
- 54 J. A. F. Compton, *Military Chemical and Biological Agents: Chemical and Toxicological Properties*, Telford Press, Caldwell, New Jersey, 1988, pp. 37–38.
- 55 C. M. Pechura and D. P. Rall, *Institute of Medicine (US) Committee on the Survey of the Health Effects of Mustard Gas and Lewisite. Veterans at Risk: The Health Effects of Mustard Gas and Lewisite*, National Academies Press, Washington (DC) (US), 1993.
- 56 G. Sandi, K. L. Brubaker, J. F. Schneider, H. J. O'Neill and P. L. Cannon Jr., *Talanta*, 2001, **54**, 913–925.
- 57 S. K. Singh, J. A. Klein, H. N. Wright and N. Tewari-Singh, *Toxicol. Mech. Methods*, 2021, **31**, 288–292.
- 58 <https://www.news9.com/story/40170458/fbi-investigationfinds-chemical-warfare-agent-inside-lawton-home>. (Accessed November 07, 2022).
- 59 T. T. Marrs, L. M. Robert and F. Sidell, *Chemical warfare agents: Toxicology and treatment*, John Wiley and Sons, Chichester, England, 2007.
- 60 L. Coentrao and D. Moura, *Am. J. Emerg. Med.*, 2011, **29**, 78–81.
- 61 F. R. Sidell, E. T. Takafuji and D. R. Franz, *Medical Aspects of Chemical and Biological Warfare*, Office of the Surgeon General, Washington, DC, 1997.
- 62 D. Henschler, Hydrogen cyanide, potassium cyanide, and sodium cyanide [MAK Value Documentation, 2003], in *The MAK-collection for occupational health and safety*, ed. M. Tschickardt, Wiley Online Library, 2012, pp. 193–95, DOI: [10.1002/3527600418.mb7490vere0019](https://doi.org/10.1002/3527600418.mb7490vere0019).
- 63 H. Babad and A. G. Zeiler, *Chem. Rev.*, 1973, **73**, 75–91.
- 64 T. Zellner and F. Eyer, *Toxicol. Lett.*, 2020, **320**, 73–79.
- 65 J. Borak and W. F. Diller, *J. Occup. Environ. Med.*, 2001, **43**, 110–119.
- 66 C. Bast and B. Bress, *Acute exposure guideline levels for selected airborne chemicals. Phosgene The National Research Council, Committee on Toxicology*, The National Academies Press, Washington, DC, vol. 2, 2002.
- 67 P. D. Anderson, *J. Pharm. Pract.*, 2012, **25**, 121–129.
- 68 M. A. Sierra and R. Martínez-Álvarez, *J. Chem. Educ.*, 2020, **97**, 1707–1714.
- 69 L. J. M. Madsen, *Clin. Lab. Med.*, 2001, **21**, 593–605.
- 70 A. P. Thottumkara, W. H. Parsons and J. D. Bois, *Angew. Chem., Int. Ed.*, 2014, **53**, 5760–5784.
- 71 W. A. Catterall, *Annu. Rev. Pharmacol. Toxicol.*, 1980, **20**, 15–43.
- 72 *Official Methods of Analysis*, ed. K. Helrich, Association of Official Analytical Chemists (AOAC), Arlington, VA, 1990, pp. 881–882.
- 73 J. F. Lawrence, B. Niedzwiedek and C. Menard, *J. AOAC Int.*, 2005, **88**, 1714–1732.
- 74 L. Polito, M. Bortolotti, M. G. Battelli, G. Calafato and A. Bolognesi, *Toxins*, 2019, **11**, 324–340.
- 75 S. Olsnes and A. Pihl, *Biochemistry*, 1973, **12**, 3121–3126.
- 76 J. M. Lord, L. M. Roberts and J. D. Robertus, *FASEB J.*, 1994, **8**, 201–208.
- 77 A. Pearson, *Nonproliferation Rev.*, 2006, **13**, 152–188.
- 78 E. J. Olajos and H. Salem, *J. Appl. Toxicol.*, 2001, **5**, 355–391.
- 79 L. J. Schep, R. J. Slaughter and D. I. McBride, *J. R. Army Med. Corps*, 2015, **161**, 94–99.
- 80 C. J. Hilmas, Riot Control Agents, in *Handbook of Toxicology of Chemical Warfare Agents*, ed. R. C. Gupta, Academic Press, 2nd edn, 2015, ch. 11, pp. 131–150.



- 81 Y. Dimitroglou, G. Rachiotis and C. Hadjichristodoulou, *Int. J. Environ. Res. Public Health*, 2015, **12**, 1397–1411.
- 82 R. Jabbour, H. Salem, B. Ballantyne and S. A. Katz, Arsenical Vomiting Agents, in *Encyclopedia of Toxicology*, ed. P. Wexler, Academic Press, 3rd edn, 2014, pp. 302–307.
- 83 J. Fusek, A. Dlabkova and J. Misik, in *Handbook of toxicology of chemical warfare agents*, ed. R. C. Gupta, Elsevier/AP, Academic Press is an imprint of Elsevier, Amsterdam, Boston, 3rd edn, 2020, ch. 14, pp. 203–213.
- 84 B. Radke, L. Jewell, S. Piketh and J. Namiesnik, Arsenic Based Warfare Agents: Production, Use, and Destruction, *Crit. Rev. Environ. Sci. Technol.*, 2014, **44**, 1525–1576.
- 85 J. M. Lakoski, W. B. Murray and J. M. Kenny, The Advantages and Limitations of Calmatives for Use as a Non-Lethal Technique (University Park, PA: Applied Research Laboratory, Pennsylvania State University, 2000), p. 48. [https://erowid.org/psychoactives/war/war\\_article1.pdf](https://erowid.org/psychoactives/war/war_article1.pdf) (Accessed November 07, 2022).
- 86 R. G. Sutherland, Chemical and Biochemical Non-lethal Weapons Political and Technical Aspects Publisher: SIPRI ISBN 978-91-85114-59-7, 2008, <https://www.sipri.org/sites/default/files/files/PP/SIPRIIPP23.pdf>, accessed November 07, 2022.
- 87 J. A. Romano Jr, B. J. Lukey and H. Salem, *Chemical Warfare Agents: Chemistry, Pharmacology, Toxicology, and Therapeutics*, CRC Press, London, 2007, pp. 367–372.
- 88 J. Bajgar, J. Kassa, J. Fusek, K. Kuca and D. Jun, in *Handbook of toxicology of chemical warfare agents*, ed. R. C. Gupta, 3rd edn, Elsevier/AP, Academic Press is an imprint of Elsevier, Amsterdam, Boston, 2020, ch. 27, pp. 403–412.
- 89 J. Matousek and I. Masek, On the new potential super-toxic lethal organophosphorus chemical warfare agents with intermediate volatility, *ASA Newsletter*, 1994, **1**, 94–95.
- 90 [https://www.opcw.org/sites/default/files/documents/2019/03/s-1731-2019\(e\).pdf](https://www.opcw.org/sites/default/files/documents/2019/03/s-1731-2019(e).pdf). (Accessed November 07, 2022).
- 91 Y. Sun and K. Y. Ong, *Detection Technologies for Chemical Warfare Agents and Toxic Vapors*, CRC Press, 2004.
- 92 Institute of Medicine (US) Committee on R&D Needs for Improving Civilian Medical Response to Chemical and Biological Terrorism Incidents. Chemical and Biological Terrorism: Research and Development to Improve Civilian Medical Response. Washington (DC), National Academies Press (US), 1999, 4, Detection and Measurement of Chemical Agents.
- 93 A. A. Fatah, R. D. Arcilesi, J. C. Peterson, C. H. Lattin, C. Y. Wells and J. A. McClintock, in *Guide for the Selection of Chemical Detection Equipment for Emergency First Responders*, ed. U. D. O. H. Security, Washington, D.C., 3rd edn, 2007.
- 94 W. Lu, M. Xue, Z. Xu, X. Dong, F. Xue, F. Wang and Z. Meng, *Curr. Org. Chem.*, 2015, **19**, 62–71.
- 95 F. N. Diauddin, J. I. A. Rashid, V. F. Knight, W. M. Z. W. Yunus, K. K. Ong, N. A. M. Kasim, N. A. Halim and S. A. M. Noor, *Sens. Bio-Sens. Res.*, 2019, **26**, 100305.
- 96 Y. Saylan, S. Akgonullu and A. Denizli, *Biosensors*, 2020, **10**, 142.
- 97 H. Yoon, *Nanomaterials*, 2013, **3**, 524–549.
- 98 Y. Sun and K. Y. Ong, *Detection Technologies for Chemical Warfare Agents and Toxic Vapors*, CRC Press, Boca Raton, Florida, 1st edn, 2004, p. 272.
- 99 Y. Seto, M. Kanamori-Kataoka, K. Tsuge, I. Ohsawa, H. Maruko, H. Sekiguchi, Y. Sano, S. Yamashiro, K. Matsushita, H. Sekiguchi, T. Itoi and K. Iura, *Toxin Rev.*, 2007, **26**, 299–312.
- 100 A. M. Marko, A. A. Osmo and E. T. S. Mika, *Anal. Chem.*, 2010, **82**, 9594–9600.
- 101 R. Sferopoulos, A Review of Chemical Warfare Agent (CWA) Detector Technologies and Commercial-Off-The-Shelf Items, <https://apps.dtic.mil/sti/pdfs/ADA502856.pdf>, retrieved on October 26, 2021.
- 102 Y. Pan, G. Zhang, T. Guo, X. Liu, C. Zhang, J. Yang, B. Cao, C. Zhang and W. Wang, *Sens. Actuators, B*, 2020, **315**, 127986.
- 103 A. T. Nimal, U. Mittal, M. Singh, M. Khaneja, G. K. Kannan, J. C. Kapoor, V. Dubey, P. K. Gutch, G. Lal, K. D. Vyas and D. C. Gupta, *Sens. Actuators, B*, 2009, **135**, 399–410.
- 104 R. R. Jones, D. C. Hooper, L. Zhang, D. Wolverson and V. K. Valev, *Nanoscale Res. Lett.*, 2019, **14**, 231–265.
- 105 E. J. Pacsial-Ong and Z. P. Aguilar, *Front. Biosci.*, 2013, **5**, 516–543.
- 106 Y. Sun and K. Y. Ong, *Detection Technologies for Chemical Warfare Agents and Toxic Vapors*, CRC Press, Boca Raton, Florida, 1st edn, 2004, pp. 190–194.
- 107 C. A. Valdez, R. N. Leif, S. Hok and B. R. Hart, *Rev. Anal. Chem.*, 2018, **37**, 20170007.
- 108 G. M. Murray, detection and Screening of Chemicals Related to the Chemical Weapons Convention. *Encyclopedia of Analytical Chemistry*, 2006, DOI: [10.1002/9780470027318.a0403.pub2](https://doi.org/10.1002/9780470027318.a0403.pub2).
- 109 J. Epstein, R. W. Rosenthal and R. J. Ess, *Anal. Chem.*, 1955, **27**, 1435–1439.
- 110 A. Bussey, A. Clarke and J. Lambert, PCT/GB2004/001083 WO/2004/081561, March 11, 2004.
- 111 B. Singh, P. P. Bhise, M. V. S. Suryanarayana, S. S. Yadav, V. K. Rao, B. G. Polke, D. Pandey, K. Ganesan and N. B. S. N. Rao, *J. Sci. Ind. Res.*, 1999, **58**, 25–30.
- 112 V. Pitschmann, I. Tušarová, E. Halánek and Z. Kobliha, *J. Serb. Chem. Soc.*, 2010, **75**, 813–822.
- 113 N. Nakano, A. Yamamoto, Y. Kobayashi and K. Nagashima, *Talanta*, 1995, **42**, 641–645.
- 114 T. W. Bell and N. M. Hext, *Chem. Soc. Rev.*, 2004, **33**, 589.
- 115 A. W. Czarnik, *Advances in Supramolecular Chemistry*, JAI Press, Greenwich, Connecticut, 1993.
- 116 V. Kumar and A. Mazumder, Detection of Chemical Warfare Agents With Chemical Sensors, in *Encyclopedia of Sensors and Biosensors*, ed. R. Narayan, Elsevier, 2022, vol. 4, pp. 667–692, DOI: [10.1016/B978-0-12-822548-6.00145-X](https://doi.org/10.1016/B978-0-12-822548-6.00145-X).
- 117 A. P. deSilva, H. N. Gunaratne, T. Gunnlaugsson, A. J. M. Huxley, C. P. McCoy, J. T. Rademacher and T. E. Rice, *Chem. Rev.*, 1997, **97**, 1515–1566.
- 118 S. Erbas-Cakmak, S. Kolemen, A. C. Sedgwick, T. Gunnlaugsson, T. D. James, J. Yoon and E. U. Akkaya, *Chem. Soc. Rev.*, 2018, **47**, 2228–2248.





- 119 A. C. Sedgwick, J. T. Brewster, T. Wu, X. Feng, S. D. Bull, X. Qian, J. L. Sessler, T. D. James, E. V. Anslyn and X. Sun., *Chem. Soc. Rev.*, 2021, **50**, 9–38.
- 120 W. Sun, M. Li, J. Fan and X. Peng, *Acc. Chem. Res.*, 2019, **52**, 2818–2831.
- 121 I. I. Ebralidze, N. O. Laschuk, J. Poisson and O. V. Zenkina, Colorimetric Sensors and Sensor Arrays, in *Micro and Nano Technologies, Nanomaterials Design for Sensing Applications*, Elsevier, 2019, ch. 1, pp. 1–39.
- 122 D. Wu, A. C. Sedgwick, T. Gunnlaugsson, E. U. Akkaya, J. Yoon and T. D. James, *Chem. Soc. Rev.*, 2017, **46**, 7105–7123.
- 123 S. Royo, R. Martinez-Manez, F. Sancenon, A. M. Costero, M. Parra and S. Gil, *Chem. Commun.*, 2007, 4839–4847.
- 124 L. Chen, D. Wu and J. Yoon, *ACS Sens.*, 2018, **3**, 27–43.
- 125 S.-W. Zhang and T. M. Swager, *J. Am. Chem. Soc.*, 2003, **125**, 3420–3421.
- 126 K. J. Wallace, J. Morey, V. M. Lynch and E. V. Anslyn, *New J. Chem.*, 2005, **29**, 1469–1474.
- 127 K. J. Wallace, R. I. Fagbemi, F. J. Folmer-Andersen, J. Morey, V. M. Lynch and E. V. Anslyn, *Chem. Commun.*, 2006, 3886–3888.
- 128 S. Bencic-Nagale, T. Sternfeld and D. R. Walt, *J. Am. Chem. Soc.*, 2006, **128**, 5041–5048.
- 129 T. J. Dale and J. Rebek, *J. Am. Chem. Soc.*, 2006, **128**, 4500–4501 (*Angew. Chem., Int. Ed.*, 2009, **48**, 7850–7852).
- 130 A. M. Costero, S. Gil, M. Parra, P. M. E. Mancini, R. Martinez-Manez, F. Sancenon and S. Royo, *Chem. Commun.*, 2008, 6002–6004.
- 131 S. Han, Z. Xue, Z. Wang and T. B. Wen, *Chem. Commun.*, 2010, **46**, 8413–8415.
- 132 S. Royo, A. M. Costero, M. Parra, S. Gil, R. Martinez-Manez and F. Sancenon, *Chem. – Eur. J.*, 2011, **17**, 6931–6934.
- 133 R. Gotor, A. M. Costero, S. Gil, M. Parra, R. Martinez-Manez and F. Sancenon, *Chem. – Eur. J.*, 2011, **17**, 11994–11997.
- 134 V. Kumar and M. P. Kaushik, *Analyst*, 2011, **136**, 5151–5156.
- 135 W. Xuan, Y. Cao, J. Zhou and W. Wang, *Chem. Commun.*, 2013, **49**, 10474–10476.
- 136 Z. Lei and Y. Yang, *J. Am. Chem. Soc.*, 2014, **136**, 6594–6597.
- 137 Y. J. Yang, O. G. Tsay, D. P. Murale, J. A. Jeong, A. Segev and D. G. Churchill, *Chem. Commun.*, 2014, **50**, 7531–7534.
- 138 G. B. Diaz de, D. Moreno, T. Torroba, A. Berg, J. Gunnars, T. Nilsson, R. Nyman, M. Persson, J. Pettersson, I. Eklind and P. Wasterby, *J. Am. Chem. Soc.*, 2014, **136**, 4125–4128.
- 139 J. G. Weis and T. M. Swager, *ACS Macro Lett.*, 2015, **4**, 138–142.
- 140 A. K. Mahapatra, K. Maiti, S. K. Manna, R. Maji, S. Mondal, C. D. Mukhopadhyay, P. Sahoo and D. Mandal, *Chem. Commun.*, 2015, **51**, 9729–9732.
- 141 V. Kumar, H. Rana, G. Raviraju, P. Garg, A. Baghel and A. K. Gupta, *RSC Adv.*, 2016, **6**, 59648–59656.
- 142 T.-I. Kim, S. B. Maity, J. Bouffard and Y. Kim, *Anal. Chem.*, 2016, **88**, 9259–9263.
- 143 X. Zhou, Y. Zeng, C. Liyan, X. Wu and J. Yoon, *Angew. Chem., Int. Ed.*, 2016, **55**, 4729–4733.
- 144 M. Gupta and H.-I. Lee, *Sens. Actuators, B*, 2017, **242**, 977–982.
- 145 Y. J. Jang, S. V. Mulay, Y. Kim, P. Jorayev and D. G. Churchill, *New J. Chem.*, 2017, **41**, 1653–1658.
- 146 X. Sun, S. D. Dahlhauser and E. V. Anslyn, *J. Am. Chem. Soc.*, 2017, **139**, 4635–4638.
- 147 Y.-C. Cai, C. Li and Q.-H. Song, *ACS Sens.*, 2017, **2**, 834–841.
- 148 Y.-C. Cai, C. Li and Q.-H. Song, *J. Mater. Chem. C*, 2017, **5**, 7337–7343.
- 149 K. Aich, S. Das, S. Gharami, L. Patra and T. K. Mondal, *New J. Chem.*, 2017, **41**, 12562–12568.
- 150 V. Kumar, G. Raviraju, H. Rana, V. K. Rao and A. K. Gupta, *Chem. Commun.*, 2017, **53**, 12954–12957.
- 151 Q. J. Luo, Z. G. Li, J. H. Lai, F. Q. Li, P. Qiu and X. L. Wang, *RSC Adv.*, 2017, **7**, 55199–55205.
- 152 M. S. J. Khan, Y.-W. Wang, M. O. Senge and Y. Peng, *J. Hazard. Mater.*, 2018, **342**, 10–19.
- 153 K. Rurack and R. Martinez-Manez, *The Supramolecular Chemistry of Organic-Inorganic Hybrid Materials*, Wiley, Hoboken, New Jersey, 2010, pp. 319–349 or 407–432.
- 154 E. Climent, M. Biyikal, K. Gawlitza, T. Dropa, M. Urban, A. M. Costero, R. Martinez-Manez and K. Rurack, *Sens. Actuators, B*, 2017, **246**, 1056–1065.
- 155 J. M. Garcia, F. C. Garcia, F. Serna and J. L. de la Pena, *Polym. Rev.*, 2011, **51**, 341–390.
- 156 H. N. Kim, Z. Guo, W. Zhu, J. Yoon and H. Tian, *Chem. Soc. Rev.*, 2011, **40**, 79–93.
- 157 M. Gupta and H.-I. Lee, *Macromolecules*, 2017, **50**, 6888–6895.
- 158 J. Yan, S. Lee, A. Zhang and J. Yoon, *Chem. Soc. Rev.*, 2018, **47**, 6900–6916.
- 159 M. E. Roth, O. Green, S. Gnaim and D. Shabat, *Chem. Rev.*, 2016, **116**(3), 1309–1352.
- 160 X. Sun and E. V. Anslyn, *Angew. Chem., Int. Ed.*, 2017, **56**, 9522–9526.
- 161 H. S. Sarkar, A. Ghosh, S. Das, P. K. Maiti, S. Maitra, S. Mandal and P. Sahoo, *Sci. Rep.*, 2018, **8**, 1–7.
- 162 X. Liu, Y. Gong, Y. Zheng, W. Xiong, C. Wang, T. Wang, Y. Che and J. Zhao, *Anal. Chem.*, 2018, **90**(3), 1498–1501.
- 163 L. Chen, H. Oh, D. Wu, M. H. Kim and J. Yoon, *Chem. Commun.*, 2018, **54**, 2276–2279.
- 164 T. Qin, Y. Huang, K. Zhu, J. Wang, C. Pan, B. Liu and L. Wang, *Anal. Chim. Acta*, 2019, **1076**, 125–130.
- 165 B. Huo, M. Du, A. Shen, M. Li, Y. Lai, X. Bai, A. Gong and Y. Yang, *Anal. Chem.*, 2019, **91**, 10979–10983.
- 166 G. Heo, R. Manivannan, H. Kim and Y.-A. Son, *Dyes Pigm.*, 2019, **171**, 107712.
- 167 X. Sun, A. A. Boulgakov, L. N. Smith, P. Metola, E. M. Marcotte and E. V. Anslyn, *ACS Cent. Sci.*, 2018, **4**, 854–861.
- 168 C. Sun, W. Xiong, W. Ye, Y. Zheng, R. Duan, Y. Che and J. Zhao, *Anal. Chem.*, 2018, **90**, 7131–7134.
- 169 K. Vymazalova, J. Kadlcak and E. Halamek, *Def. Sci. J.*, 2012, **62**, 399–403.
- 170 V. Pitschmann, L. Matejovsky, D. Vetchy and Z. Kobliha, *Anal. Lett.*, 2016, **49**, 2418–2426.





- 171 V. Pitschmann, L. Matejovsky, M. Lobotka, J. Dedic, M. Urban and M. Dymak, *Biosensors*, 2018, **8**, 81–90.
- 172 L. Matejovsky and V. Pitschmann, *ACS Omega*, 2019, **4**(25), 20978–20986.
- 173 N. Zehra, A. Kalita, A. H. Malik, U. Barman, M. A. Afroz and P. KrishnanIyer, *ACS Sens.*, 2020, **5**, 191–198.
- 174 M. C. de Koning, G. W. Peterson, M. V. Grol, I. Iordanov and M. McEntee, *Chem. Mater.*, 2019, **31**, 7417–7424.
- 175 G. L. Ellman, K. D. Courtney, V. Andres Jr. and R. M. Featherstone, *Biochem. Pharmacol.*, 1961, **7**, 88–95.
- 176 L. Zeng, H. Zeng, L. Jiang, S. Wang, J.-T. Hou and J. Yoon, *Anal. Chem.*, 2019, **91**, 12070–12076.
- 177 N. Boens, V. Leen and W. Dehaen, *Chem. Soc. Rev.*, 2012, **41**, 1130–1172.
- 178 T. Kowada, H. Maeda and K. Kikuchi, *Chem. Soc. Rev.*, 2015, **44**, 4953–4972.
- 179 A. C. Sedgwick, R. S. L. Chapman, J. E. Gardiner, L. R. Peacock, G. Kim, J. Yoon, S. D. Bull and T. D. James, *Chem. Commun.*, 2017, **53**, 10441–10443.
- 180 Z. Lu, W. Fan, X. Shi, C. A. Black, C. Fan and F. Wang, *Sens. Actuators, B*, 2018, **255**, 176–182.
- 181 S.-S. Li, Y.-C. Zheng, X.-M. Zhu, H.-B. Wang, L.-H. Liang, X.-Z. Wang, L. Yuan, F.-H. Zhang, H. Zheng and C.-L. Zhao, *Sens. Actuators, B*, 2021, **337**, 129804.
- 182 J. G. Mao, *Coord. Chem. Rev.*, 2007, **251**, 1493–1520.
- 183 E. Butera, A. Zammataro, A. Pappalardo and G. T. Sfrazzetto, *ChemPlusChem*, 2021, **86**, 681–695.
- 184 C. M. A. Gangemi, U. Rimkaite, A. Pappalardo and G. T. Sfrazzetto, *RSC Adv.*, 2021, **11**, 13047–13050.
- 185 X. Hua, H. Zeng, T. Chen, H. Q. Yuan, L. Zeng and G. M. Bao, *Sens. Actuators, B*, 2020, **319**, 128282.
- 186 S. K. Sheet, B. Sen and S. Khatua, *Inorg. Chem.*, 2019, **58**, 3635–3645.
- 187 W. Weihui, S. Shaohui, L. Jian, Z. Liang, L. Dan, X. Yanhua, W. Lianyuan, Z. Haiyan, S. Yonglin and J. Zhigang, *Analyst*, 2020, **145**, 5425–5429.
- 188 X. Wang, H. Chang, J. Xie, B. Zhao, B. Liu, S. Xu, W. Pei, N. Ren, L. Huang and W. Huang, *Coord. Chem. Rev.*, 2014, **273–274**, 201–212.
- 189 K. Gupta and A. K. Patra, *ACS Sens.*, 2020, **5**, 1268–1272.
- 190 M. Sathiyaraja and V. Thiagarajan, *RSC Adv.*, 2020, **10**, 25848–25855.
- 191 H. Xu, H. Zhang, L. Zhao, C. Peng, G. Liu and T. Cheng, *New J. Chem.*, 2020, **44**, 10713–10718.
- 192 K. C. Behera and B. Bag, *Chem. Commun.*, 2020, **56**, 9308–9311.
- 193 T. N. Annisa, S.-H. Jung, M. Gupta, J. Y. Bae, J. M. Park and H.-L. Lee, *ACS Appl. Mater. Interfaces*, 2020, **12**, 11055–11062.
- 194 S.-H. Jung, Y. J. Jung, B. C. Park, H. Kong, B. Lim, J. M. Park and H.-L. Lee, *Sens. Actuators, B*, 2020, **323**, 128698.
- 195 F. Takahashi, Y. Kazui, H. Miyaguchi, T. Ohmori, R. Tanaka and J. Jin, *Sens. Actuators, B*, 2021, **327**, 128902.
- 196 Y. Zhang, H. Mu, P. Zheng, Y. Zhao and M. Zhang, *Sens. Actuators, B*, 2021, **343**, 130140.
- 197 Q. Q. Wang, R. A. Begum, V. W. Day and K. Bowman-James, *Org. Biomol. Chem.*, 2012, **10**, 8786–8793.
- 198 Y. C. Yang, J. R. Ward and T. Luteran, *J. Org. Chem.*, 1986, **51**, 2756–2759.
- 199 <https://www.science.org/news/2013/09/un-experts-find-convincing-evidence-large-scale-sarin-attack-syria>. (Accessed November 07, 2022).
- 200 S. Tal, H. Salman, Y. Abraham, M. Botoshansky and Y. Eichen, *Chem. – Eur. J.*, 2006, **12**, 4858–4864.
- 201 V. Kumar and E. V. Anslyn, *J. Am. Chem. Soc.*, 2013, **135**, 6338–6344.
- 202 H. Rana, G. Raviraju, A. Kumar, J. Acharya, A. K. Gupta and V. Kumar, *Sens. Lett.*, 2019, **17**, 352–357.
- 203 V. Kumar and E. V. Anslyn, *Chem. Sci.*, 2013, **4**, 4292–4297.
- 204 V. Kumar and H. Rana, *RSC Adv.*, 2015, **5**, 91946–91950.
- 205 D. R. Goud, A. K. Purohit, V. Tak, D. K. Dubey, P. Kumar and D. Pardasani, *Chem. Commun.*, 2014, **50**, 12363–12366.
- 206 H. Wang, J. Guan, X. Han, S. W. Chen, T. Li, Y. Zhang, M. S. Yuan and J. Wang, *Talanta*, 2018, **189**, 39–44.
- 207 Y. M. Poronik, K. V. Vygranenko, D. Gryko and D. T. Gryko, *Chem. Soc. Rev.*, 2019, **48**, 5242–5265.
- 208 S. Bidmanova, M. S. Steiner, M. Stepan, K. Vymazalova, M. A. Gruber, A. Duerkop, J. Damborsky, Z. Prokop and O. S. Wolfbeis, *Anal. Chem.*, 2016, **88**(11), 6044–6049.
- 209 H. Wang, D.-E. Wang, J. Guan, X. Han, P. Xue, W. Liu, M.-S. Yuan and J. Wang, *J. Mater. Chem. C*, 2017, **5**, 11565–11572.
- 210 V. Kumar, H. Rana, G. Raviraju and A. K. Gupta, *Anal. Chem.*, 2018, **90**, 1417–1422.
- 211 Y. Zhang, Y. Lv, X. Wang, A. Peng, K. Zhang, X. Jie, J. Huang and Z. Tian, *Anal. Chem.*, 2018, **90**, 5481–5488.
- 212 Y. L. Jiang and A.-M. Broome, *ACS Sens.*, 2019, **4**, 1791–1797.
- 213 Z. Guo, S. Park, J. Yoon and I. Shin, *Chem. Soc. Rev.*, 2014, **43**, 16–29.
- 214 W. Meng, M. Sun, Q. Xu, J. Cen, Y. Cao, Z. Li and K. Xiao, *ACS Sens.*, 2019, **4**, 2794–2801.
- 215 W. Xiong, Y. Gong, Y. Che and J. Zhao, *Anal. Chem.*, 2019, **91**, 1711–1714.
- 216 C. Qiu, X. Liu, C. Cheng, Y. Gong, W. Xiong, Y. Guo, C. Wang, J. Zhao and Y. Che, *Anal. Chem.*, 2019, **91**, 6408–6412.
- 217 W. Tuo, J. Bouquet, F. Taran and T. L. Gall, *Chem. Commun.*, 2019, **55**, 8655–8658.
- 218 V. V. Singh, V. Kumar, U. Biswas, M. Boopathi, K. Ganesan and A. K. Gupta, *Anal. Chem.*, 2021, **93**, 1193–1199.
- 219 R. C. Knighton, M. R. Sambrook, J. C. Vincent, S. A. Smith, C. J. Serpell, J. Cookson, M. S. Vickers and P. D. Beer, *Chem. Commun.*, 2013, **49**, 2293–2295.
- 220 D. Pardasani, V. Tak, A. K. Purohit and D. K. Dubey, *Analyst*, 2012, **137**, 5648–5653.
- 221 M. Boopathi, M. V. S. Suryanarayana, A. K. Nigam, P. Pandey, K. Ganesan, B. Singh and K. Sekhar, *Biosens. Bioelectron.*, 2006, **21**, 2339–2344.
- 222 S. Kaur, M. Singh and S. S. Flora, *Appl. Biochem. Biotechnol.*, 2013, **171**, 1405–1415.
- 223 B. Li, S. Li, B. Wang, Z. Meng, Y. Wang, Q. Meng and C. Li, *iScience*, 2020, **23**, 101443.



- 224 Q.-Q. Wang, R. A. Begum, V. W. Day and K. Bowman-James, *J. Am. Chem. Soc.*, 2013, **135**, 17193–17199.
- 225 N. Li, P. Zhao, N. Liu, M. Echeverria, S. Moya, L. Salmon, J. Ruiz and D. Astruc, *Chem. – Eur. J.*, 2014, **20**, 8363–8369.
- 226 N. V. Singha, B. Shankar, R. Shanmugam, S. K. Awasthi and R. D. Gupta, *Sens. Actuators, B*, 2016, **227**, 85–91.
- 227 D. Li, H. Xi, S. Han and S. Zhao, *Anal. Methods*, 2021, **13**, 484–490.
- 228 W. Menga, H. Zhang, L. Xiao, X. Chend, M. Sunb, Q. Xub, Y. Cao, K. Xiao and Z. Li, *Sens. Actuators, B*, 2019, **296**, 126678.
- 229 M.-J. Xue, X.-Z. Wei, W. Feng, Z.-F. Xing, S.-L. Liu and Q.-H. Song, *J. Hazard. Mater.*, 2021, **416**, 125789.
- 230 O. Abuzalat, S. Homayoonnia, D. Wong, H. R. Tantawy and S. Kim, *Dalton Trans.*, 2021, **50**, 3261–3268.
- 231 S. Shrivastava, T. Q. Trung and N.-E. Lee, *Chem. Soc. Rev.*, 2020, **49**, 1812–1866.
- 232 N. Colozza, K. Kehe, G. Dionisi, T. Popp, A. Tsoutsouloupoulos, D. Steinritz, D. Moscone and F. Arduini, *Biosens. Bioelectron.*, 2019, **129**, 15–23.
- 233 D.-H. Lee, D.-N. Lee and J.-I. Hong, *New J. Chem.*, 2016, **40**, 9021–9024.
- 234 R. Gotor, A. M. Costero, S. Gil, M. Parra, R. Martinez-Manez, F. Sancenon and P. Gavina, *Chem. Commun.*, 2013, **49**, 5669–5671.
- 235 L. Zhong, H. Li, S.-L. Wang and Q.-H. Song, *Sens. Actuators, B*, 2018, **266**, 703–709.
- 236 L. A. Greenawald, J. L. Snyder, N. L. Fry, M. J. Sailor, G. R. Boss, H. O. Finklea and S. Bell, *Sens. Actuators, B*, 2015, **221**, 379–385.
- 237 L. A. Greenawald, G. R. Boss, J. L. Snyder, A. Reeder and S. Bell, *ACS Sens.*, 2017, **2**(10), 1458–1466.
- 238 R. C. Gupta, S. K. Dwivedi, R. Ali and A. Misra, *ChemistrySelect*, 2018, **3**, 2025–2031.
- 239 X. Liu, N. Li, M. Li, H. Chen, N. Zhang, Y. Wang and K. Zheng, *Coord. Chem. Rev.*, 2020, **404**, 213109.
- 240 C. Guo, A. C. Sedgwick, T. Hirao and J. L. Sessler, *Coord. Chem. Rev.*, 2021, **427**, 213560.
- 241 R. E. Gawley, S. Pinet, C. M. Cardona, P. K. Datta, T. Ren, W. C. Guida, J. Nydick and R. M. Leblanc, *J. Am. Chem. Soc.*, 2002, **124**, 13448–13453.
- 242 H. Mao, J. B. Thorne, J. S. Pharr and R. E. Gawley, *Can. J. Chem.*, 2006, **84**, 1273–1279.
- 243 P. Kele, J. Orbulescu, T. L. Calhoun, R. E. Gawley and R. M. Leblanc, *Tetrahedron Lett.*, 2002, **43**, 4413–4416.
- 244 J. Lago, L. P. Rodríguez, L. Blanco, J. M. Vieites and A. G. Cabado, *Mar. Drugs*, 2015, **13**, 6384–6406.
- 245 S. Burrell, S. Crum, B. Foley and A. D. Turner, *TrAC, Trends Anal. Chem.*, 2016, **75**, 10–23.
- 246 R. E. Gawley, M. Shanmugasundaram, J. B. Thorne and R. M. Tarkka, *Toxicon*, 2005, **45**, 783–787; Corrigendum 46, 477.
- 247 R. E. Gawley, H. Mao, M. M. Haque, J. B. Thorne and J. S. Pharr, *J. Org. Chem.*, 2007, **72**, 2187–2191.
- 248 J. Orbulescu, P. Kele, A. Kotschy and R. M. Leblanc, *J. Mater. Chem.*, 2005, **15**, 3084–3088.
- 249 P. Kele, J. Orbulescu, R. E. Gawley and R. M. Leblanc, *Chem. Commun.*, 2006, 1494–1496.
- 250 A. Sun, J. Chai, T. Xiao, X. Shi, X. Li, Q. Zhao, D. Li and J. Chen, *Sens. Actuators, B*, 2018, **258**, 408–414.
- 251 L. Qiang, Y. Zhang, X. Guo, Y. Gao, Y. Han, J. Sun and L. Han, *RSC Adv.*, 2020, **10**, 15293–15298.
- 252 X. He, Current technologies for detection of ricin in different matrices, in *Ricin Toxin*, ed. J. W. Cherwonogrodsky, Bentham Science, Oak Park, Illinois, 2014, ch. 2, pp. 38–56.
- 253 J. Hu, H. Dai, Y. Sun, P. Ni, Y. Wang, S. Jiang and Z. Li, *RSC Adv.*, 2014, **4**, 43998–44003.
- 254 J. Hu, P. Ni, H. Dai, Y. Sun, Y. Wang, S. Jiang and Z. Li, *RSC Adv.*, 2015, **5**, 16036–16041.
- 255 C. L. Schofield, B. Mukhopadhyay, S. M. Hardy, M. B. McDonnell, R. A. Field and D. A. Russell, *Analyst*, 2008, **133**, 626–634.
- 256 S. Pradhan, M. Boopathi, O. Kumar, A. Baghel, P. Pandey, T. H. Mahato, B. Singh and R. Vijayaraghavan, *Biosens. Bioelectron.*, 2009, **25**, 592–598.
- 257 B. Esteban-Fernández de Ávila, M. A. Lopez-Ramirez, D. F. Báez, A. Jodra, V. V. Singh, K. Kaufmann and J. Wang, *ACS Sens.*, 2016, **1**, 217–221.
- 258 S. Fan, G. H. Dennison, N. FitzGerald, P. L. Burn, I. R. Gentle and P. E. Shaw, *Commun. Chem.*, 2021, **4**, 1–11.
- 259 T. M. Alam, M. K. Kinnan, B. W. Wilson and D. R. Wheeler, *ChemistrySelect*, 2016, **1**, 2698–2705.
- 260 W. Q. Meng, A. C. Sedgwick, N. Kwon, M. Sun, K. Xiao, X. P. He, E. V. Anslyn, T. D. James and J. Yoon, *Chem. Soc. Rev.*, 2022, DOI: [10.1039/D2CS00650B](https://doi.org/10.1039/D2CS00650B).
- 261 L. Zeng, T. Chen, B. Zhu, S. Koo, Y. Tang, W. Lin, T. D. James and J. S. Kim, *Chem. Sci.*, 2022, **13**, 4523–4532.

